Shear strength comparison of the natural and reconstituted form of Upper Globigerina Limestone in the undrained state using triaxial testing

Jerome Phil Ciantar

Dissertation submitted to the Faculty for the Built Environment, University of Malta in part fulfilment of the requirements for the attainment of the degree of Master of Engineering (Engineering with Management).

July 2024

L-Università
ta' Malta

FACULTY/INSTITUTE/CENTRE/SCHOOL Faculty for the Built Environment

DECLARATIONS BY POSTGRADUATE STUDENTS

(a) Authenticity of Dissertation

I hereby declare that I am the legitimate author of this Dissertation and that it is my original work.

No portion of this work has been submitted in support of an application for another degree or qualification of this or any other university or institution of higher education.

I hold the University of Malta harmless against any third party claims with regard to copyright violation, breach of confidentiality, defamation and any other third party right infringement.

(b) Research Code of Practice and Ethics Review Procedures

I declare that I have abided by the University's Research Ethics Review Procedures. Research Ethics & Data Protection form code BEN - 2023 - 00128.

As a Master's student, as per Regulation 77 of the General Regulations for University Postgraduate Awards 2021, I accept that should my dissertation be awarded a Grade A, it will be made publicly available on the University of Malta Institutional Repository.

Acknowledgments

I want to express my deepest gratitude to my tutor, Dr. Adrian Mifsud. His invaluable knowledge and guidance have been immensely helpful, making a significant difference in my journey. Thank you, Dr. Mifsud, for your endless help and support!

A sincere thank you to Ms. Tiffany Camilleri and Mr. Sven Grima for their help and support throughout this dissertation.

A heartfelt thanks to my family and friends, especially my parents Philip and Maria and my sisters Tamsin and Kelsey, for being my backbone.

Finally, I would like to give a special thanks to my girlfriend, Anna Marie, for her constant support, patience and encouragement.

I take full responsibility for any shortcomings in this dissertation.

Abstract

The Upper member of the Globigerina limestone formation is a peculiar sedimentary ground material found within the Maltese stratification, which poses difficulties in classification as it can be considered both a hard soil and a soft rock. Geologically, the Upper Globigerina Limestone is one of the weakest layers in the Maltese stratigraphy. However, currently there is very limited literature on the geotechnical engineering behaviour of this material. Such material is well-known for causing foundation issues, and many areas across Malta and Gozo are surmounted on this ground material.

Leroueil and Vaughan (1990) and Burland (1990) outlined that natural sedimentary deposits have a bonded structure and that the strength and stiffness of these deposits cannot be fully explained by void ratio and stress history alone. They emphasized that the soil's structure plays an equally significant role in influencing the material's mechanical behaviour. This theory will be further explored by comparing the mechanical behaviour of the soil in both its intact state, which retains structure, and its destructured state, which lacks such structure. This comparison will highlight the impact the soil's structure has on this material's mechanical properties.

Multiple triaxial tests were conducted to compare the shear strength and the mechanical behaviour of the Upper Globigerina Limestone in both its natural state and its reconstituted equivalent, under undrained conditions. These comparisons enabled determination of how the observed results align with the theory mentioned by Leroueil and Vaughan (1990) and Burland (1990). Additionally, this analysis will offer valuable insights into the mechanical behaviour of this unique facies within the Maltese stratigraphy when subjected to load under isotropic, undrained conditions.

Keywords: Upper Globigerina Limestone, Sedimentary Deposits, Maltese Stratigraphy, Structured, Destructured, Shear Strength, Natural, Reconstituted, Isotropic Conditions, Undrained State and Triaxial Test.

Table of Contents

List of Figures

List of Tables

List of Equations

Glossary

Abbreviation	Meaning
CSL	Critical State Line
CU	Consolidated Undrained
CD	Consolidated Drained
ERF	Electrostatic Repulsive Forces
GL	Globigerina Limestone
INCL	Intrinsic Compression Line
LGLM	Lower Globigerina Limestone
LCL	Lower Coralline Limestone
MGLM	Middle Globigerina Limestone
NCL	Normal Compression line
OCR	Overconsolidation Ratio
RRS	Roscoe-Rendulic Surface
SBS	State Boundary Surface
SCC	Sedimentation Compression Curve
SCL	Sedimentation Compression Line
SHRF	Surface Hydration Repulsive Forces
UGLM	Upper Globigerina Limestone
UU	Unconsolidated Undrained
vDWAF	Van der Waals Attractive Forces
YSR	Yield Stress Ratio

List of Symbols

Symbol	Meaning
Cv	Coefficient of consolidation
c'	Cohesion
c_u	Undrained shear strength
e	Void ratio
ε_a	Axial strain
ε_s	Shear strain
I_v	Void Index
k	Coefficient of permeability
K_0	One Dimensional compression line
M	Gradient
m_v	Coefficient of volume compressibility
p'	Mean effective stress
p'_0	Lower mean effective stress
p'_e	Initial Isotropic stress
$p'_{\max}$	Max experienced mean effective stress
q	Deviatoric stress
S_t	Strength sensitivity
Γ	Location parameter of CSL at yield (following Hvorslev's normalisation)
τ_f	Shear stress
μ	Pore water pressure
ν	Specific volume
W_L	Liquid Limit
$\emptyset'$	Angle of shearing resistance
λ	The slope of a compression line
$\asymp$	A location parameter
ϕ_u	Basic friction angle of the grain material
σ	Total stress
σ'	Effective stress
σ_{vp}	Resultant preconsolidation stress
σ_v'	Vertical effective stress
σ'_{vc}	Past maximum stress (preconsolidation stress)
σ^*_{vy}	The equivalent pressure on K_0CL corresponding to the void ratio of the natural soil
σ'_{vy}	Gross yield stress

1. Introduction

Geotechnical engineering, a relatively young field of study, has gained prominence in recent years. It elicits comprehensive research into the mechanical behaviour of the ground which we build upon and excavate in. This field is critical in the construction sector, as factors such as cost, schedule, and risk are heavily influenced by geological and geomorphological conditions. Understanding the geological situation of a site is crucial not only for ensuring structural integrity but also for maintaining operational functionality. Geotechnical assessments are conducted both for planned construction projects and to safeguard adjacent structures, particularly during excavation activities.

The geological stratification of the Maltese Islands has long been relevant in the construction of a variety of structures, ranging from lightweight to heavy and from simple to intricate. Many of the geological formations found in Malta have already been built upon, making the local ground materials familiar to the locals. In recent decades, the construction sector has seen significant expansion, with projects becoming increasingly complex and excavations going deeper. Compounding this, land scarcity in Mata necessitates development, regardless of the underlying geological conditions. Consequently, there is a pressing need to enhance our understanding of available geological materials, to analyse their limitations and to optimize their utilization while considering their stress limitations in terms of the imposed stress states.

Geological characteristics differ among various ground materials, and even within the same material. A significant challenge in geotechnical engineering arises from the heterogeneous and non-linear nature of the ground. As a result, ground materials can exhibit unusual weaknesses or strengths. Thus, each development necessitates careful and tailored analysis of the ground material to ensure accurate assessment and planning.

1.1 The Maltese Geological Stratigraphy and its Weak 'Rocks'

The Maltese Islands are located in the centre of the Mediterranean Sea and are situated 93 km south of Sicily and 290 km north of the African coast (Schembri, 2003), as indicated in Figure 1.1.

The geographical features of the Maltese Islands have been formed by two primary elements. Galea (2019) outlines that these elements comprise of regional tectonic activities occurring approximately 30 million years ago and the composition of marine sedimentary rock formations. The sedimentary geology is particularly significant as it influences varying rates of erosion and contributes to the formation of distinct and recognizable landforms.

The rock formations found on the Maltese Islands were created by a marine deposition process which occurred during the Late Oligocene-Miocene epochs. This happened within a context of intricate shifts in plate boundaries, plate movements, and stress patterns that unfolded in the Mediterranean throughout the Tertiary period (Scerri, 2019).

Figure 1.1 - Location of the Maltese Islands (Google Maps)

Made up of a series of marine sedimentary rocks, Scerri (2019) reports that the Maltese stratification has accumulated to a thickness of approximately 250 meters. This sequence comprises various types of rocks including limestones, marls, and clays. The stratigraphy of the rock sequence has been divided into five formations. These formations, from oldest to youngest, include the Lower Coralline Limestone (LCL), Globigerina Limestone (GL), Blue Clay, Greensand, and Upper Coralline Limestone (UCL) (Pedley, 2011). Galea (2019) explains that the LCL and UCL share the same lithology, both composed of algal reef limestones formed in shallow waters. These materials are relatively hard, brittle, and competent from an engineering perspective. Between these two hard layers lie the Globigerina Limestone and Blue Clay formations, which originate from sediments deposited in low-energy, deep-marine environments. These formations consist of fine-grained clays, marls, and pelagic limestones. Blue Clay is notably rich in echinoids, molluscs, and solitary corals, fish remnants and marine animals. Additionally, Greensand, made up of glauconitic sand, is located between the Blue Clay and UCL, although it is not always present (Scerri, 2019).

The broad classification outlined above can be developed further by considering the different facies within each formation, some of which are now referred to as 'members.' The Globigerina Limestone formation, for example, is sub-divided in three layers: the Lower Globigerina Limestone (LGL), the Middle Globigerina Limestone (MGL), and the Upper Globigerina Limestone (UGL). The interfaces between these members are demarcated by marker layers of phosphorite clasts frozen within the same limestone matrix of micro-organism skeletons. The marker layer, which separate the LGLM from the MGLM is known as Phosphorite Conglomerate Bed C1 and another Phosphorite Conglomerate Bed, referred to as C2, marks the separation between the MGLM and the UGLM (Oil Exploration Directorate, 1993).

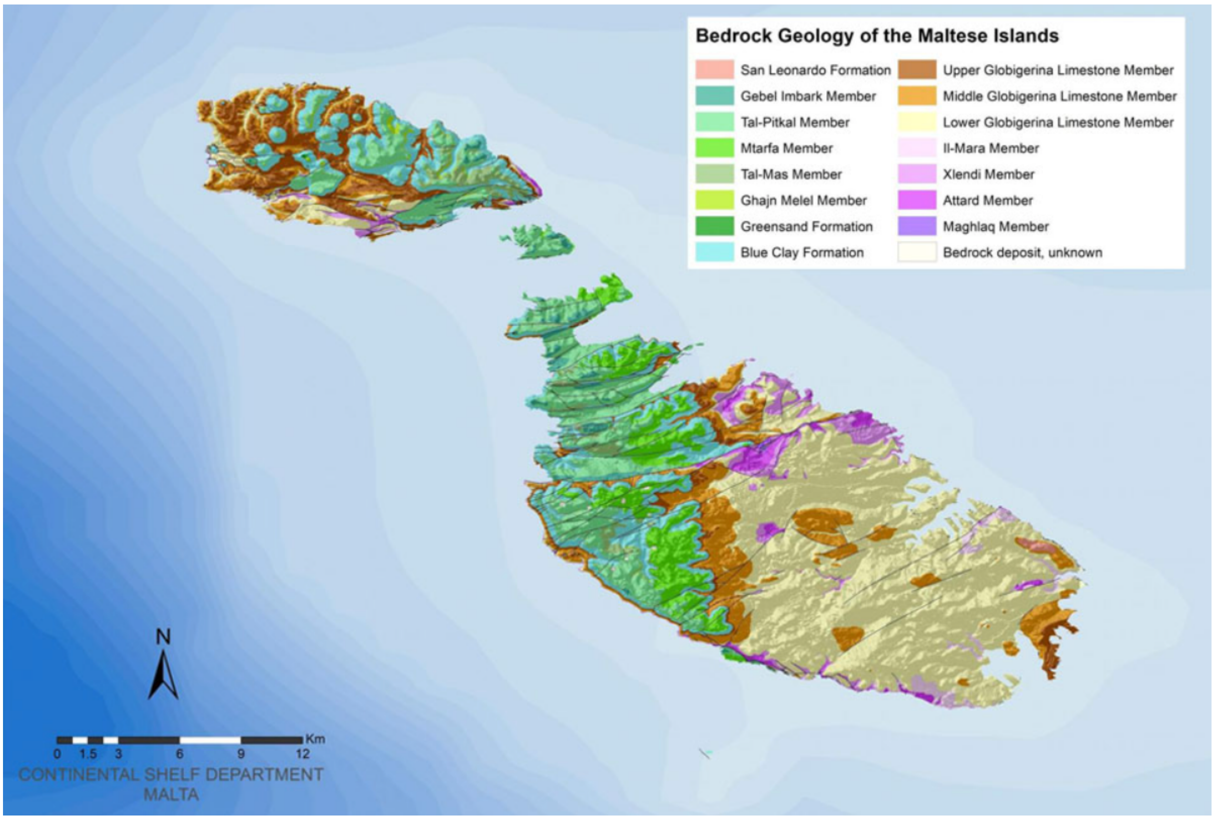

Figure 1.2 – The Geological Map of the Maltese Islands (Continental Shelf Department, 2022)

EPOCH (Stage)	Formation	Member	Strength
PLEISTOCENE (Calabrian)			
MIOCENE (Messinian)	Upper Coralline Limestone	Gebel Imbark	Medium strong to weak
(Tortonian/Messinian)		Tal-Pitkal	Medium strong to weak
(Tortonian)		Mtarfa	Medium strong to weak
		Ghajn Melel	Weak
MIOCENE (Lhangian/Tortonian)	Greensand		Weak to very weak
MIOCENE (Lhangian/Tortonian)	Blue Clay		Very weak to extremely weak
MIOCENE (Burdigalian/Lhangian)	Globigerina Limestone	Upper Globigerina Limestone	Very weak
(Aqiutanian/Burdiglian)		Middle Globigerina Limestone	Very weak
(Aqiutanian)		Lower Globigerina Limestone	Weak
OLIGOCENE (Chattian)	Lower Coralline Limestone	Il-Mara	Medium strong to weak
		Xlendi	Medium strong to weak
(Chattian)		Attard	Medium strong to weak
(Chattian)		Wied Maghlaq	Medium strong to weak

Table 1.1 - The Maltese sedimentary rock stratigraphic sequence (arranged from youngest to oldest) and their characterised strength (Based on Gauci & Schembri, 2019 & Oil Exploration Directorate, 1993)

According to Oil Exploration Directorate, (1993), all stratified layers are categorized into ground materials of varying strengths, ranging from very weak to medium strong, as illustrated in Table 1.1. This demonstrates that different members possess distinct engineering properties, however, such characterisation is very vague. Oil Exploration Directorate (1993) distinguishes the strength of the three Globigerina Limestone members in geological terms; however, no reference is made to the geotechnical engineering behaviour of these distinct layers. While this classification may indicate similarity in terms of their formation between these three members, this is not the case in terms of geotechnical behaviour (Mifsud, 2019). The Maltese geology is well-documented and thoroughly researched, but there are significant gaps in literature regarding the geotechnical engineering properties of these same materials.

1.2 The Upper Globigerina Limestone and its Context

The significance of weak rock formations across the Maltese islands often goes overlooked, with scant research available on these less popular materials, from a geotechnical perspective. This dissertation aims to investigate the Upper Globigerina Limestone, a peculiar and one of the weakest ground materials within the Maltese stratification. Despite its intriguing properties, its geotechnical engineering characteristics remains relatively unexplored. This dissertation is one of a series focused on this specific member, some of which have already been completed in previous years.

The Upper Globigerina Limestone is a distinctive ground material that is part of Malta's geological stratification. The UGL was previously overlaid by additional layers, including Blue Clay, Greensand, and the Upper Coralline Limestone (Scerri, 2019). Over time, these upper layers eroded, gradually exposing the Upper Globigerina Limestone in some places. Areas such as parts of Saint Paul’s Bay in Malta and Xewkija in Gozo are built on top of this ground material. Additionally, such material can be found in other locations across the Maltese Islands, including Mellieha, Delimara, Victoria, and much of the western part of Gozo, such as Ghasri, Gharb, and Kercem.

The Upper Globigerina Limestone is a peculiar ground material, presenting challenges in characterization, as it falls into a classification somewhere between that of hard soil and soft rock. The transition from sediment to rock presents challenges in determining whether argillaceous deposits should be classified as engineering soils or rocks. Terzaghi and Peck (1948) provide a definition of soil as "natural aggregates of mineral grains that can be separated by such gentle mechanical means as agitation in water" and define rocks as "a natural aggregate of minerals connected by strong and permanent cohesive forces." This research will provide guidance on the classification of this specific material.

Bennett (1979) identified that the UGL member is further sub-divided into three specific beds: the Qala, Mgiebaħ and Daħlet Qorrot beds. While the uppermost and lowermost beds are classified as weak rocks, the middle bed is actually a softer facies. Despite being labelled as a very weak and soft by Bennett (1979), this characteristic is not quantified and remains vague. The middle UGL bed is also known for causing foundation issues for overlying structures (Solidbase, 2023). Therefore, this dissertation aims to explore the middle bed of the Upper Globigerina Limestone (UGL-2) to determine the stress limits it can endure, aiming to enhance the understanding of its mechanical properties. This analysis will provide deeper insights into the material's strength and stiffness limitations.

Recent studies by Leroueil and Vaughan (1990) and Burland (1990) highlight that sedimentary deposits possess a bonded structure, and this structure significantly influences the strength and stiffness of these deposits. Mitchell (1976) describes structure as the combination of 'fabric' and interparticle 'bonding.' Czerewko and Cripps (2006) outlines that the structure of natural soils is formed by various factors, which depend heavily on the material's composition, lithification, and diagenetic history. Despite these varying factors, the overall impact on structure is similar, resulting in increased strength and an expanded yield domain, which significantly affects the engineering behaviour of these soils, and which facilitates use of nomenclature such as ‘weak rock’ when describing these materials.

Structure in soils is just as important in determining its strength and stiffness as porosity and stress history. This observation is relevant not only to soft and stiff clays but also to granular and residual soils, and also weak and weathered rock formations (Leroueil and Vaughan, 1990).

Soils can exist either as naturally structured ground material or as man-made destructured reconstituted ground material, which are made in laboratories. Burland (1990) explains that these two forms differ significantly due to the effects of their micro and macro structures.

Burland (1990) explains reconstituted soils as materials mixed with 1 to 1.5 times its liquid limit, then consolidating it one-dimensionally. This process removes all bonding within the soil skeleton, leading to these soils being termed destructured soils. In contrast, natural soils, which retain their original structure, are referred to as structured soils.

Natural soils behave differently from their reconstituted counterparts due to their inherent structure. Burland (1990) explains that natural soils can withstand greater shear stresses compared to reconstituted soils, which lack this structure. Consequently, the mechanical properties of both natural and reconstituted soils are distinctly influenced by their micro and macro structures. Therefore, soil structure reflects various properties and conditions of the soil, and its heterogeneous nature makes it a significant area of study within soil mechanics (Kruse, Gerard, Dijkstra & Schokking, 2007). The properties and characteristics of reconstituted soils are labelled as 'intrinsic' since they are independent of the soil's natural state. These intrinsic properties serve as a benchmark for comparing reconstituted soils to natural soils.

The theories stated by Burland (1990) and Leroueil and Vaughan (1990) will be applied in this dissertation to study the middle bed of the Upper Globigerina Limestone (UGL-2). This ground material will undergo analyses to determine whether this material is consistent with these theories. This study will investigate the engineering behaviour of the UGL-2 in both its natural (structured) and reconstituted (destructured) states. Testing will involve analysing the engineering properties of both forms to identify differences and understand the impact structure has on the mechanical behaviour of UGL-2. The findings will provide valuable insights into the geotechnical engineering characteristics of UGL-2, serving as a benchmark for further studies. Hoek (1999) highlights that soil properties can vary significantly over short distances. Therefore, the mechanical behaviour observed in the UGL-2 specimens in this dissertation may differ from the UGL-2 of just a few meters away and significantly in different localities.

1.3 Scope

The scope of this dissertation is to subject the Upper Globigerina Limestone to isotropic compression and shearing in the triaxial equipment, in both its natural and reconstituted forms. By testing the Upper Globigerina Limestone in both states, the objective is to comprehend the impact soil structure has on its mechanical behaviour, under stress. Testing will be conducted in the undrained state to simulate short-term in situ stresses before water escapes. Careful analysis of the tests will be carried out to ensure error-free results. Finally, these tests can serve as a foundational reference for future studies on such material.

1.4 Research Question

How does structure influence the mechanical behaviour of the natural (structured) UGL-2 specimens when compared to the reconstituted (destructured) UGL-2 specimens under isotropic, undrained conditions?

1.5 Research Methods

The shear strength characteristics of the UGL-2 can be best analysed using the triaxial apparatus. This apparatus is very versatile as it can saturate the ground material, consolidate the material isotropically or anisotropically, as well as shear the material both in drained and undrained conditions whilst it is subject to varying degrees of confinement to simulate ground conditions to a certain extent (Lade, 2016). Thus, such apparatus is beneficial in analysing the material's engineering properties. While anisotropic consolidation tests offer a more accurate reflection of on-site conditions by implying larger vertical stresses compared to horizontal stresses, such tests require complex and specialized apparatus as well as professionals trained in its operation, thus, in the case of this dissertation, isotropic conditions will be assumed.

Triaxial testing has been conducted on both forms of UGL-2. These tests are complex and time-consuming, but during the course of this research work, seven tests were completed: four tests on specimens in the natural state, and three tests on specimens in the reconstituted state.

1.6 Structure of this Dissertation

Geological Background of Sample Retrieval Site – Chapter 2 provides a concise geological and geomorphological overview of the sample retrieval site, followed by a detailed examination of the Maltese Globigerina Limestone, with a specific emphasis on the Upper Globigerina Limestone. This focus is essential as the Upper Globigerina Limestone is the material analysed in this dissertation.

Literature Review – Chapter 3 comprises the literature review, which initially delves into the constituents, diagenesis, and structure of sedimentary deposits. This section aims to elucidate the processes that contributed to the formation of the UGL-2 and consequently, its structure. Subsequently, the literature review transitions to expound on the critical state framework, which is pivotal to this dissertation. This chapter continues by discussing the types of strength experienced by such materials when subjected to stress. Understanding this framework is crucial for comprehending the mechanical behaviour of such materials when subjected to load. The chapter then proceeds to elucidate the influence of the material's structure, providing evidence that the structure plays a significant role in its mechanical behaviour.

Methodology – Chapter 4 encompasses the methodology, offering a detailed description of the laboratory testing method employed to attain the necessary results for a comprehensive analysis. It provides why the testing method was chosen and outlines how it was implemented. Additionally, details on the sample's sourcing methodology are included.

Results – Chapter 5 provides the results obtained from laboratory testing of undrained shear on both the reconstituted and natural sample of the UGL-2.

Conclusion – Chapter 6 compiles and summarizes the results obtained from the laboratory tests.

1.7 Additional Note

In this dissertation, it is worth mentioning that the reconstituted sample of the UGL-2, which is a crucial component of this research, was prepared by another student (Sven Grima) as part of his own dissertation project. Grima's dissertation was conducted simultaneously with this dissertation. While this collaboration allowed sharing of resources and expertise, it is important to note that similar, yet distinctive objectives were pursued. The intention was to examine the same ground material from different perspectives, thus enriching the overall understanding of the subject matter. While each dissertation was focused on individual research endeavours, the nature of the work necessitated mutual assistance and cooperation to successfully carry out these respective dissertations.

2. Geological Background of Sample Retrieval Site

The natural middle bed of the Upper Globigerina Limestone studied in this dissertation was sourced from Mellieha, situated in the northern part of Malta, as highlighted in red in Figure 2.1. This chapter presents a concise overview of the geology and geomorphology of the area.

The ground material tested in this dissertation, referred to as UGL-2 in a ground investigation report by Solidbase (2023), was sourced from an area near the Mellieha Bay Hotel (with the location to be identified later in this chapter). The report observed that this ground material, due to its weak and soft nature, caused foundation issues at the hotel. Specifically, it led to settlement cracks within the building, rendering the hotel unserviceable.

Figure 2.1 - Location of Mellieha, Malta (Wikimedia, 2007)

The Mellieha Bay Hotel is built on the UGL bed, which is composed of three layers with varying strengths. Most of the hotel rests on UGL-1, a relatively weak layer, while a portion of the hotel is situated on UGL-2, a very weak layer consisting of silty clay or hard clayey silt. The hotel's placement on these different layers, each with distinct properties, has caused uneven settling in some areas The depth of the UGL-2 layer varies significantly due to the extensive faulting in the area, ranging from just a few centimetres to nearly 15 metres (Solidbase, 2023).

2.1 Mellieha Horst and Graben System

The initial extensional regime impacting the islands began in the early Miocene, leading to the formation of fractures oriented in the NE-SW direction. These fractures developed into a remarkable block faulting sequence, forming the horst-and-graben landscape characteristic of northwestern Malta, (Galea 2019) including Mellieha, as depicted in Figure 2.3.

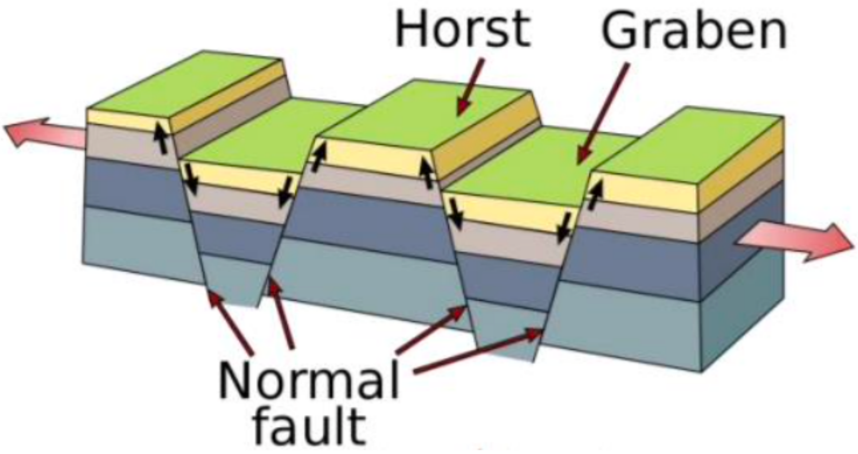

Figure 2.2 – Horst and Graben System formed during tectonic activities (Continental Shelf, 2022)

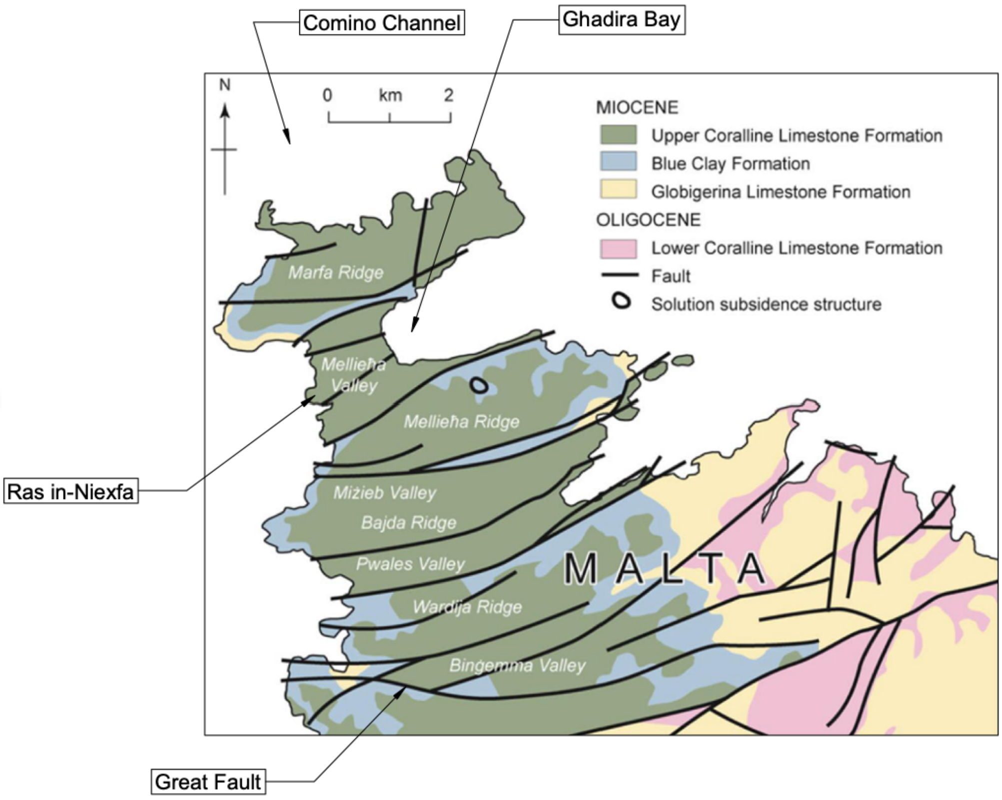

Figure 2.3 - Horst and Graben systems in the Northern part of Malta (Oil Exploration Directorate, 1993)

The northern part of Malta, especially Mellieha, consists of several ridges and valleys as depicted in Figure 2.3. Of particular significance for this dissertation are the Marfa Ridge Peninsula and the Mellieha Valley, as the sample was extracted from an area located between them. Both are situated to the north of the Great Fault and constituting part of the horst-and-graben sequence.

Scerri (2019) describes the Marfa Ridge Peninsula as a ridge that attains a peak elevation of 120 meters towards its western end, with a sharp inclined slope located on the southern edge of the peninsula, overlooking the Mellieha Isthmus with a dramatic fault-line scarp that drops from 120 meters in the west to just over 30 meters in the east. The Marfa Peninsula itself is an inclined fault block that gently slopes to the north, heading towards the Comino Channel and is intersected by several small-scaled valleys draining north along the Marfa coastline. The island of Comino is thought to be an exposed portion of a submerged graben north of Marfa Ridge (Pedley, 1976). The western and eastern shores of this Peninsula uncovered the Blue Clay member and exhibits areas of large boulders and slopes of loose rocks, created through varying erosion and landslide mechanisms (Soldati, 2019).

Scerri (2019) further explains that the Mellieha Valley (isthmus) is characterized by northern and southern alluvial depressions, such as l-Ghadira and il-Hofra, divided by a small Upper Coralline Limestone ridge that peaks at 60 meters near Ras in-Niexfa. At this point, two prominent hills reveal the Gebel Imbark member, the youngest member of the UCL. The area's stepped morphology results from bedding, featuring narrow, dry channels draining northward to Ghadira, where alluvial fans developed across the plain. This ridge and valley system continues up to the Great Fault.

2.2 Geology of site

2.2.1 Location

The location of the site is situated within the Mellieha Valley in Ghadira, which is one of the subdivisions of Mellieha. Characterized as a low-developed area, it hosts some hotels attracted by the stunning view of Ghadira Bay, along with several boathouses and Triq Il-Marfa, serving as the primary route linking Mellieha to Cirkewwa. The remaining portion of the area comprises the sandy expanse of Ghadira Bay, interspersed with vegetated regions, and also holds a protected site under Natura 2000.

The precise location of the sample is illustrated in red in the aerial photographs shown in Figure 2.4. It is positioned between the Marfa Ridge Peninsula and the Mellieha Valley (isthmus). The site is very close to the Mellieha Bay Hotel and was chosen to investigate the ground below this building, as part of the redevelopment of this same hotel.

Figure 2.4 - Aerial photograph showing location of site (Google Maps)

2.2.2 Topography and Rainwater Drainage

Rainwater drainage flows from higher altitude areas towards the shore. Figure 2.5 illustrates the topographic map of Malta and highlights its numerous valleys. Mellieħa is distinguished by its numerous valleys that contribute to the town's steep hills characteristic. The selected site is positioned along a valley's flank, as illustrated by the red dashed circle in Figure 2.5.

The section in Figure 2.6 illustrate the slope descending from the North-West (the top of the slope) to the South-East (the bottom of the slope). While Figure 2.7 illustrates the section from North-East to South-West, where the site remains relatively horizontal. The red arrows in Figure 2.6 & Figure 2.7 indicate the location of the retrieval site of the sample in relation to the slope.

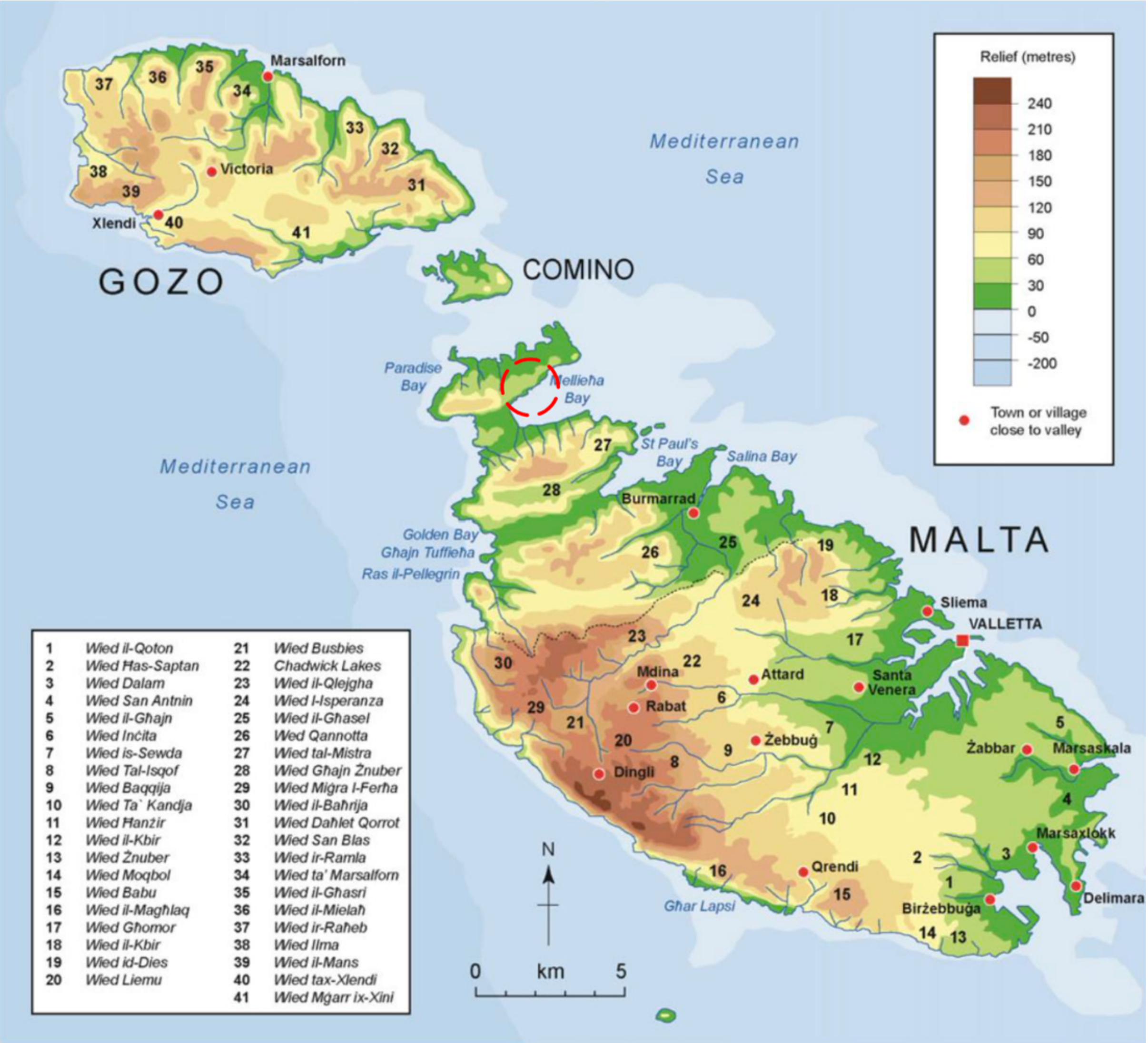

Figure 2.5 – Topographic Map of the Maltese Islands (Scerri, 2019)

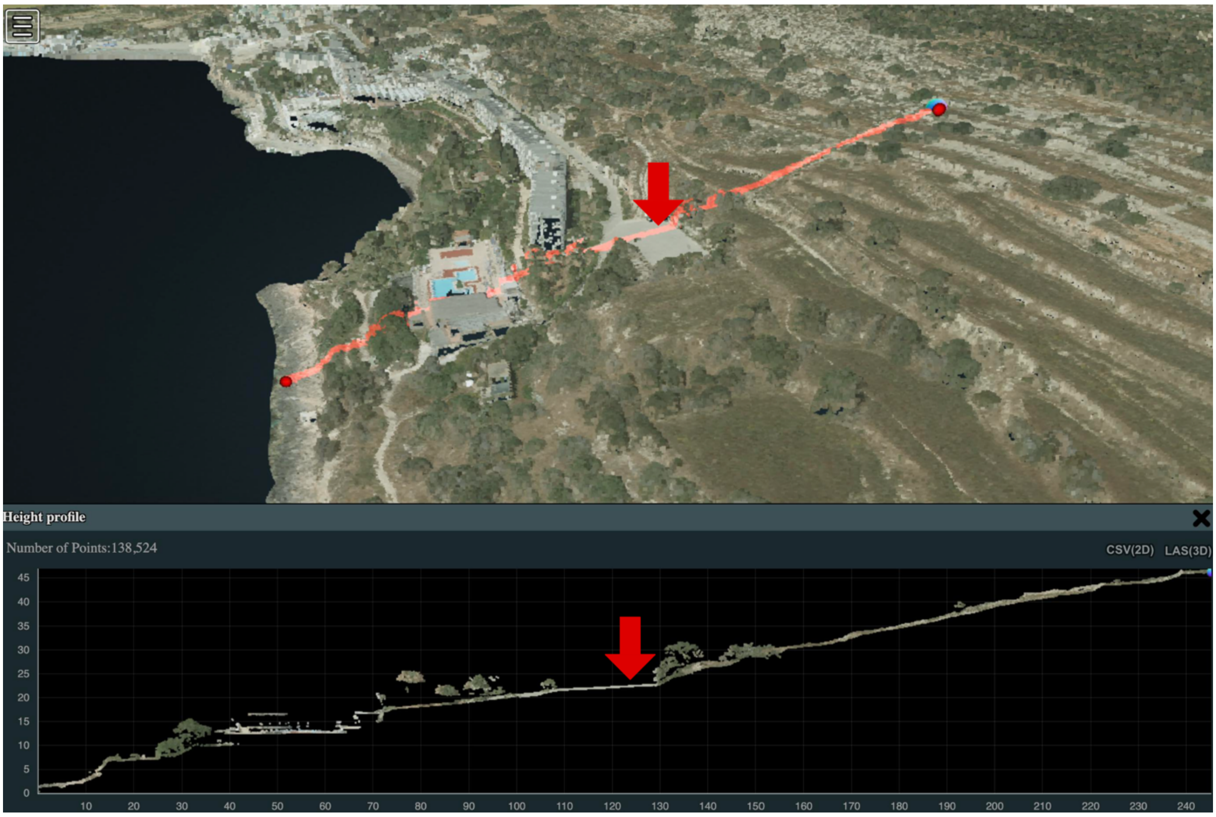

Number of Points:138,524

Figure 2.6 – North-West to South-East sections of the site from where the samples were sourced (CloudIsle, 2018)

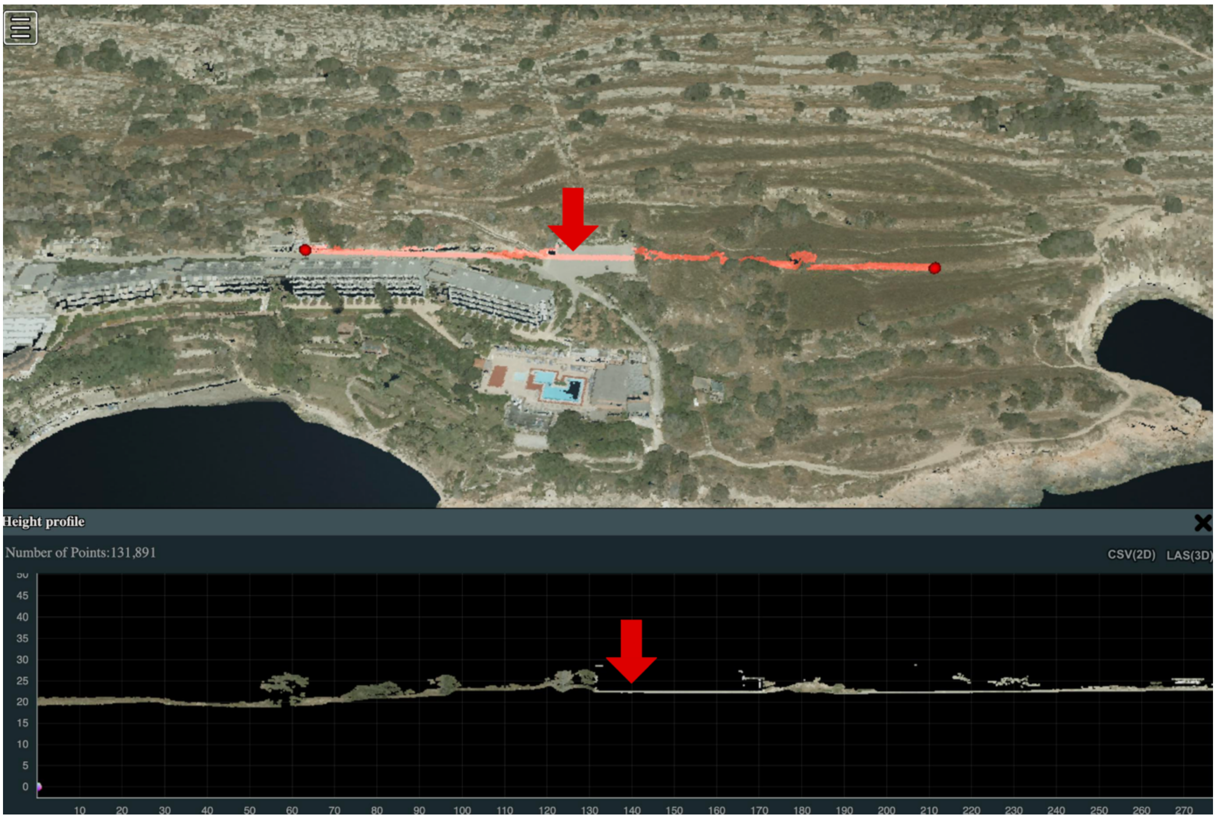

Number of Points:131,891

Figure 2.7 - North-East to South-West sections of the site from where the samples were sourced (CloudIsle, 2018)

2.2.3 Site Geology

The geological maps in Figure 2.8 highlights the relationship between the site and the numerous fault lines present in the region. Notably, the site is situated between two of these fault lines, providing important context for understanding the geological dynamics of the area.

Upon reference to the geological map depicted in Figure 2.8, it becomes apparent that the sample was obtained from an area distinguished by the Upper Globigerina Limestone formation. Therefore, it is clear that the sample belongs to the Upper Globigerina Limestone stratum.

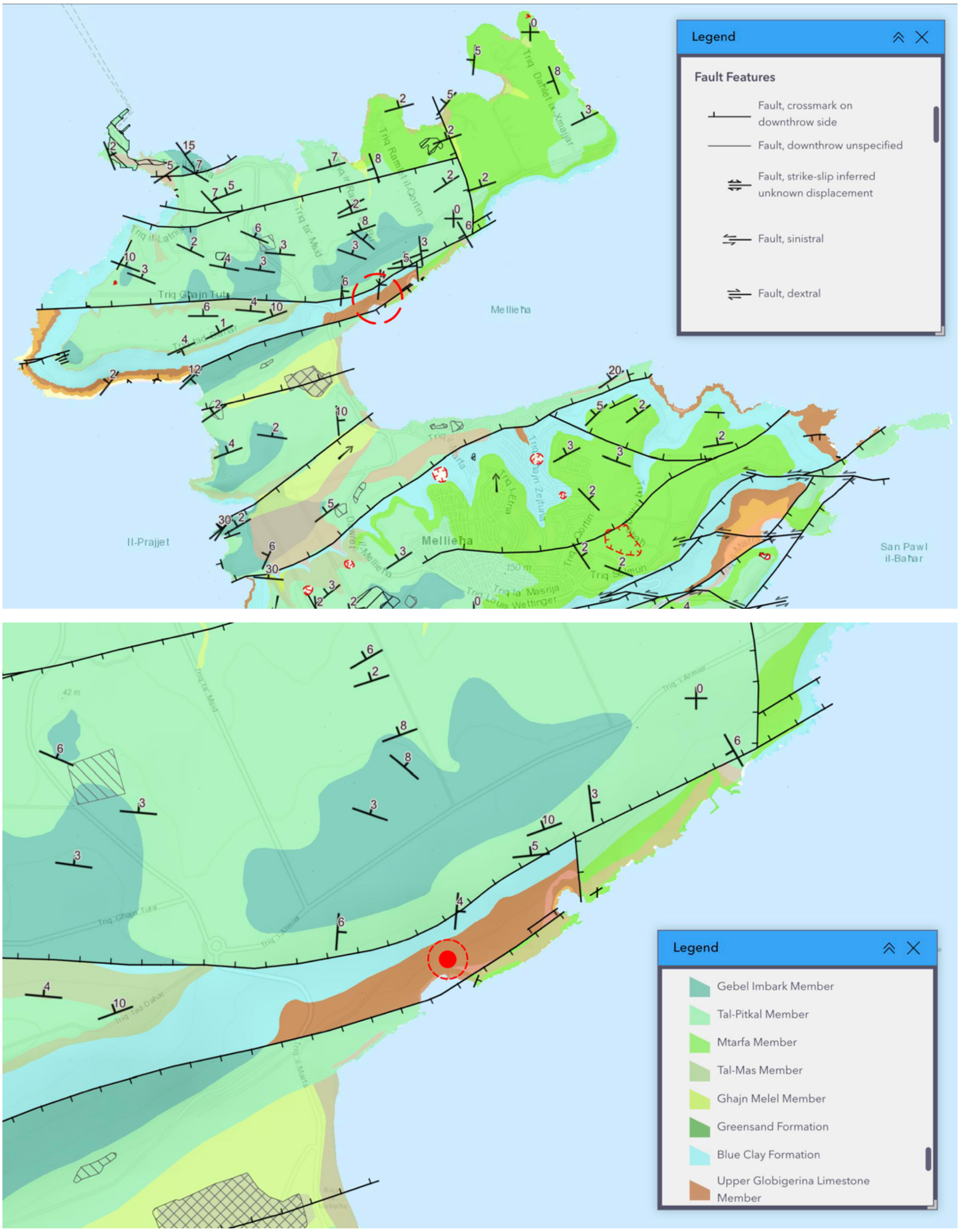

Figure 2.8 - Geological Map of Mellieha (Top) and of site (Bottom) (Geological Map of the Maltese Islands, 2022)

Furthermore, the lack of Upper Coralline Limestone (UCL), Greensand, and Blue Clay above this stratum suggests erosion that uncovered the Upper Globigerina Limestone. This corresponds with the conclusions drawn by Scerri (2019) mentioned in Chapter 1 of this dissertation. Moreover, this implies that the UGL-2 endured higher stress levels in the past, as indicated by the erosion of overlying layers.

2.3 The Globigerina Limestone

The Globigerina Limestone, which is rich in planktonic foraminifera, is widely found in the Maltese Islands (Pedley, 1978). The stratigraphic member of the Globigerina Limestone occupies approximately 44.5 percent of the Maltese island's surface area. Globigerina limestone is characterized by a gently sloping rock/shore platform, serving as its main geomorphological feature (Schembri, 2003).

Gauci & Inkpen (2019) document that this type of limestone is susceptible to weathering and gives rise to softly undulating terrains and gradual inclines. However, this terrain is interrupted by two narrow layers of conglomerate beds that resist weathering, resulting in prominent outcrops or forming elevated steps within the slopes. The occurrence of pebbles within the conglomerate beds suggests a shift in the way materials were deposited.

The Globigerina Limestone layer is relatively softer compared to the underlying Mara Member and, as it erodes, it forms gradual, terraced slopes. The Lower Globigerina Limestone layer exhibits a pale-yellow hue and is the most uniform and resilient layer. Fossils within these formations primarily include scallop shells and burrowing sea urchins (Pedley, 2002).

The following section will focus exclusively on the UGL, as it is the primary subject of this dissertation.

2.3.1 The Upper Globigerina Limestone

Specifically, the Upper Globigerina Limestone (UGL) alone encompasses about 8.4 percent of the entire Maltese Islands (Schembri, 2003). Scerri (2019) described the middle and upper members of the Globigerina Limestone as being softer in texture, with a greater presence of marl and a higher proportion of clay content.

Scerri (2019) states that UGL consist of finely grained limestone created from the remnants of foraminifera and other planktonic creatures. The nature of this layer suggests its deposition in a deeper marine setting that remained undisturbed by wave activity.

The clasts within this bed are consistently smaller than 5 centimetres in size, and fish teeth are frequently present. Due to the presence of a marly lime mud that provides structural support, this bed is highly susceptible to erosion and doesn't form distinct, prominent ledges. Often, it remains concealed beneath weathered material that originates from the bed of grey marl facies located above it (Gauci and Inkpen, 2019).

The three aforementioned UGL sub-divisions are different from each other. The upper and lower beds share similar lithological characteristics, being a paler yellowish and heterogenous material, possessing ferruginous nodules and subject to honeycomb weathering (Pedley, 1976). Felix (1973) described the uppermost bed as a foraminiferal wackestone facies with a mottled yellow and orange hue, while the lowermost bed also exhibits a mottled yellow and orange hue and characterized as a foraminiferal wackestone facies. The middle (Mgiebaħ) bed has a higher clay content compared to the other two beds (John, Mutti, & Adatte, 2003). The middle bed is described as an argillaceous marl (House, Dunham, & Wigglesworth, 1960), pale grey marl biomicrite (Pedley, 1976), or a marly limestone (Gatt, 2006). Felix (1973) described the middle bed as a dark grey foram-coccolith marly facies.

At the upper boundary of this member, there is a quick transition, occurring over a depth of approximately one meter to the Blue Clay member. This transition is marked by a notable rise in clay content within the layer (Scerri, 2019).

Figure 2.9 – Yellow Upper Globigerina Limestone formation at Il-Hofra l-Kbira near Marsaxlokk (Malta) (Agius, 2023)

It is worth mentioning that this dissertation will focus solely on testing the middle bed of the Upper Globigerina Limestone (UGL-2), which is the weakest and most problematic of the three beds, thus, justifying its selection for this study.

3. Literature Review

3.1 Constituents, diagenesis and structure of Globigerina Limestone and similar sedimentary deposits

The Globigerina Limestone, a prominent sedimentary deposit in the Maltese islands, exhibits a composition influenced by various factors. Its formation is intricately linked to the physical elements governing sedimentation, the aggregation process on the seabed, and subsequent alterations upon burial. A comprehensive understanding of the constituents, diagenesis and structure is essential for unravelling the unique engineering characteristics of this material.

3.1.1 Constituents

Sedimentary deposits are composed of two primary components: biogenic material (represented by microfossils, shallow water organisms and biota), and non-biogenic material (which takes form of water-borne clay, silt, and mud particles). The varying proportions of these components result in a diverse spectrum of mechanical behaviours exhibited by sediments.

3.1.1.1 Biogenic

Pelagic sediments accumulate biogenic input when the remnants of planktonic organisms from the upper layers of the seawater column descend to the seabed in deep sea environments (Nichols, 2009). These remains can be either composed of calcium carbonate or silica.

Biogenic material can be produced by various carbonate-forming organisms. One example is the Foraminifera, which are tiny, single-celled marine organisms that vary in size from a few tens of microns to several millimetres in diameter. These organisms can either be planktonic, floating in the water, or benthic, residing on the sea floor. Most contemporary and ancient foraminifera possess hard outer shells (tests) composed of either high or low-magnesium calcite.

Additionally, biogenic material can be produced from carbonate-forming plants. One such example are corals which forms either in large colonies that span several meters or exists as solitary organisms. Corals maintain a symbiotic relationship with algae, which thrive in clear, warm, shallow marine waters (Nichols, 2009). Biogenic materials are also made from calcareous algae, which produce much smaller skeletons that make up the Upper and Middle Globigerinae (John et al. 2003).

3.1.1.2 Non-Biogenic

Erosion of landmasses through various weathering processes generates the majority of non-biogenic content. Physical, chemical, or biological factors break down exposed rocks, resulting in the accumulation of clay particles in different layers. Components such as the environment, climate, and the type of bedrock influence the extent of leaching and soil pH levels, which in turn affect the formation of various clay minerals, quartz, and feldspars. Additionally, non-biogenic material can have volcanic origins, with volcanic ash being particularly prone to decomposing into various clay minerals. Another source of non-biogenic material is the immediate precipitation of mineral ions dissolved within the pore water of freshly deposited sediment material in microscopic levels (Nichols, 2009).

3.1.2 Diagenetic Processes

Diagenesis refers to the process through which sediments undergo both chemical and physical changes as they transform from loose deposits into solid rocks after their initial deposition. Described by Twenhofel (1939), the term "diagenesis" specifically denotes alterations that occur in sediments after their deposition, encompassing various changes that influence the sediments as they progress towards becoming sedimentary rocks.

3.1.2.1 Compaction

Compaction is the process where sediment volume decreases, resulting in higher density. This alteration in physical properties occurs after deposition and is influenced by factors such as the stress imposed from overlying material (gravitational compaction) and biological or chemical reactions that involve the dissolution and precipitation of minerals. The compaction process is instrumental in shaping the characteristics of sedimentary rocks (Bjørlykke, 2013). Compaction stands out as a primary physical post-depositional process that significantly impacts soils. The ongoing cycle of burial and exhumation leads to a constant evolution in the structure and composition of the soil fabric. This dynamic process plays a crucial role in shaping the characteristics of the sediment over time (Middleton, 2003).

3.1.2.2 Cementation

Cementation is a pivotal diagenetic process involving the precipitation of mineral matter, referred to as cements, within the pores of sediments or rocks. This process is part of a broader spectrum of diagenetic phenomena, which includes mechanical and chemical compaction, as well as mineral replacement. Collectively, these processes contribute to the gradual reduction of porosity and the lithification of sedimentary layers as they age or become more deeply buried. Cementation takes place in various types of voids, ranging from open intergranular or intragranular pores (between or within grains) to larger spaces such as caves, or fractures. It is noteworthy that cements can even form crusts on surfaces at interfaces with sediment-water or sediment-air. The precipitation of cements is not restricted to a specific diagenetic stage; it can occur during deposition, burial, and subsequent uplift and exposure (Middleton, 2003).

3.1.3 Structure

The three-dimensional structure of a soil is an outcome of a sedimentary process that took place in the distant past. Soils consist of heterogeneous materials, and their attributes are intimately tied to their three-dimensional structure. A soil's structure is an intricate arrangement comprising particles, pores, and voids that vary in shape and size (Totsche, 2018).

The constituents make up the particles of various forms and sizes which create the ground material. The way in which these particles are arranged give the material its unique engineering characteristics. Such features are later shaped by the ground material’s diagenetic history and weathering process. Diagenesis causes particles to compress, possibly resulting in the formation of an interlocking structure whose variation corresponds to the degree of diagenesis (Holtz & Kovacs, 1981). The characteristics exhibited by this distinctive arrangement of particles are referred to as the "structure" of these sedimentary deposits. According to Lambe and Whitman (1969), structure is described as the combination of "fabric" and "bonding" being the spatial orientation and arrangement of particles within a soil mass, along with the interparticle forces that exist between adjacent soil particles.

Fabric, as introduced in the first part of Lambe and Whitman's (1969) definition of structure, describes the diverse orientations and distributions of clay particles, attributed to their plate-like nature. The next component of this definition, bonding, encompasses the interparticle forces. Such interparticle forces include, Van der Waals attractive forces (vDWAF), electrostatic repulsive forces (ERF), and surface hydration repulsive forces (SHRF) which are significant factors that collectively contribute to the stability of aggregates within soil. ERF arise when the electric double layers of two adjacent particles, both carrying the same charge, overlap. On the other hand, vDWAF originate from the electromagnetic interactions between the molecules that make up the particles. Moreover, the interaction between water molecules and clay is a result of SHRF. All three factors mentioned contribute to attractive or repulsive interparticle forces (Zhenghong, 2020). Additionally, bonding includes the impacts of cementation between individual particles, significantly influencing the mechanical behaviour of the sediment, regardless of its mineral composition.

Leroueil and Vaughan (1990) outline that structure is one of the fundamental principles in soil mechanics, alongside other factors like initial void ratio and stress history, as they hold comparable significance. While the void ratio serves as a fundamental mechanical property in soils as it provides insight into the degree of grain packing, structure of a soil holds equal significance in determining its strength and stiffness (Leroueil & Vaughan 1990). Void ratio offer clues as to whether a soil will contract or dilate when subjected to shearing forces. In the critical state framework, this material's pore structure characteristic is utilized to delineate the critical state, aiding in the differentiation between densely packed and loosely packed soils (Wen & Zhang, 2022).

Both void ratio and soil structure serve as quantitative measures of the internal structure of soil. Understanding the relationship between these two parameters is crucial for integrating the critical state and the critical fabric surface (Wen & Zhang, 2022).

3.1.3.1 Natural (structured) and reconstituted (destructured) soils

Many naturally occurring sedimentary deposits exhibit a particular structure that significantly impacts their mechanical properties (Leroueil & Vaughan, 1990). The impact of structure on the engineering behaviour of these soils can be assessed by comparing them with destructured soils, which lack this inherent structure and bonding. Destructured soils can be created in the laboratory in the form of reconstituted soils where the internal bonding is removed, thus eliminating any interparticle bonding within the soil matrix. Thus, the mechanical properties of reconstituted soils are intrinsic to the soil itself and do not depend on its natural state. Such reconstituted soils are labelled as intrinsic materials because their characteristics are inherent, depending only on interparticle friction and particle arrangement, and are created in a specific method, independent of their natural state. Therefore, natural and reconstituted soils exhibit different mechanical properties influenced by the presence or otherwise of their micro and macro structure (Burland, 1990).

Burland (1990) explains that the primary benefit of the reconstitution process is that it produces soil with a standardized, repeatable particle arrangement that lacks structure. This reconstituted structure serves as a benchmark for comparing it to natural soils, which are influenced by structure. As a result, compression curves for a natural soil sample may differ from those of a reconstituted sample of the same material, even when they share identical soil parameters. This highlights the contrasting behaviour observed between reconstituted versus natural soils.

The primary objective of this dissertation is to analyse the effect structure has on the engineering behaviour of soils. Therefore, the natural UGL-2 will be used as the natural structured soil (which contains bonding), and the reconstituted UGL-2 will serve as the destructured soil (with its bonding removed). These two forms of UGL-2 will be subjected to shear tests to analyse the impact of bonding on the mechanical behaviour of this material.

In summary, the structure of soil and the manner in which the material was deposited have an impact on natural soils. These soils exhibit different behaviours when subjected to remoulding (Mitchell, 1976). Comprehending the behaviour of these forms of soil requires accounting for the influences of structure, which holds equal significance to factors like initial void ratio and stress history in characterizing their response (Leroueil & Vaughan, 1990).

3.2 The frictional behaviour of granular soils

The resistance to shearing in any assembly of solid particles is influenced by the particle shape and their level of packing (interlocking is ‘structure’). Research indicates that when a stress is applied perpendicular to an assembly of particles undergoing shearing, there is an increase in contact forces between the particles, making them more resistant to displacement (Schofield & Wroth, 2004).

3.2.1 The principle of effective stress

This behaviour is observed not only in dry soils but also in saturated soils. In saturated conditions, however, the impact of pore water pressure on particle interactions must be considered. Terzaghi (1925) articulated this concept as the principle of effective stress, which is fundamental to soil mechanics. According to this principle, the stresses exerted on the soil skeleton (σ') are the difference between the total applied stress (σ) and the pore water pressure (u).

$$\sigma' = \sigma - \mu \qquad \text{(Eq. 3.1)}$$

Thus, in dry materials, shear is resisted primarily by the interaction within the assembly of particles, or the soil skeleton, whereas in saturated soils, shear is resisted by both the soil skeleton and the fluid in between. In cases where the fluid is incompressible, such as with water-saturated sediment, the pressure of the fluid within the soil's pores can change when the sediment is subjected to external stress. If the fluid cannot escape, or escapes very slowly, the resulting pressure helps resist the applied external stress (Schofield & Wroth, 2004).

Terzaghi underscores the importance of effective stress, asserting that any measurable impact from stress alterations is solely due to changes in effective stresses. In soil engineering, it is essential to account for effective stresses as most soils are saturated to a certain degree.

3.2.2 Invariants of stress

In triaxial testing, soils are subjected to two types of stresses: normal (direct) stress and shear stress.

Normal (direct) stress is a compressive stress exerted perpendicular to the cross-sectional plane of the specimen. The compressibility of soil which reflect changes in volume under normal stress, is primarily influenced by alterations in effective stress rather than total stress. These compressive forces cause soil particles to rearrange, resulting in a more compact assembly (Head, 1998).

Shear stresses occur parallel to the plane being considered and arise when forces induce particles to slide past each other. Shear stress resists angular deformation in the same way that normal stress resists compression. In soil, shear stresses are transferred purely through frictional forces at the points of intergranular contact, indicating that they are supported by the soil skeleton itself. Hence, the ability to withstand shear stress on a specific plane relies on the effective normal stress rather than the total normal stress (Head, 1998).

In a triaxial test, stresses are applied to the soil specimen in two stages, according to Head (1998):

- **All-round Pressure**: This is the cell pressure, denoted as $\Delta\sigma_3$, which causes a rise in pore pressure. This stress is associated with the mean stress (p'), which forces soil particles to move closer together.
- **Additional Axial Stress Increment**: This is the deviator stress, calculated as $\Delta\sigma_1 - \Delta\sigma_3$, which causes a further increase in pore pressure. This stress is associated with the deviator stress (q), which forces particles to move relative to each other.

Figure 3.1 depicts the following: (a) the original specimen in an unstressed state, (b) the impact of the mean stress (p) denoted as $\Delta\sigma_3$, which induces particles to draw nearer to each other, (c) the influence of the deviator stress (q) represented as $\Delta\sigma_1 - \Delta\sigma_3$, where shear stresses are introduced, prompting particle movement relative to one another, and (d) the resultant stresses arising from both aforementioned stress components.

Where:

$$p' = \frac{\sigma_1 + 2\sigma_3}{3} \qquad \text{(Eq. 3.2)}$$

$$q = \sigma_1 - \sigma_3 \qquad \text{(Eq. 3.3)}$$

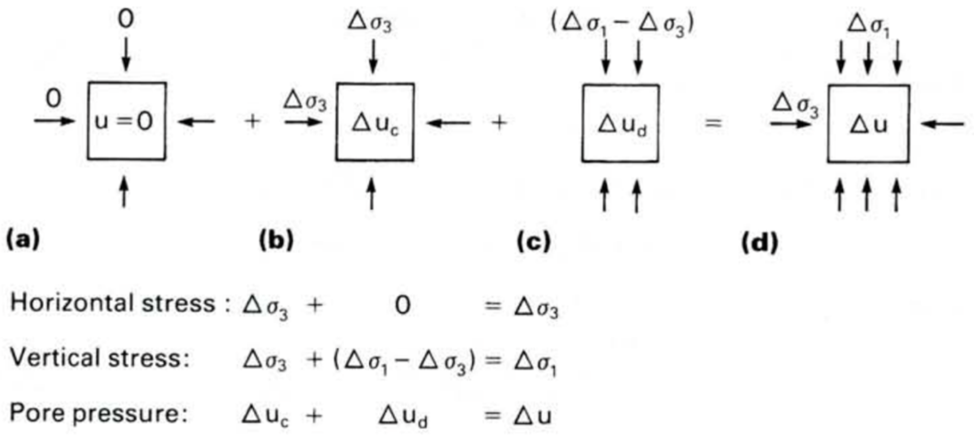

Figure 3.1 – Stress stages applied to a soil in a typical triaxial test: (a) initial, (b) cell pressure increment, (c) deviator stress increment and (d) combined (Head, 1998)

3.3 The critical state framework

This sub-chapter provides an overview of the mechanical behaviour of sedimentary ground materials in context to the critical state framework.

3.3.1 Compression and swelling lines

Considering cohesive materials placed in triaxial or oedometer cells in the drained state, where different confinement pressures are applied (mean effective stress, p', for the triaxial and vertical effective stress σ_v' for the oedometer), when plotting the specific volumes against these confining pressures, in the drained state, it is observed that a curve is formed when plotted in logarithmic form. This line is called the Compression Line. The equation of such a curve is (Atkinson & Bransby, 1978):

$$\nu = \asymp -\lambda\, logp' \qquad \text{(Eq. 3.4)}$$

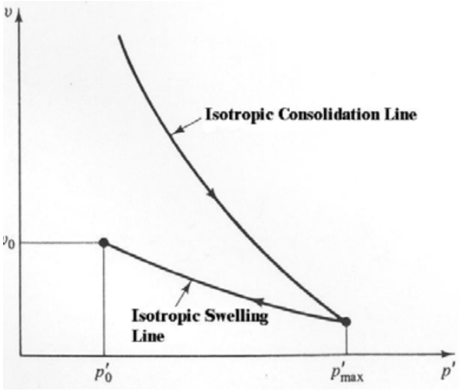

Figure 3.2 - Isotropic Consolidation Line & Isotropic Swelling Line (Atkinson & Bransby, 1978)

Different specimens, of the same or different materials, result in different Compression Line positions, which can be a result of a range of causes, such as the consolidation procedure, to the different materials and also, the effects of structure of the material. When the considered sample is unloaded, it will not travel along the Compression Line again in the $\nu - p'$ space, but will move along a family of curves, named as swelling line. A swelling line, therefore, will always initiate from a Compression Line. Consolidation in a swelling line, which is a result of unloading, is less than the consolidation arising from an identical unloading happening along a compression line (Atkinson & Bransby, 1978).

In this dissertation, and for the specific case of the UGL-2 material, specimens found on a compression line are referred to as normally consolidated samples, while those initially located on a swelling line are termed overconsolidated specimens. The normally consolidated samples refer to the laboratory-produced reconstituted specimens, and the overconsolidated specimens refer to natural specimens, sampled directly from the site.

3.3.2 Typical undrained stress paths of normally consolidated materials

The stress path behaviour of a series of normally consolidated specimens, under isotropic triaxial compression testing is depicted in Figure 3.3. Each test is subjected to a different mean effective stress p', denoted as p'_e, representing the maximum stress the specimen has ever experienced.

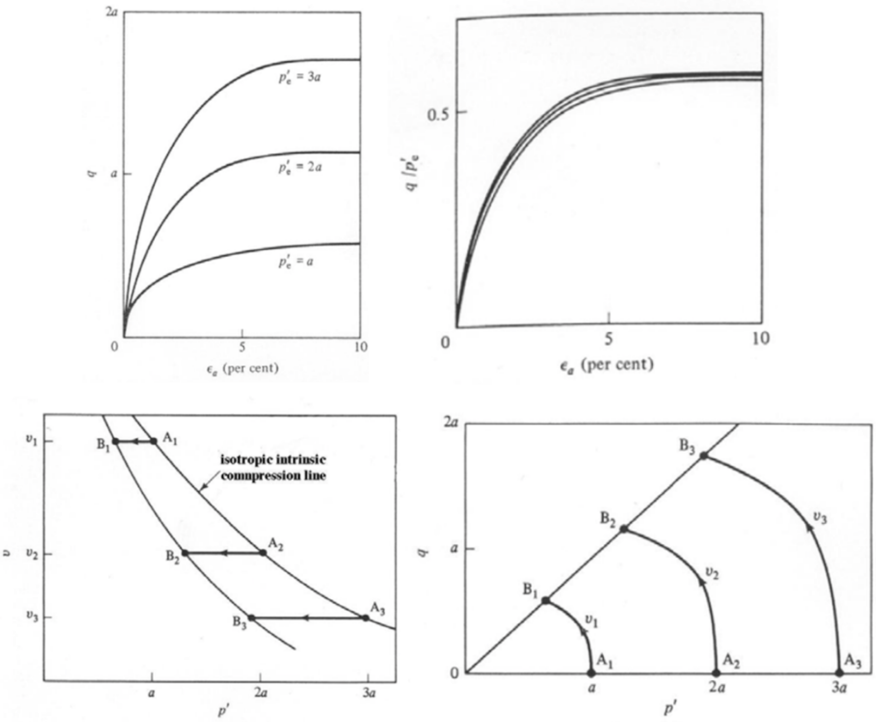

Figure 3.3 - Normally consolidated undrained stress paths in $q - \varepsilon_a$ space (top - left), $q/p'_e - \varepsilon_a$ space (top – right), $\nu - p'$ space (bottom - left) and $q - p'$ space (bottom - right) (Atkinson & Bransby, 1978)

Specimens compressed to a higher p' value exhibit higher values of q at failure. While variations in mean effective stress result in different q values, all curves display a similar overall shape. This allows for normalization by plotting q/p'_e against ε_a. The stress paths visualized in a $\nu - p'$ space follow a horizontal line, a characteristic of undrained tests where no change in volume occurs.

Samples begin at the normal consolidation line (A1, A2, A3) and move leftward until reaching failure points (B1, B2, B3). Additionally, the stress path in $q - p'$ space exhibit curves which rise in their initial stage and then move to the left. Interestingly, different stress paths display similar shapes. The failure points B1-B3 form a straight line in $q - p'$ space and a smooth curve, resembling the normal consolidation line, in $v - p'$ space (Atkinson & Bransby, 1978).

Figure 3.4 illustrates a $q - p' - v$ space, where stress path AB follows an undrained plane.

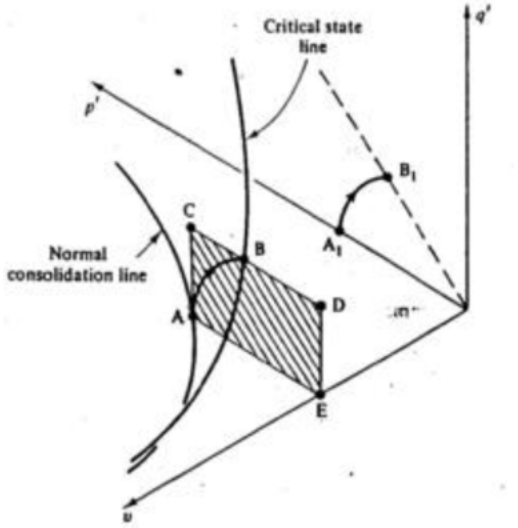

Figure 3.4 - Stress path of an undrained test in a q - p' - v space (Atkinson & Bransby, 1978)

3.3.3 Typical undrained stress paths of overconsolidated materials

Overconsolidated materials are samples that have undergone isotropic consolidation, reaching some mean effective stress p'_{max}, and then subjected to unloading/swelling isotropically to some lower mean normal stress p'_0. The overconsolidation ratio is equal to p'_{max} / p'_0, thus normally consolidated specimens have an OCR value of 1, while overconsolidated samples have an OCR greater than 1 (Atkinson & Bransby, 1978).

$$\mathrm{OCR} = \frac{p'_{max}}{p'_0} \qquad \text{(Eq. 3.5)}$$

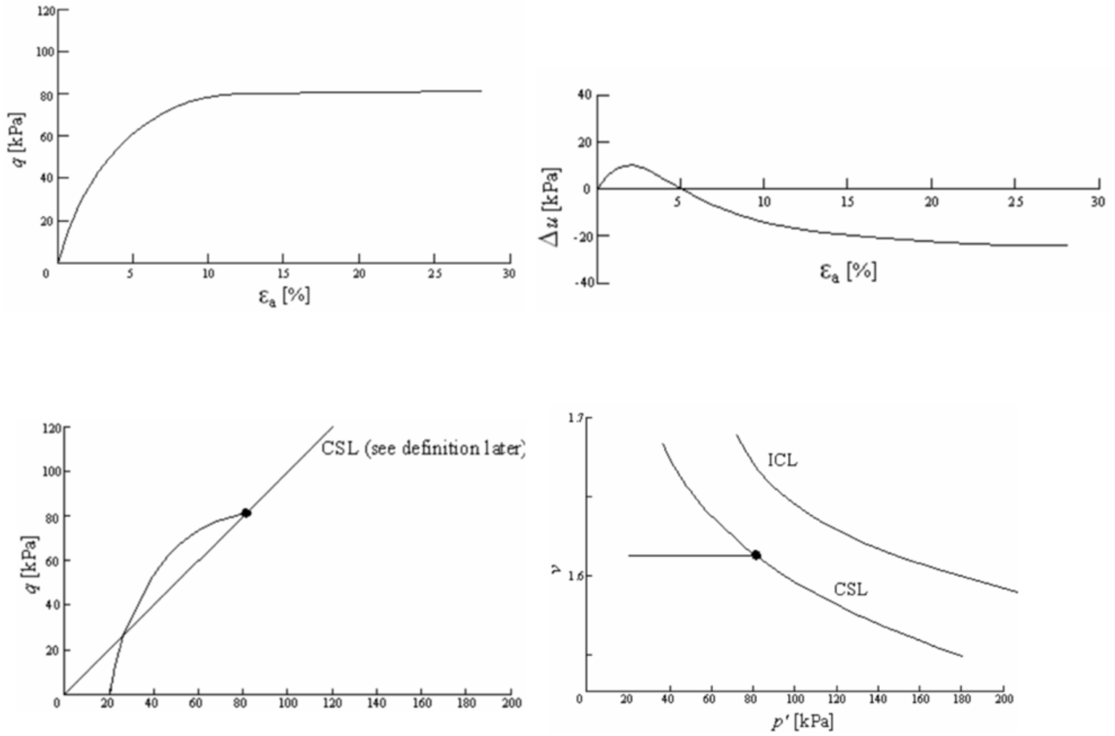

Figure 3.5 - Overconsolidated undrained stress paths in q – ε_a space (top left), Δu – ε_a space (top right), q – p' space (bottom left) and v – p' space (bottom right) (Viladesau Franquesa, 2004)

Figure 3.5 illustrate the theoretical stress paths of q – ε_a and u – ε_a of overconsolidated samples. A notable difference from normally consolidated samples is that the pore pressure is positive in the initial stage of the undrained test, however, over time, it becomes negative and eventually reaches a steady value, indicating the completion of the test. The deviator stress q increase and eventually reach a steady value as well. In the $q - p'$ plot, the stress path rises nearly upright and then smoothly turns to the right until a steady value is reached, indicating that the pore water pressure has stabilized. Similarly, the $v - p'$ space can be plotted as shown below (Atkinson & Bransby, 1978).

The stress paths depicted are theoretical representations based on the Critical State Framework. However, actual stress paths often display brittle behaviour due to strain localization. This phenomenon is not accurately predicted by the framework, leading to discrepancies between theoretical predictions and real-world observations (Atkinson & Bransby, 1978).

3.3.4 The Critical State Line

It is noticeable, that in both the normally consolidated and heavily overconsolidated samples under undrained conditions, all failure points align approximately along the same straight line. This line of failure is also evident in the $v - p'$ plot, resembling the intrinsic compression line. Termed the Critical State Line, its significance lies in the fact that failure of samples which are initially isotropically compressed occurs once their stress states reach this line, regardless of the path taken during testing. The failure will manifest as a state in which extensive shear deformation occur without any alteration in stress or void ratio. Moreover, at critical state, samples experience zero change in volumetric strain and thus shear at constant volume (Atkinson & Bransby, 1978).

The critical state line in a $q - p'$ space, is described as (Atkinson & Bransby, 1978).

$$q = Mp' \tag{Eq. 3.6}$$

While the critical state line in a $v - p'$ space is curved, the critical state plotted in a $v - \log p'$ is straight, which is parallel to the intrinsic compression line, described as (Atkinson & Bransby, 1978).

$$v = \Gamma - \lambda \, logp' \tag{Eq. 3.7}$$

Both the above equations combined defines the curve in a $q - p' - v$ space.

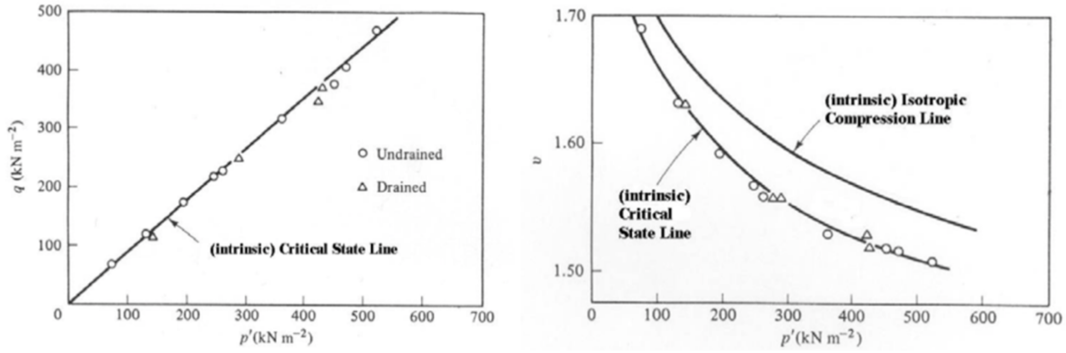

Figure 3.6 – Critical State Line in a q – p' space (left) and in a v – p' space (right) (Atkinson & Bransby, 1978)

Figure 3.7 shows the q, p' and v functions of a soil in a 3D space. Points ABC on the critical line project curves to the $q - p'$ space and intersects on points $A_1B_1C_1$, and also project curves to the $v - p'$ space and intersects as $A_2B_2C_2$. Thus, it is useful to conceptualize the critical state line within a three-dimensional $v - p' - q$ space.

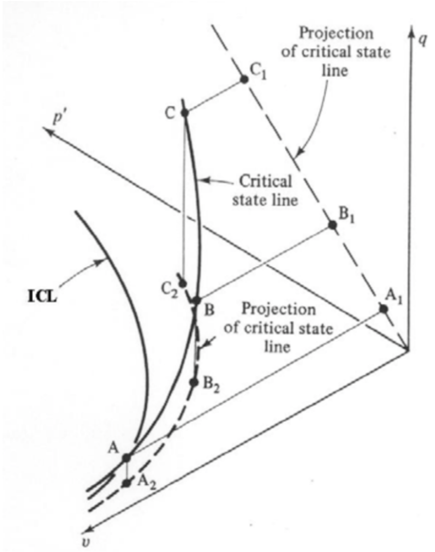

Figure 3.7 - The Critical State Framework in a 3-dimensional space (Atkinson & Bransby, 1978)

3.3.5 The Roscoe-Rendulic Surface (behaviour of normally consolidated samples)

In a $q - p' - v$ space, stress paths obtained from a triaxial test can be illustrated. A typical specimen undergoes isotropic consolidation followed by triaxial compression until it reaches the CSL, where failure occurs. Figure 3.8 illustrates different undrained planes for varying values of p'_0. Each value of p'_0 represents the stress path on a distinct undrained plane. However, all values of p'_0 collectively define a 3D surface that connects the consolidation compression line to the CSL.

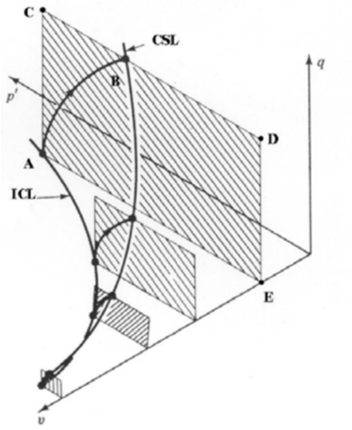

Figure 3.8 - Stress paths moving on an undrained plane (Atkinson & Bransby, 1978)

Hence, it is concluded that all stress paths end up on a distinct 3D surface. This is because each stress path starts from a compression line and ends at a point on the same CSL. Drained tests also conclude at the same CSL but follow a different curve. This surface is termed the Roscoe-Rendulic Surface (Atkinson & Bransby, 1978).

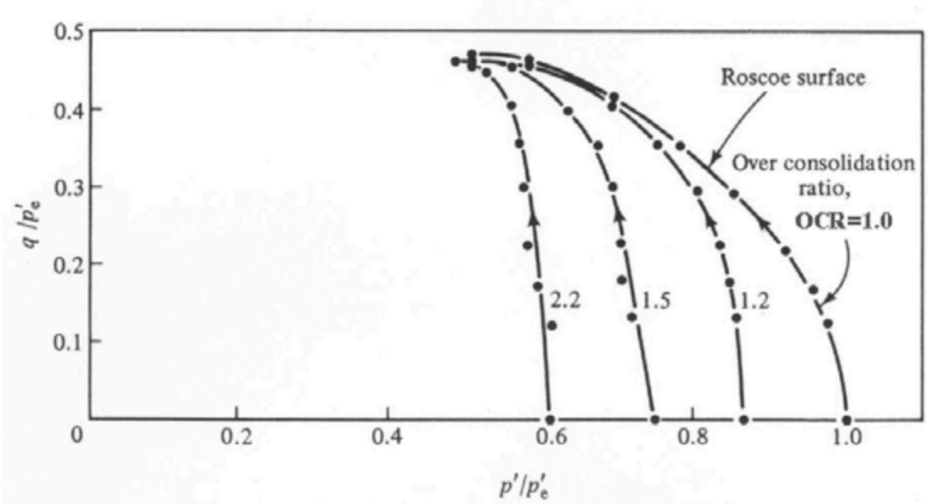

Figure 3.9 - Undrained stress path of normally & lightly consolidated samples of Kaolin clay (Atkinson & Bransby, 1978)

It is noticed that samples that follow a Roscoe-Rendulic surface are normally consolidated and lightly overconsolidated samples. From Figure 3.9, it can be noticed that both samples fail on the same CSL.

The Roscoe-Rendulic surface forms a boundary surface that stress paths cannot surpass.

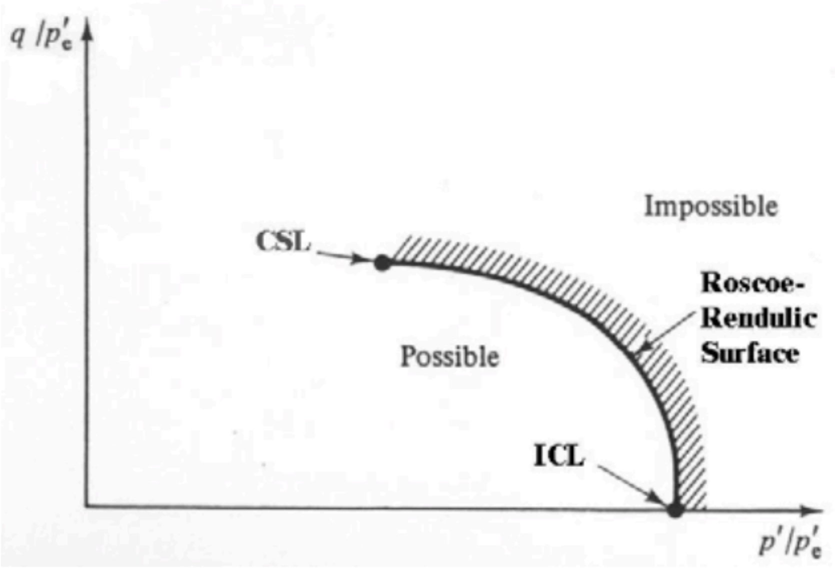

Figure 3.10 - Roscoe-Rendulic surface parting possible from impossible states (Atkinson & Bransby, 1978)

3.3.6 The Hvorslev Surface (behaviour of overconsolidated samples)

The stress paths considered here are exclusively for heavily overconsolidated samples. The failure states of samples subjected to triaxial compression testing and then normalized, are illustrated in Figure 3.11. Both the stress paths of drained and undrained overconsolidated samples align on a single curve in the q/p'_e vs p'/p'_e space, representing a single plane (Atkinson & Bransby, 1978).

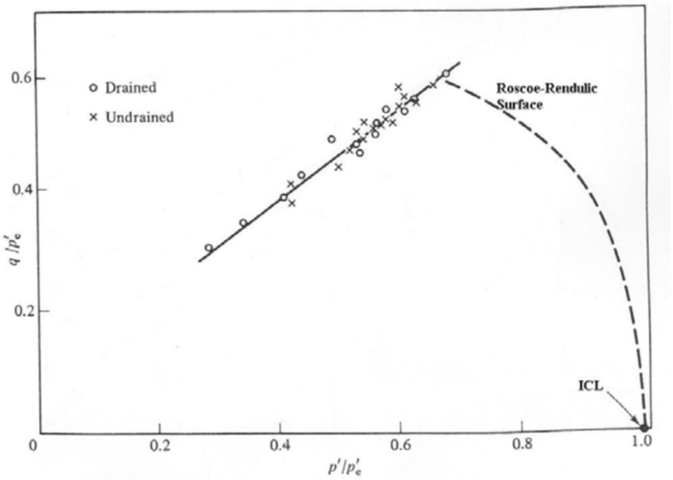

Figure 3.11 - Failure envelope of both drained and undrained overconsolidated samples of Weald Clay (Atkinson & Bransby, 1978)

In Figure 3.12, the idealized failure points are represented by line CB. This line is bounded on the left by line OC, which has a gradient of 1:3, indicating tensile failure. Furthermore, it is bounded by the CSL (point B), and the Roscoe-Rendulic surface illustrated as curve AB. The set of failure points along line CB is known as the Hvorslev surface (Atkinson & Bransby, 1978).

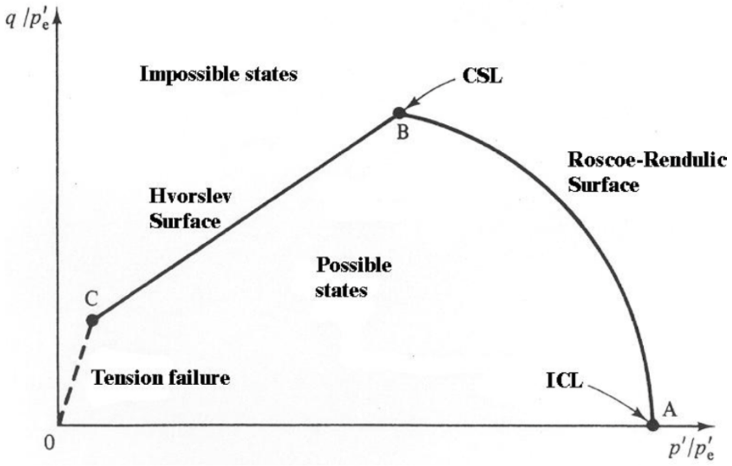

Figure 3.12 – A normalised complete State Boundary Surface (Atkinson & Bransby, 1978)

The deviator stress at failure of an overconsolidated sample is composed of two components. The initial parameter is proportional to mean normal effective stress, and it is most probably due to the generated frictional behaviour by nature. The second component is the current specific volume, and thus this concludes that strength of the soil is enhanced by a decrease in void ratio (Atkinson & Bransby, 1978).

It is anticipated that specimens at failure move outward as much as possible in a $q - p' - v$ space. Therefore, it is inferred that stress paths of overconsolidated samples adhere to the Hvorslev surface as their state boundary surface, analogous to how stress paths of normally and lightly consolidated samples conform to a Roscoe-Rendulic surface as their state boundary surface. Consequently, both boundary surfaces meet at a unique line, which is the CSL (Atkinson & Bransby, 1978).

3.3.7 The complete State Boundary Surface

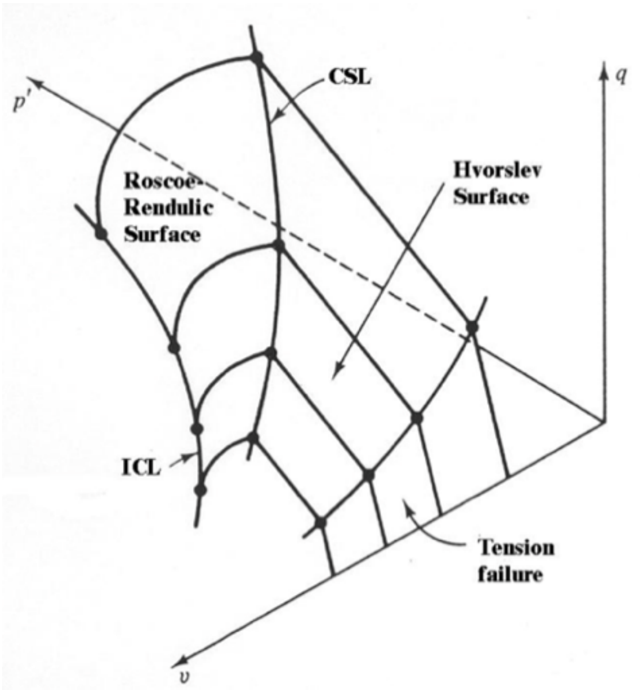

Figure 3.13 - The complete State Boundary Surface in a q - p' - v space (Atkinson & Bransby, 1978)

Figure 3.13 illustrates the complete State Boundary Surface in a $q - p' - v$ space. This surface comprises a tension cut-off limit, the Hvorslev surface, the CSL, and the Roscoe-Rendulic surface. All stress paths originate from either an intrinsic compression line or a swelling line. It is evident that the CSL forms a ridge that separates the Hvorslev surface from the Roscoe-Rendulic surface. Additionally, the height and gradient of this ridge increase with an increase in the mean normal effective stress (Atkinson & Bransby, 1978).

3.3.8 Pore Water Pressure changes for different overconsolidation ratios

Triaxial tests can be carried out either under drained or undrained conditions. In drained tests, the drainage valve remains open, allowing the soil specimen to change volume during the shearing stage. This volume change can involve contraction, where the specimen expels pore fluid, or expansion (dilation), where it absorbs water. Conversely, in undrained tests, the drainage valve is closed, preventing any water drainage and thus maintaining a constant volume. Such behaviour is reflected by observed changes in pore pressure during shearing stage. In undrained tests, a positive pore pressure indicates that the material is attempting to expand (dilate), while a negative pore pressure signifies that the specimen is trying to contract (Lade, 2016).

Atkinson & Bransby (1978) provide test paths for a normally consolidated and an overconsolidated specimen, as depicted in Figure 3.14. It is evident that the normally consolidated specimen, A, fails with a significantly high positive pore water pressure, while the overconsolidated specimen, B, fails with a negative pore water pressure. This observation highlights that the pore water pressure at the point of failure is substantially influenced by the initial overconsolidation ratios of the specimens.

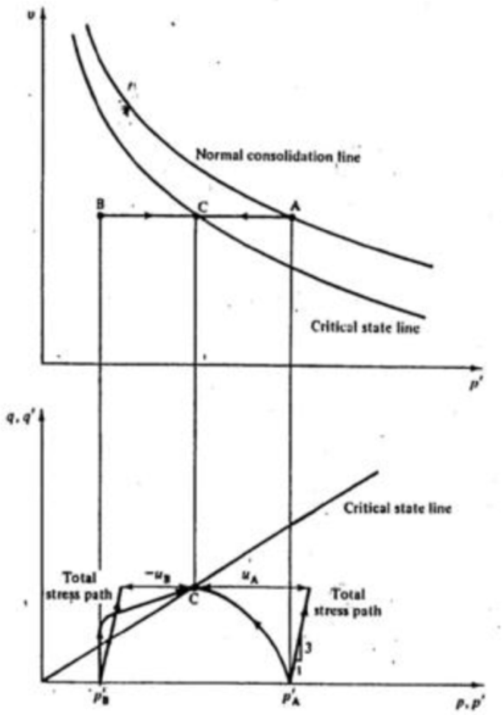

Figure 3.14 – Undrained stress paths on normally and overconsolidated samples of clay (Atkinson & Bransby, 1978)

3.3.9 Mohr-Coulomb failure criterion and the critical state line

Failure in Mohr's Coulomb criterion happens when the outer Mohr Circle, meets the failure line. The Mohr-Coulomb failure concept represents the stress threshold that a soil can endure before potential rupture planes might emerge within it. The Mohr-Coulomb failure criterion is established as the juncture where a soil body experiences failure as the shear stress τ on any plane within that soil unit reaches a certain critical value (Wood, 1990). It can be expressed as:

$$\tau_f = c' + \sigma'_p \tan\emptyset \qquad \text{(Eq. 3.8)}$$

This equation consists of a pair of straight lines (failure envelopes) in a $\tau - \sigma'$ plane. Sliding on any plane on the soil mass will occur when the frictional resistance $\sigma'_p\tan\emptyset$ is smaller than the shear stress τ_f. Sliding is influenced by the effective normal stress σ', the friction angle $\emptyset$ and cohesion c' of the soil mass. Thus, when the Mohr's circle of effective stress reaches the failure envelope, failure will occur (Wood, 1990).

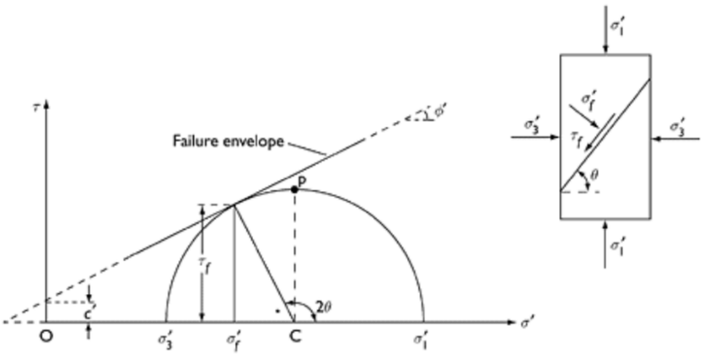

Figure 3.15 - The Mohr-Coulomb failure criterion (Craig, 2004)

Wood (1990) expresses the Mohr-Coulomb failure in terms of $q - p'$ space. Since 'M' is the gradient of the critical state line, the critical state angle of shearing resistance can be obtained from (Eq. 3.9).

$$M = \frac{6 \sin \emptyset'_{cs}}{3 - sin\emptyset'_{cs}} \qquad \text{(Eq. 3.9)}$$

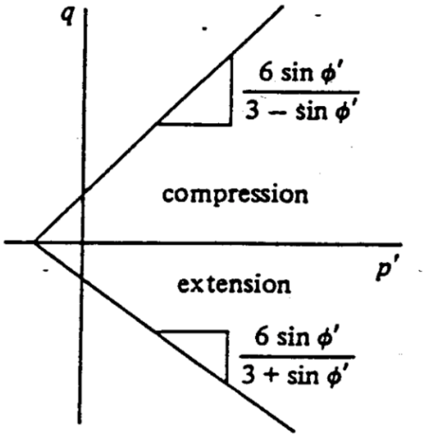

Figure 3.16 - Mohr-Coulomb failure criterion (Wood, 1990)

The failure of soil arises from the interaction between shear stress and effective normal stress at any particular point. The ability to withstand shear is a result of the interparticle forces present within the soil. Consequently, shearing resistance will be negligible when the effective normal stress is equal to zero, unless particles are held together by cementation (Craig & Knappett, 2012).

3.3.10 Mechanical behaviour and critical states for clays

Data from four conventional triaxial compression tests on reconstituted Weald clay samples, sourced from Bishop and Henkel (1957), were analysed.

In undrained tests, pore pressures arise because the soil seeks to change volume during shear, but this is prevented by the test conditions. In normally consolidated samples, as the soil is sheared, it tends to collapse, leading to the generation of positive pore pressures. These pressures serve to reduce the mean effective stress carried by the soil particles, with the expansion offsetting the collapse that cannot occur. Conversely, in overconsolidated samples, negative pore pressures are observed. In this case, the soil skeleton is restrained by the pore pressure to prevent the sample from expanding (Wood, 1990).

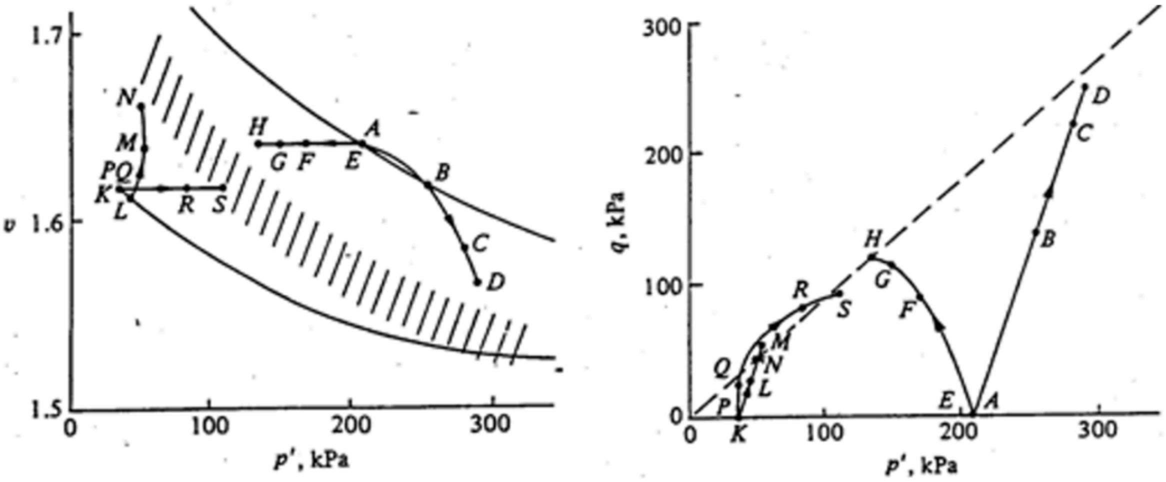

Figure 3.17 – Drained and Undrained stress paths on Weald Clay of $v - p'$ space (left) and $q - p'$ space (right) (Bishop & Henkel, 1957)

In Figure 3.18, the endpoints of multiple tests conducted on Weald clay are plotted, revealing a straight line in the $q - p'$ space and a curved line in the $v - p'$ space. These lines can be drawn from the origin through these points. Thus, all undrained tests appear to converge toward this same line.

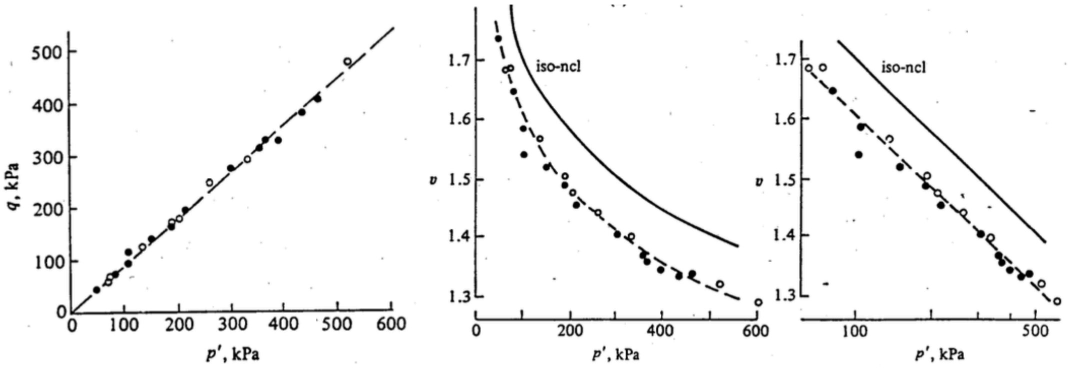

Figure 3.18 – Undrained triaxial compression end points of Weald Clay of $q - p'$ space (left), $v - p'$ space (middle) and $v - logp'$ (right) (Roscoe, Schofield & Wroth, 1958)

This dataset offers evidence of an existing line in the $v - q - p'$ space, regardless of the consolidation history of the samples. The shape of this line resembles that of the critical state line, indicating that Weald clay exhibits typical engineering characteristics of soil response.

3.3.11 Mechanical behaviour and critical state for sands and granular material

In experimental observations, it has been noted that normally consolidated clay contracts, whereas overconsolidated clays expand when sheared under drained conditions. Additionally, it is widely recognized that dense sand expands, while loose sand contracts when sheared (Wood, 1990). This observation suggests the presence of critical states in sands, which may represent a fundamental aspect of the mechanical behaviour of soils.

Loose particles tend to be unstable and collapse under shear, whereas dense particles have the ability to deform as particles stack atop each other. Although particles in practice are often more irregular, this theory can still be applied (Wood, 1990).

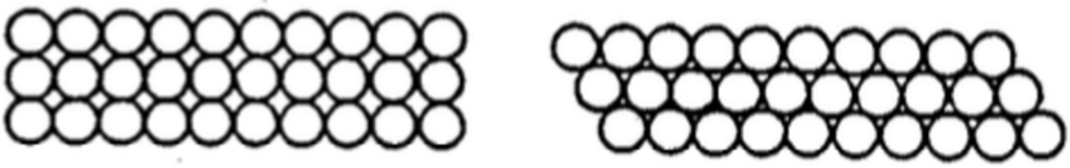

Figure 3.19 - Spherical particles loosely packed (left) and densely packed (right) (Wood, 1990)

Typical triaxial test data on loose and dense Brasted sand, are presented below.

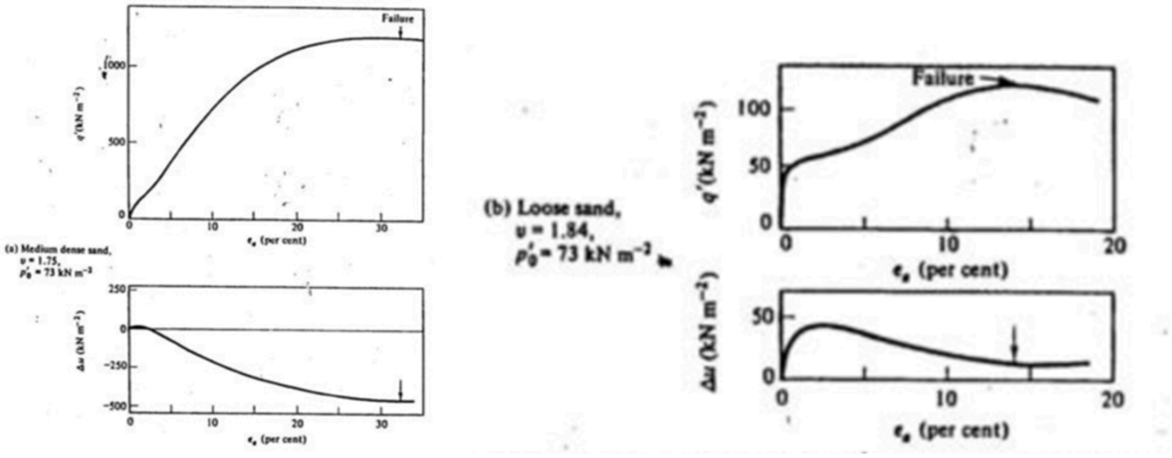

Figure 3.20 – Undrained triaxial tests on medium dense (left) and loose Brasted sand (Bishop and Henkel, 1962)

Both medium and dense samples, which are consolidated to an equivalent value, exhibit similar shapes. However, the q value is noticeably higher for the more densely packed specimen. The most notable difference lies in the pore pressure changes at failure: the loose sand experiences a positive pore water pressure at failure, while the medium dense specimen has a substantial negative pore pressure at failure. This disparity in pore water pressures at failure is the primary reason for the substantial contrast in the observed strength of the two specimens, as the effective radial stress at failure in the dense sand is greater than that in the loose sand (Atkinson & Bransby, 1978).

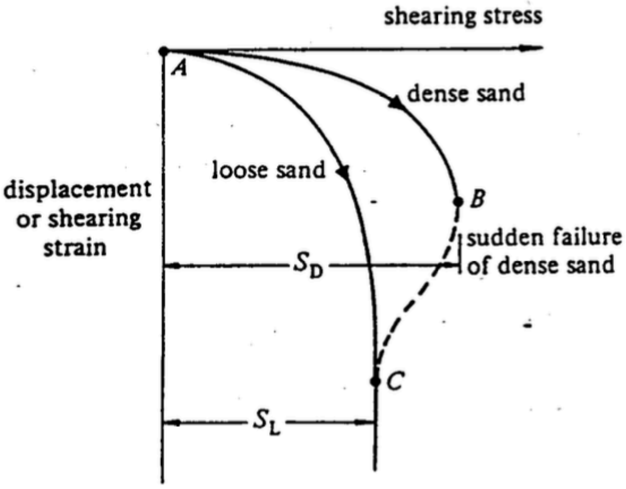

Figure 3.21 - Effect of shearing strain with shear on loose and dense sand (Casagrande, 1936)

When dense sand is subjected to shear, it reaches a peak, and as deformation continues, the shearing stress drops in value. Sand keeps expanding under shear stress until it reaches a critical state. At this point, continuous distortion can occur while maintaining a constant shearing stress. Conversely, when loose sand is subjected to shearing, shear stress increases until a certain level is attained. Beyond this point, the resistance to deformation remains constant. In this state, the sand volume must correspond to the critical state. Consequently, both loose and dense materials eventually reach the critical state. This implies that the volume curves for both loose and dense states intersect at the critical point when a stable condition is achieved. It is concluded by Casagrande that “every cohesionless soil has a certain critical state it can undergo any amount of deformation without volume change” (Casagrande, 1936).

In the drained test, loose sample contracts, whereas in the undrained test, it generates positive pore water pressures. Conversely, the denser specimen expands in the drained test and generates negative pore water pressures in the undrained test. This behaviour pattern is reminiscent of clay, where heavily overconsolidated clay specimens expand during shear and generate negative pore water pressures, while normally consolidated clay specimens’ contract during shear and generate positive pore water pressures (Atkinson & Bransby, 1978).

The critical state line, as observed in $v - ln\, p'$ space, is relatively flat. At stress levels commonly encountered in laboratory testing, samples that fall on the critical state line tend to be extremely loose. Achieving such very loose critical states for sands often requires dilation during shear. It is anticipated that the shear behaviour of sand samples, especially those that are dense, will resemble the behaviour of heavily overconsolidated clay specimens. Consequently, an undrained test on a dense sand is expected to follow the test path O'A as depicted in Figure 3.22. This test path is likely constrained by a state boundary surface similar to the Hvorslev surface, with the Roscoe surface being less relevant for heavily overconsolidated specimens. In this context, the position of the critical state line suggests the accumulation of a very large negative pore pressure (Atkinson & Bransby, 1978).

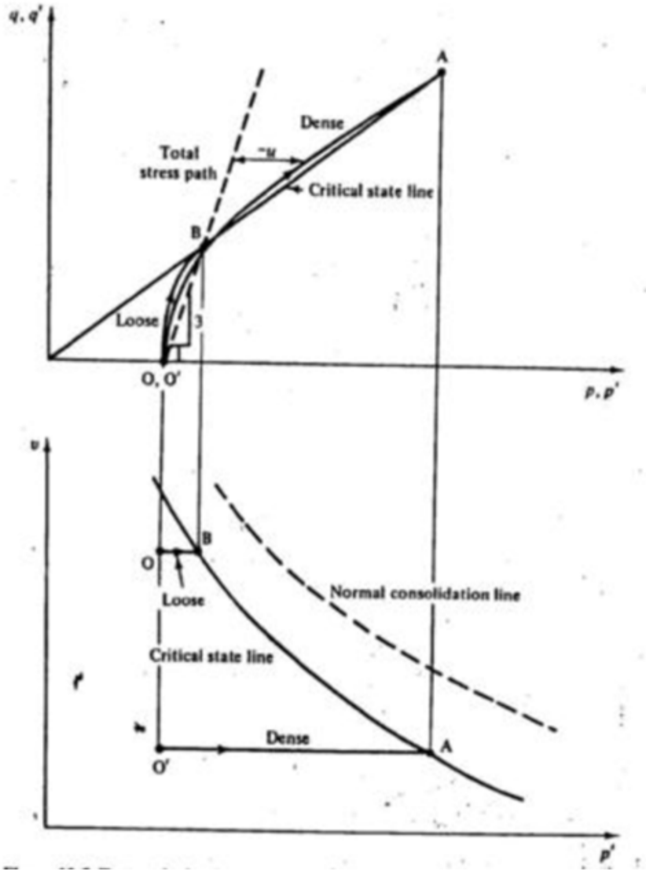

Figure 3.22 – Undrained Stress paths for dense and loose sand (Atkinson & Bransby, 1978)

The data from the two undrained tests in Figure 3.23 are not contradictory to the concepts discussed earlier, which were derived from our understanding of clay behaviour. It is important to note that the size of the constant specific volume segment of the state boundary surface is greater for the denser specimen and smaller for the looser specimen. Consequently, it is anticipated that at the ultimate points along the critical state line, q' will be greater for the dense specimen as compared to the looser specimen (Atkinson & Bransby, 1978).

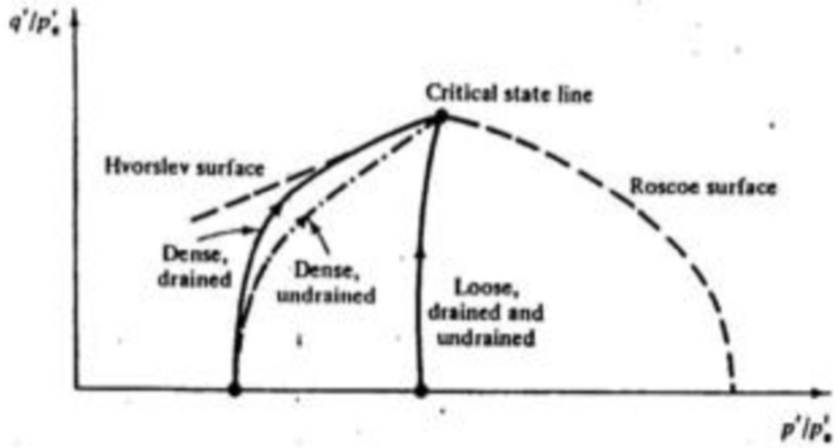

Figure 3.23 - Normalised stress paths on dense and loose samples of sand (Atkinson & Bransby, 1978)

3.3.12 Plasticity and the CSF

When stress paths reach the yield curve, they cannot extend beyond the SBS, as is typical in plasticity theory. The only option is for the stress path to revert to the elastic region and move along the yield curve, allowing samples to reach regions previously inaccessible (hardening) (Viladesau Franquesa, 2004).

In theoretical terms, undrained tests on samples are not expected to exhibit a brittle behaviour or a distinct peak. This is because specific volume is constrained from changing, preventing any shrinkage of the yield curve. However, in practical testing scenarios, undrained samples often do display a peak followed by post-rupture behaviour. This real brittle behaviour is particularly evident in overconsolidated samples when subjected to undrained shearing (Viladesau Franquesa, 2004).

The explanation for this phenomenon lies in the fact that although the sample is undrained, conditions are not uniform throughout. In reality, the shear plane that forms during testing draws water towards it. Consequently, the yield curve in the vicinity of the shear plane lowers until the specimen in that region reaches critical state. This dynamic process leads to undrained tests exhibiting a more extended "plateau" at peak strength, as water needs to be drawn towards the shear plane before going to the post-rupture state (Coop, 2004).

Figure 3.24 below depict an undrained shear test conducted on an overconsolidated sample. Unlike the theoretical expectation of reaching the critical state, these tests do not align with the predicted behaviour.

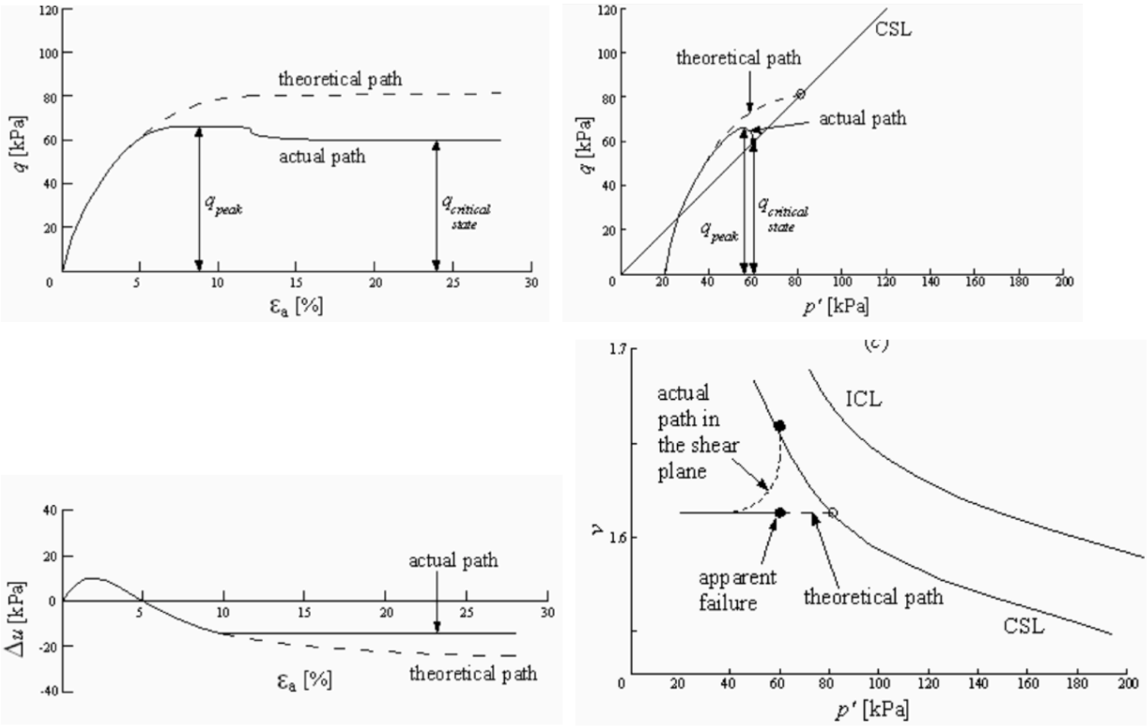

Figure 3.24 - Theoretical vs actual stress paths of $q - \varepsilon_a$ (top left), $q - p'$ (top right), $\Delta\mu - \varepsilon_a$ (bottom left) and $v - p'$ (bottom right) (Based on Coop, 2004)

The behaviour of overconsolidated samples is more complex due to their varied stress history. Geological processes and anisotropy can introduce complexities that deviate from theoretical predictions. Additionally, structural effects and heterogeneous conditions within the sample may further influence its behaviour. Therefore, while theoretical models provide valuable insights, the actual behaviour of overconsolidated samples may differ due to these factors (Viladesau Franquesa, 2004).

3.4 The influence of Structure

Burland (1990) highlights the significance of both micro and macro structural characteristics in understanding the characteristics of natural soils when comparing them to reconstituted soils. These intrinsic properties are crucial in influencing the mechanical response of soils under different stresses. Burland (1990) defines structure as "*the combination of fabric, that is, the arrangement of particles and bonding, defined as those interparticle forces which are not of a purely frictional nature*".

Both natural and reconstituted clays exhibit an anisotropic fabric that is aligned coaxially with the upright direction of sedimentation (McConnachie, 1974). In contrast, the mechanical characteristics of natural sedimentary clays differ from their reconstituted counterparts. The notable distinctions are associated with the presence of inter-particle bonds that form during the diagenesis of natural clay deposits (Burland, 1990). The presence of these bonds imparts significant strength anisotropy to natural clays, resulting in yield surfaces that extend well beyond the critical state line. The bonding in natural clays primarily influences the shape and size of the yield surface rather than elastic anisotropy.

Subsequent research has unveiled numerous potential mechanisms influencing the formation of bonded structures in these soils (Leroueil & Vaughan, 1990).

3.4.1 Effects of structure on compression behaviour

During sedimentary compaction, the overburden stress on sediments increases, causing particles to rearrange as water trapped between them is expelled. This process compacts the particles further, thereby increasing the sediment's density. Consequently, density changes with depth. Skempton (1970) plotted the void ratio against depth for various sediments, all resulting in a curve known as the sedimentation compression curve (SCC) as seen in Figure 3.25. Clays with different mineral compositions (liquid limits) followed distinct sedimentation compression curves.

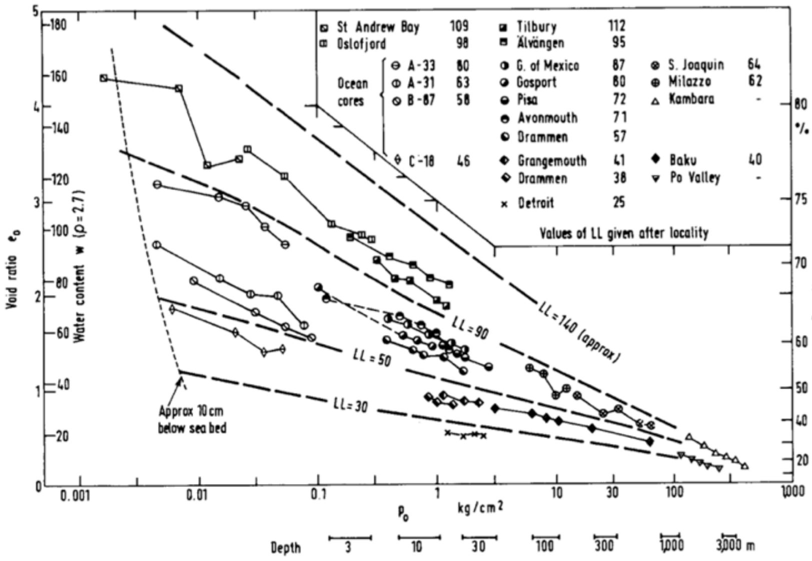

Figure 3.25 – Sedimentation compression curves for normally consolidated argillaceous sediments (Skempton, 1970)

Burland (1990) normalized the referenced data set using specific void ratios. For each type of structured clay, a corresponding reconstituted sample was created, and the void ratios were determined at vertical effective stresses of 100kPa and 1000kPa during one-dimensional compression. The in-situ void ratio was then normalized to a metric known as the Void Index (I_v), defined as:

$$\mathrm{I_v} = \frac{\mathrm{e} - \mathrm{e}_{100}^{*}}{\mathrm{e}_{100}^{*} - \mathrm{e}_{1000}^{*}} \qquad \text{(Eq. 3.10)}$$

Where $e_{\mathbf{100}}^{*}$ *and* $e_{\mathbf{1000}}^{*}$ represent the void ratios of the reconstituted material at 100kPa and 1000kPa, respectively, Burland used the Void Index to standardize the one-dimensional compression lines for various reconstituted soils. All test results aligned on a specific line known as the Intrinsic Compression Line (ICL).

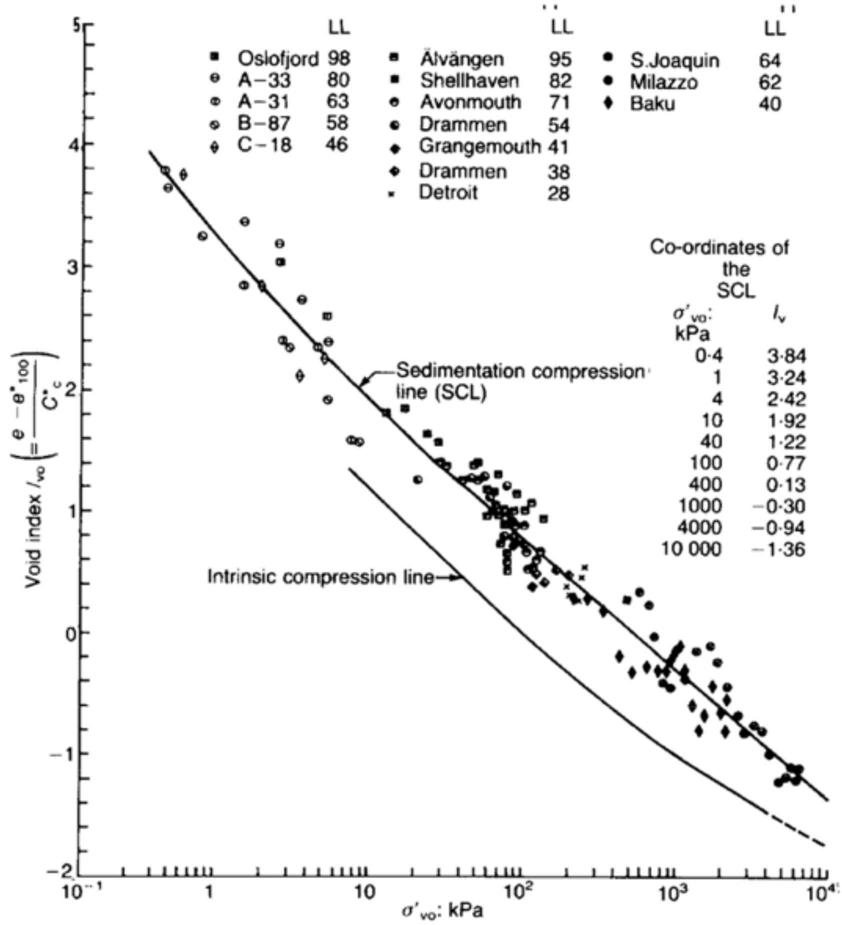

Figure 3.26 - A sedimentary fitted compression line for many normally consolidated clays (Burland 1990)

The same method was subsequently applied to intact materials, where the SCC for each sediment was normalized similarly, creating multiple lines in the void index versus log vertical effective stress space. These curves were found to fall within a very narrow range, leading Burland (1990) to average them into a particular line, termed the Sedimentation Compression Line (SCL). Both the ICL and the SCL are illustrated in Figure 3.26. The same figure illustrates that the ICL is positioned to the left of the SCL, though both lines run approximately parallel. This indicates that intact materials exhibit higher void ratios compared to reconstituted materials under an identical vertical effective stress.

Figure 3.26 suggests that the effective overburden pressure of intact specimens is greater than that of its reconstituted counterpart at certain void index ratios. Thus, this serves as evidence of the heightened strength of naturally deposited clay compared to reconstituted clay. This increase in strength is attributed to differences in the fabric and bonding (structure) of the sediment. The significance of structure was initially acknowledged by Terzaghi (1941) and later verified by Skempton (1994).

The behaviour of a destructured clay in comparison to a structured clay for a specific intact specimen can be illustrated by Figure 3.27. Large strains are highly improbable when a structured soil occupies the space allotted for its destructured nature, even as stress states extend into areas permitted by the structure. Yielding subsequently results in a significant alteration in volume and strain, greatly surpassing those under pre-yield stress. This underscores the importance of structure which is as crucial as void ratio and stress history in dictating the strength of ground materials (Leroueil & Vaughan, 1990).

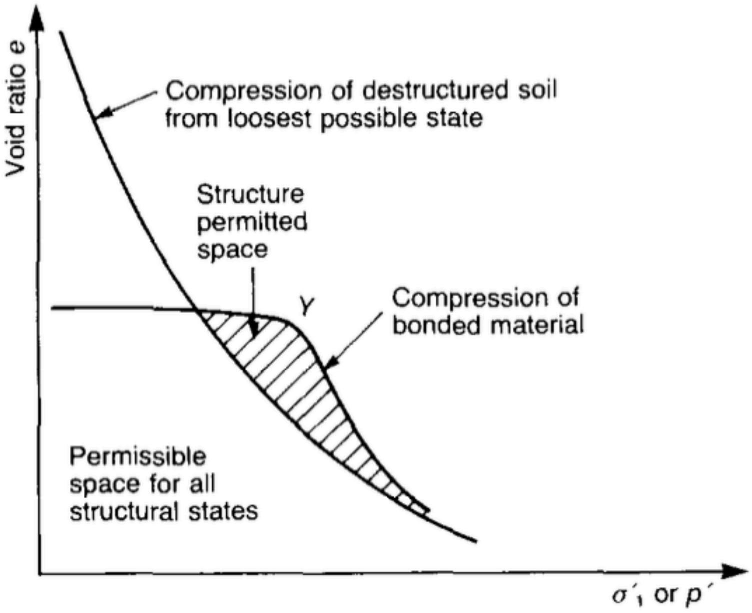

Figure 3.27 – The comparison of structured and destructured clay compressed one-dimensionally (Leroueil & Vaughan, 1990)

3.4.2 An extended state boundary state

It has been observed that soils with a structured arrangement demonstrate higher shear strength compared to unstructured soils and thus, Burland (1996), highlights that natural samples can withstand larger vertical effective stresses compared to reconstituted samples. This discrepancy is attributed to the microstructure of the samples, encompassing factors such as bonding and fabric within the specimen. Leroueil and Vaughan (1990) conducted numerous shear tests on various types of clays and found that structured soils consistently exhibited a normalized yield surpassing that of their unstructured counterparts. As depicted in Figure 3.28, the SBS of the structured material exceeded the SBS of the destructured material. Leroueil and Vaughan (1990) noted this phenomenon in soft and stiff clays, granular and residual soils, and also in weak and weathered rocks.

This indicates that the natural UGL-2 tested in this dissertation is expected to exhibit greater strength compared to the reconstituted specimens, due to the inherent structure the natural UGL-2 possesses.

This increase in resistance to one-dimensional compression, resulting from the natural microstructure, is quantified by a parameter known as the Yield Stress Ratio (YSR). This ratio is defined by (Burland, 1996):

$$YSR = \frac{\sigma'_{\mathrm{vy}}}{\sigma^{*}_{\mathrm{vy}}} \qquad \text{(Eq. 3.11)}$$

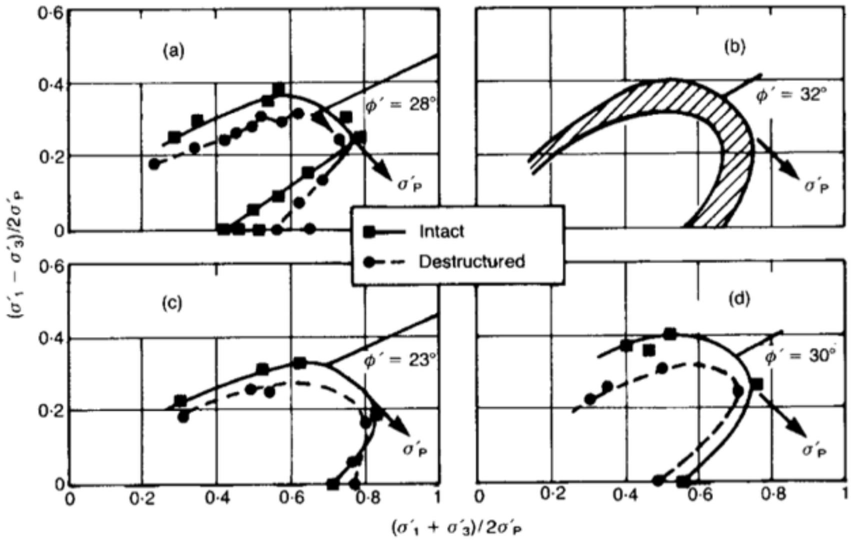

Figure 3.28 - Normalised Yield curves for intact and deconstructed different types of clays (Leroueil and Vaughan, 1990)

Burland, Rampello, Georgiannou & Calabresi (1996), also verified that natural soils containing structure experience states beyond the SBS reached by reconstituted soils. The SBS for the natural soil is similar in shape, however larger than the SBS shown by reconstituted samples. This means that structure of soil effects the scale of the SBS, however keeping the same shape. This is illustrated in Figure 3.29.

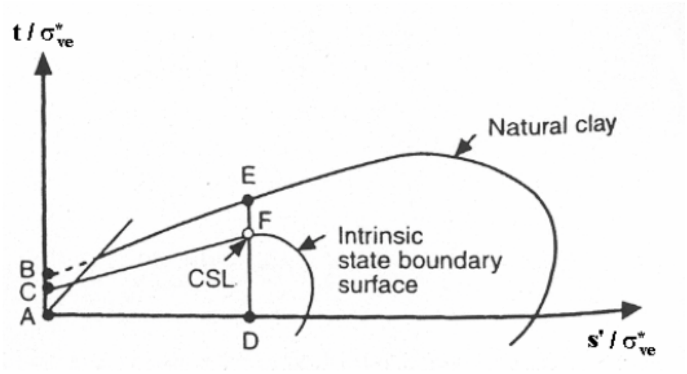

Figure 3.29 - SBS of natural specimen vs SBS of reconstituted Specimen, similar in shape but different in size Burland, (Rampello, Georgiannou & Calabresi, 1996)

3.4.3 Behaviour under load

3.4.3.1 Pre-yield behaviour in structured materials

Yield in structure as explained in previous sub-sections, is described as a significant discontinuity in stress-strain behaviour, which happens suddenly and can be easily observed (Vaughan, 1988). Prior to yield, the material is stiff, however, not necessary elastic. While there may be a zone of elastic behaviour (Elliot & Brown, 1985), some structure may be lost owing to stress changes within the primary yield curve. Vaughan (1988) suggest that an initial yield occurs at stresses less than primary yield.

3.4.3.2 Post-yield behaviour in structured materials

Substantial post-yielding is required to completely remove structure, as the process is a progressive one. Yield of structure can be more logical to make it a function of strain energy. When sufficient strain occurs, the material becomes destructured (Leroueil and Vaughan, 1990).

3.4.3.3 Stress strain response

Under consistent changes in stress levels, the occurrence of yield is marked by a distinct discontinuity in the stress-strain relationship. Yielding can be understood as a permanent alteration in both strength and rigidity beyond the point of yield. It is noted that the yield stress rises with developing strain, a phenomenon evident in materials like structured soft clay and fragile rock formations (Tavenas, Leroueil, La Rochelle & Roy, 1978)

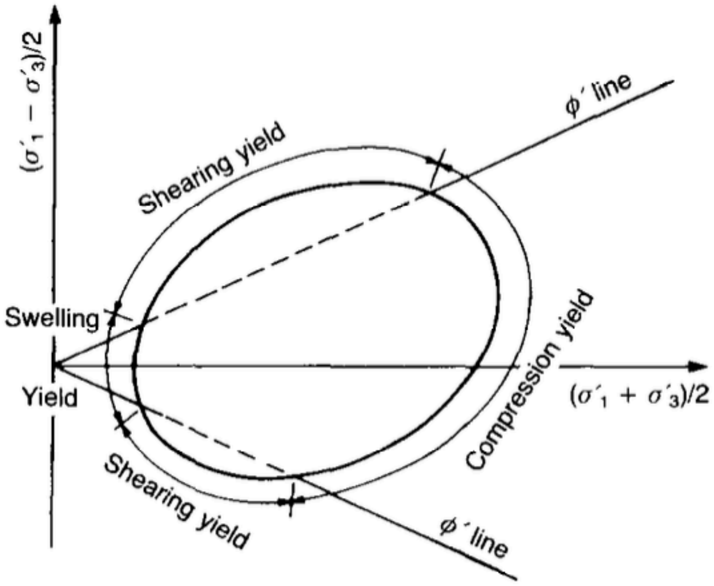

Figure 3.30 - Types of yielding (Leroueil and Vaughan, 1990)

Figure 3.30 illustrates a compression yield, characterized by yielding happening beyond the peak shear strength envelope, prompted by a rise in average and/or shear stress. Shearing yield arises when yielding happens prior to shear failure, whereas swelling yield takes place when yielding moves away from the failure envelope during swelling, a consequence of the structure's inability to preserve stored strain energy (Leroueil & Vaughan, 1990).

Compression and swelling yield involve alterations in stress levels while shearing yield leads to the formation of discontinuities as yielding initiates. This discontinuity leads to a decrease in strength, with the rest of the soil remaining unaffected by yielding (Leroueil & Vaughan, 1990).

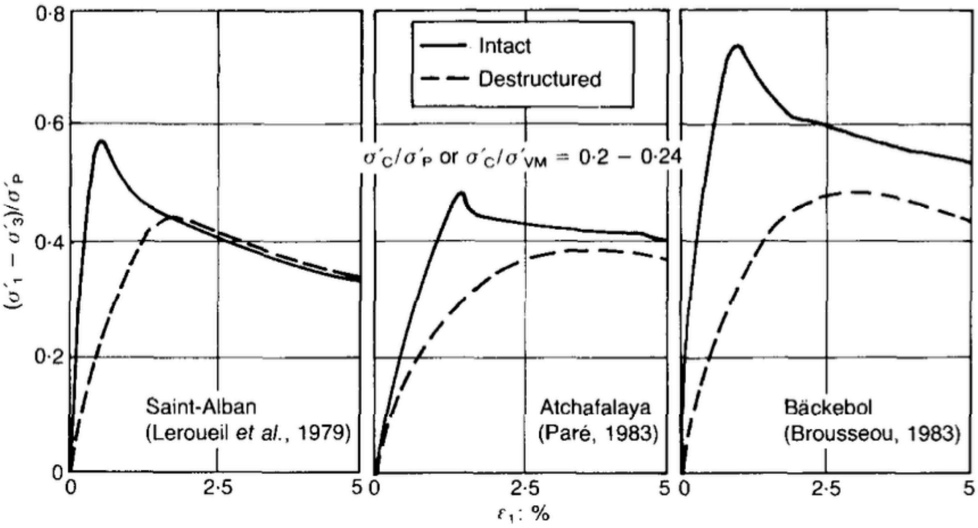

Figure 3.31 - Stress vs strain graphs for undrained triaxial tests on intact and destructured clays (Tavenas & Leroueil, 1985)

A series of soft clays had their structure removed and were subsequently tested under undrained conditions after undergoing consolidation. The results obtained were then compared to those of soft clay in their natural structured state. These results are depicted in Figure 3.31. Although all materials demonstrate similar behaviour, the destructed clays exhibit less stiffness and a lower peak strength at larger failure strains. Thus, the failure envelope for the destructured material is inferior to the intact equivalent.

Cemented sands show a particular increase in peak strength, initial stiffness and brittleness as shown in Figure 3.32, while giving some tensile strength as well as compared to the uncemented counterparts.

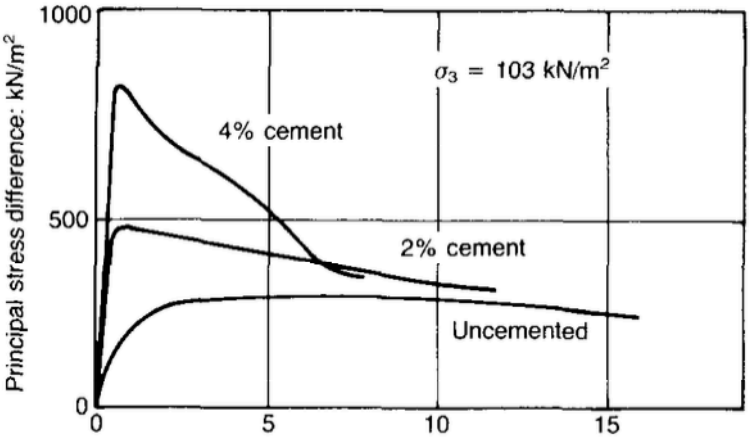

Figure 3.32 - Behaviour comparison of cemented and uncemented sands (Clough, 1981)

The stress-strain data presented in Figure 3.33 shows the behaviour of both the reconstituted and natural clayey loess specimens. A notable observation is that the undisturbed soil tested exhibit a stiffer behaviour compared to the reconstituted soil under similar stress levels. Upon reaching gross yield, the undrained intact specimen experiences rapid strain softening, a feature not observed in the reconstituted soils. This difference in behaviour could be originating due to the structural variations between the intact and reconstituted soils (Ling, 2015).

The below diagrams depict: R = Reconstituted specimen, U = Undisturbed specimen, D = Drained tests, U = Undrained Tests

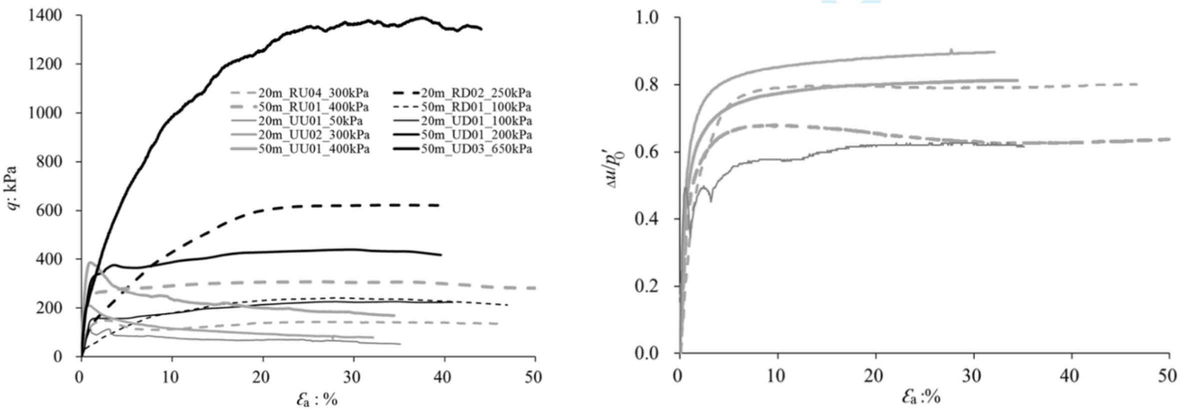

Figure 3.33 - Undrained triaxial tests $q' - \varepsilon_a$ (left) & $\Delta u - \varepsilon_a$ (right) of clayey loess specimens (Ling, 2015)

The stress paths depicted in Figure 3.34 illustrate the behaviour of both intact and reconstituted specimens in the undrained and drained state. These stress paths provide a basis for comparing the effects of structure between the undisturbed and reconstituted specimens. It is evident that the undisturbed paths exhibit a more pronounced strain-softening behaviour (Ling, 2015).

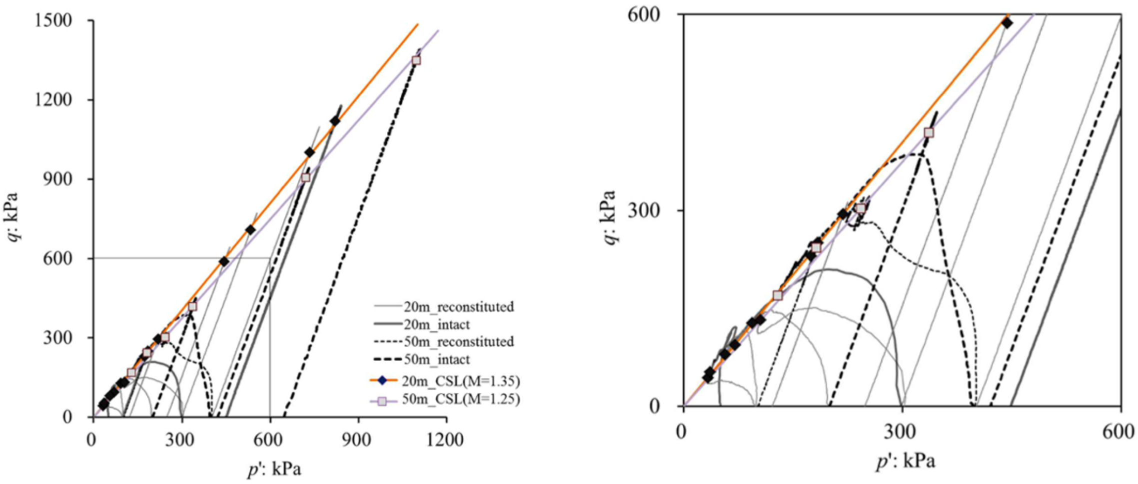

Figure 3.34 - Stress paths for intact and reconstituted specimens zoomed out (left) and zoomed in (right) (Ling, 2015)

3.4.4 Strength in soils

In geotechnical analysis, understanding the actual strength characteristics of soils is a fundamental concern. Different stress-strain curves are used to represent soils exhibiting either brittle or ductile failure behaviour. In the case of ductile rupture, the stress-strain curve typically exhibits a continuous increase in strength until failure, with no distinct peak, where strength gradually increases throughout the test until reaching a unique maximum value at the end. On the other hand, brittle rupture is characterized by a distinct peak in the stress-strain curve, indicating a sudden decrease in strength. Following the peak, there may be a stabilization of strength at minor deformations, followed by a continuing decrease to a stable strength level at a large deformation.

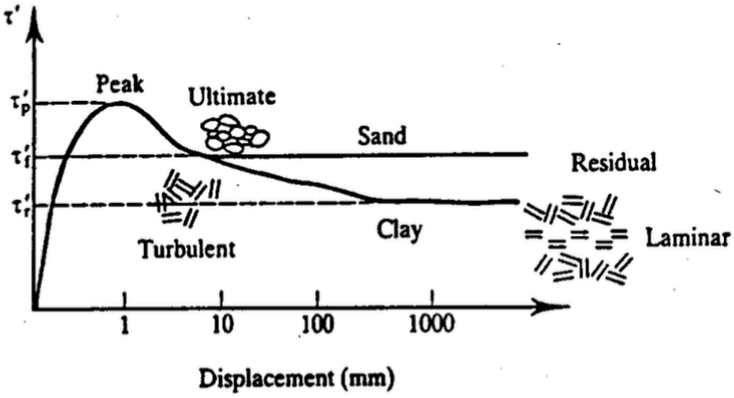

Figure 3.35 – Range of Strength Types (Atkinson, 1993)

3.4.4.1 Intrinsic Strength

The phrase "intrinsic strength" is employed by Burland (1990) to describe the distinct Critical State strength demonstrated by reconstituted samples, as opposed to the peak strength observed in their undisturbed equivalents. Reconstituted samples, lacking inherent structure, typically display ductile failure behaviour when normally consolidated. This absence of a distinct peak in their stress-strain curve results in a single strength parameter for such samples.

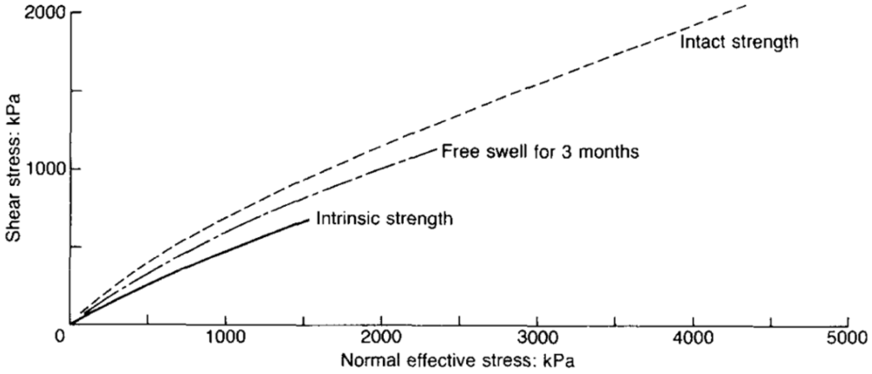

Figure 3.36 - Mohr-Coulomb failure envelopes for Todi Clay (Burland, 1990)

Figure 3.36 illustrates some Mohr-Coulomb failure envelopes for a particular clay. The intact envelope represents samples that were consolidated and then swelled, while the intrinsic envelope pertains to normally consolidated reconstituted samples. The variation in strength displayed can be attributed to two primary parameters: the void ratio at failure and the soil structure (Burland, 1990).

3.4.4.2 Peak Strength

Soils initially situated on the dry side of the critical line attain peak shear stress states before reaching the ultimate state. The peak state is typically achieved at strains around 1%, while the ultimate state is reached after strains exceeding 10%. At the peak state, the soil experiences maximum dilation rate. In contrast, soils positioned on the wet side of critical undergo continuous compression throughout the shearing process until reaching the ultimate state, without exhibiting a distinct peak (Atkinson, 1993).

Burland (1990), emphasises that most often, the peak undrained strength is primarily influenced by the soil fabric rather than its void index or liquidity index.

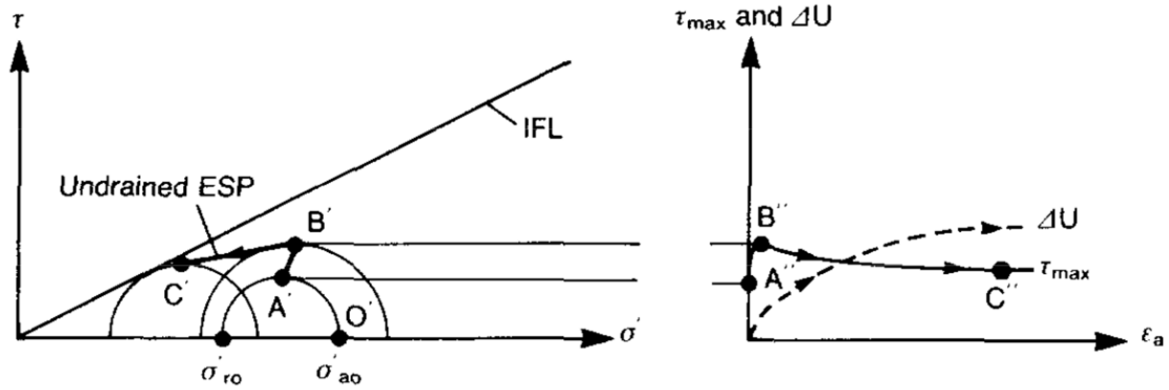

Figure 3.37 – Ideal undrained triaxial compression behaviour of reconstituted clay (Burland 1990)

Point B in Figure 3.37 shows the undrained peak compression strength, which is reached at a very small strain. Upon reaching peak, the specimen continues experiencing contract behaviour indicated by the increase in pore pressure. The critical state strength is denoted by C. Although the strength is decreasing along path BC, the stress ratio is actually increasing and thus the soil skeleton is strain hardening (Burland, 1990).

3.4.4.3 Post-rupture strength

In natural stiff clays, a brittle behaviour is often observed, featured by reaching a peak strength and then followed a stabilizing strength reaching a well-defined plateau. Burland (1990) termed this as post-rupture strength.

The post-rupture strength is attained when an intact sample fails along a singular slip surface, which develops at peak deviatoric strength. Following this peak, the graph representing deviator force against axial strain sharply declines to reach a clearly defined plateau. The fluctuations in excess pore pressure suddenly halt after peak is achieved. Subsequently, local axial strains diminish due to unloading, leading to post-rupture deformation characterized by almost rigid sliding along the failure plane. Initially, the shear stress experiences a rapid drop, but eventually stabilizes at a nearly constant level after a certain displacement. The post-rupture failure envelope is observed to be situated significantly below the intact failure line and slightly above the residual failure line (Burland, 1990).

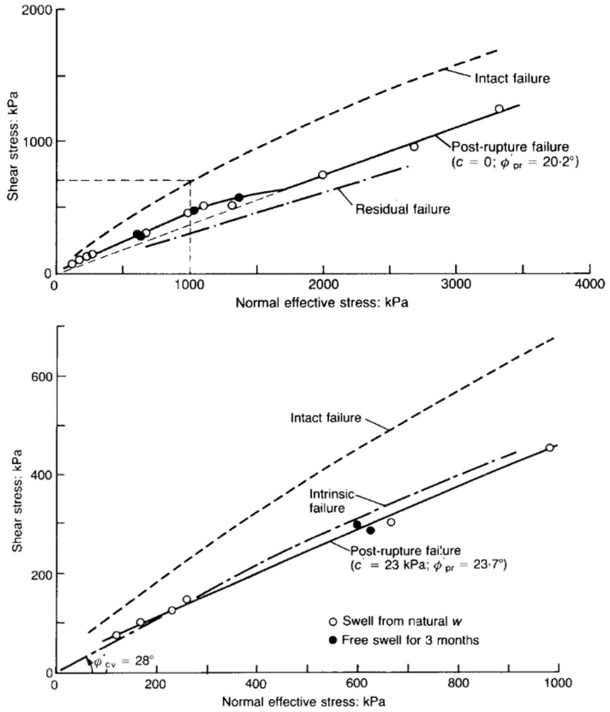

Figure 3.38 – Post-rupture failure envelope of Todi Clay for high pressures (top) & for low to medium pressures compared with intact, intrinsic and residual failure lines (Burland, 1990)

3.4.4.4 Residual strength

At major displacements, strength tends to head towards another steady but at significantly lower resistance known as the residual strength. The residual state refers to the minimum shear stress attained following significant displacements. It is identified by the laminar flow of flat clay grains oriented parallel to the rupture zone (Atkinson, 1993).

3.4.5 The Sensitivity Framework

The behavioural difference between natural and reconstituted clays has been actively researched over the last few decades (Viladesau Franquesa, 2004). Various clays in their present form can be attributed to one of the two geological processes: The "sedimentation" structure or "post-sedimentation" structure which are explained by Cotecchia & Chandler (2000). Sedimentation structure encompasses all internal structures (patterns and nature of particle arrangement) that develop during and immediately after the deposition process due to one-consolidation compression. This type of structure is exclusively found in normally consolidated clays, which may exhibit different fabrics and degrees of bonding. When the YSR equals the OCR, it suggests that the clay possesses a sedimentary structure. "Post-sedimentary" structured clay emerges when geological processes occurring after normal consolidation alter the sedimentation structure. These processes may include mechanical loading and unloading, as well as creep, thixotropy, post-deposition bonding, or more broadly, diagenesis. When the YSR exceeds the OCR, it indicates that the clay possesses a post-sedimentation structure.

The space separating the ICL and SCL was further developed by Cotecchia & Chandler (2000). They included a parameter, termed stress sensitivity which is the relative proximity of the mentioned curves. Reconstituted clays, comprise a Stress Sensitivity, St = 1. These findings contribute to the formulation of an overarching behavioural pattern, the sensitivity framework, depicted in Figure 3.40. It is evident that the SCLs are quasi-parallel, with the reconstituted curve positioned furthest left, reflecting its association with a reconstituted soil. SCLs with St values greater than 1 are situated to the right, indicating higher sensitivity (Cotecchia & Chandler, 2000).

Figure 3.39 illustrates reconstituted and natural clays, both possessing identical mineralogical compositions. However, their distinct compression line paths result from differing sedimentation structures. Distinguishing between post-sedimentation structures resulting purely from geological unloading and those involving additional geological processes can be beneficial.

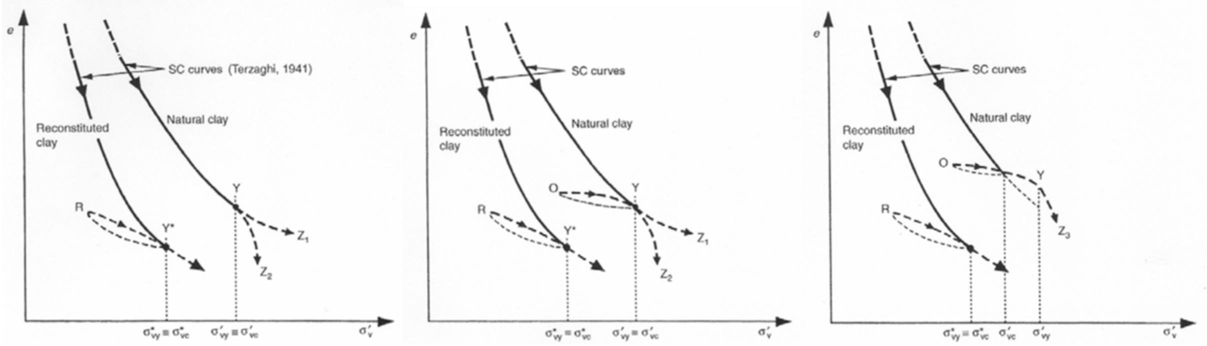

Figure 3.39 - Response of clays to one-dimensional compression. (Left) The natural clay is normally consolidated with a sedimentation structure, (middle) the natural clay is simply overconsolidated and (right) the natural clay is overconsolidated with a post-sedimentation structure at gross yield (Cotecchia & Chandler, 2000)

The term "gross yield" is a state in the effective stress area is located at the exterior of the elastic domain, where the soil stiffness undergoes a significant reduction. Beyond the gross yield point, plastic strain increments for a given applied stress increment become more pronounced due to the degradation of the soil structure. Typically, there is a notable variation in the hardening relationship at the gross yield point, which manifests as alterations in both the strength and stiffness relationships with the compression state $v - p'$ state. Therefore, soil behaviour can be categorized as either pre-gross yield or post-gross yield. The locus of the gross yield states, both in compression and shear, is considered significant in soil behaviour modelling (Cotecchia & Chandler, 2000).

When a reconstituted equivalent of clay is prepared, the impact of processes such as post-diagenetic cementation is completely eliminated. However, if the reconstituted soil is left undisturbed for an extended period, some bonding may naturally develop within the soil mass (Cotecchia & Chandler, 2000). Thus, the post-sedimentation structure observed in reconstituted clays often arises from factors such as particle interlock or creep (Mifsud et al 2019). Conversely, many natural clays may exhibit a post-sedimentation structure influenced by varying degrees of diagenesis. Consequently, during reloading in oedometer tests, these clays retain elements of the post-sedimentation structure, crossing the SCL and shifting rightward before reaching gross yield, as depicted by the O-Y path in Figure 3.39. In such scenarios, the post-sedimentation structure continues to impact the clay's behaviour at stress levels exceeding those of prior geological loading. Following gross yield (path Y-Z3), the sample adopts a trajectory steeper than the SCL, its slope contingent upon progressive structural alterations (Cotecchia & Chandler, 2000).

Therefore, the behaviour of clay at gross yield hinges on whether it solely possesses a sedimentation structure or retains elements of a post-sedimentation structure at that juncture. Clays exhibiting a sedimentation structure at gross yield will exhibit a YSR, equivalent to the OCR. Conversely, clays retaining a post-sedimentation structure at gross yield will display a YSR exceeding the OCR. Hence, the compression and strength behaviour of clay is primarily dictated by the YSR rather than the geological OCR (Cotecchia & Chandler, 2000).

The SCL for reconstituted clays is nearly coincident, indicating that they exhibit similar structural behaviour with one-dimensional response. In contrast, the SCL for natural clays varies, reflecting differences in behaviour attributable to their sedimentation structure. Each natural clay is situated on an SCL approximately corresponding to the clay's sensitivity. These curves run parallel to the distinct SCL resulting from reconstituted specimens (Cotecchia & Chandler, 2000).

The strength sensitivity of clays, whether they possess a sedimentation or post-sedimentation structure, is assessed by comparing the ratio of undrained strength after consolidation to gross yield strength of each specimen with the strength of a reconstituted clay normally consolidated to the same water content as the natural clay at gross yield. Consequently, for reconstituted clays, St = 1. These findings contribute to the formulation of an overarching behavioural pattern, the sensitivity framework, depicted in Figure 3.40. It is evident that the SCLs are quasi-parallel, with the reconstituted curve positioned furthest left, reflecting its association with a reconstituted soil. SCLs with St values greater than 1 are situated to the right, indicating higher sensitivity (Cotecchia & Chandler, 2000).

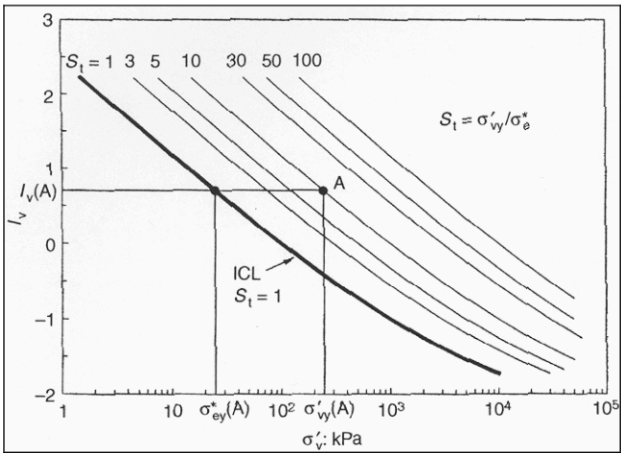

Figure 3.40 - Sedimentation compression curves in the idealized sensitivity framework (Cotecchia & Chandler, 2000)

The implications of this are as follows: natural clays, consolidated to gross yield prior to shearing and thus sheared from a YSR of 1, typically demonstrate their peak undrained strength at the apex of the SBS, with a strength represented by q_{peak}, as illustrated in Figure 3.41. Consequently, sensitivity can be redefined as the ratio of the vertical extent of the SBS of the natural clay to that of the reconstituted clay (at the same specific volume) (Cotecchia & Chandler, 2000).

There exists a geometric resemblance between the natural State Boundary Surface and the corresponding intrinsic SBS, as suggested by (Burland 1996), and the ratio between the sizes of the boundary surfaces remains consistent for clays with equal strength sensitivity St (Cotecchia & Chandler, 2000).

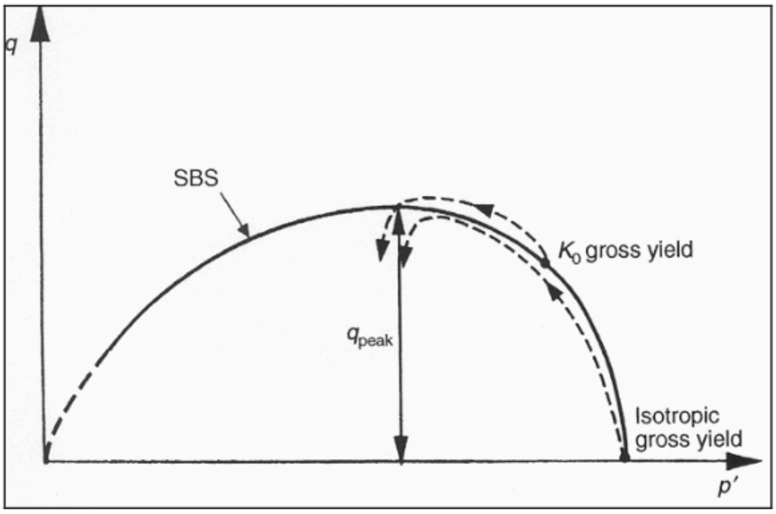

Figure 3.41 - Undrained stress paths for clay samples consolidated to gross yield (Cotecchia & Chandler, 2000)

3.4.6 Additional causes to loss of structure

Leroueil and Vaughan (1990) reported that the loss of structure in soil can occur due to external factors such as geological processes. Such processes result in induced yield or the removal of bonding agents. Soils and weak rocks undergo a loss of structure through mechanical and chemical weathering processes. Chemical reactions may lead to the elimination of structure through the leaching of bonding agents. Chandler and Apted (1988) documented a reduction in the strength of an intact London clay sample due to weathering. Weathering induces destructuring, resulting in a decrease in the material's stiffness. Additionally, structured soils, susceptible to expansion and contraction, may experience yielding and destructuring, a phenomenon observed in materials prone to seasonal changes in water content.

3.5 Drained Tests on UGL-2 (Solidbase, 2023)

Several tests were carried out which is too extensive to summarise, however, in summary, the UGL-2 tested by Soildbase (2023) is classified as high plasticity clay of normal activity and variable clay sized content. Void ratio varies between 1.0 and 0.5 (blue clay is around 1, for comparison, and most local rocks (the harder ones) are around 0.3-0.5). It was generally too weak for specimen preparation to conduct UCS testing in normal manner. Triaxial tests and oedometer tests carried out are typically overconsolidated soil, with bonding (structure). Stress-strain curves invariably show peaks and oedometer loading stages close to yield exhibit a lot of creep or secondary compressions.

4. Methodology

The main objective of this dissertation is to examine the mechanical properties and primarily determine the shear strength characteristics of the Upper Globigerina Limestone in both its natural (structured) and reconstituted (destructured) forms. The hypothesis is that there will be a significant difference in the mechanical behaviour and shear strength between the two forms, with the structured UGL-2 expected to show much higher shear strength than the destructured UGL-2.

To test this hypothesis, tests were conducted on both the natural and reconstituted forms of UGL-2. The natural form represents the structured UGL-2, while the reconstituted form, representing the destructured UGL-2, was prepared by another student (Grima, 2024) as part of his dissertation.

To examine the mechanical properties of both forms of UGL-2, isotropic triaxial tests were performed. This apparatus was selected because it can replicate in-situ conditions to a certain extent and enables a detailed analysis of shear strength characteristics.

4.1 The Triaxial Test

The triaxial apparatus was employed to examine the mechanical behaviour of both the natural and reconstituted forms of UGL-2. This test is highly versatile and frequently utilized in geotechnical laboratories. It involves three main procedures: saturation, consolidation, and shear. Triaxial tests can be performed in various ways, including unconsolidated and consolidated forms, which can be further classified as either isotropic or anisotropic, and conducted under drained or undrained conditions (Lade 2016). The triaxial apparatus used is shown in Figure 4.1.

Figure 4.1 - The Triaxial Apparatus at UoM

Lade (2016) states that triaxial testing is used to evaluate multiple mechanical properties, including stress-strain relationships, volume changes, pore pressure behaviour, and shear strength. Additionally, triaxial tests can measure various geotechnical parameters such as shear strength (c_u), shear stiffness (G), angle of shearing resistance (φ), cohesion (c), and permeability (k).

Triaxial tests can mimic in-situ conditions to a certain degree, which is why various types of these tests are available for different situations. Despite this versatility, there are some limitations. Isotropic consolidation is commonly used and generally sufficient, but it doesn't perfectly replicate real ground conditions, where vertical stresses from overlying sedimentary layers are significantly higher than horizontal stresses. Anisotropic tests provide more precise in-situ data, yet they are more costly and challenging to perform.

Consolidated undrained testing will be applied in this dissertation, as drained tests on UGL-2 have already been conducted previously by Solidbase (2023). Lade (2016) explains that undrained tests simulate the short-term strength of the material in situ. This represents the strength of relatively impermeable soils that are loaded for a certain period of time after undergoing initial consolidation under existing pressures before loading.

The main components of the triaxial apparatus include the triaxial cell, base pedestal, cell top and the piston which are illustrated in Figure 4.2.

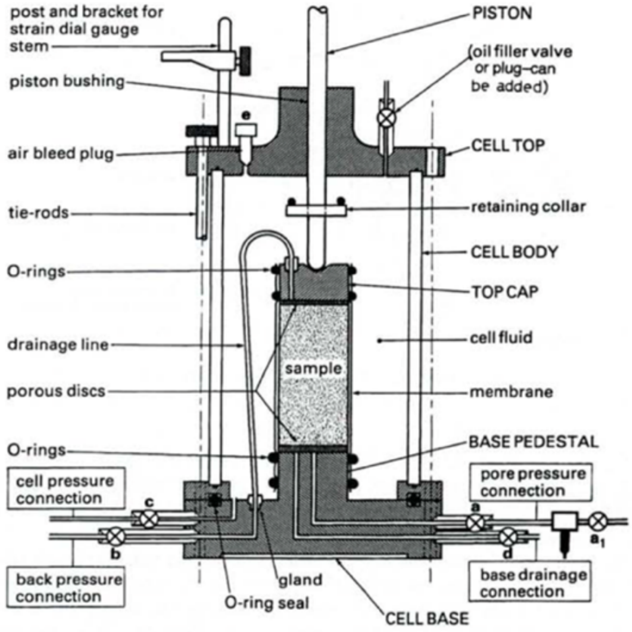

Figure 4.2 - A typical triaxial cell (Head, 1998)

Henkel (1956) notes that normally consolidated and overconsolidated clays (the latter having a past stress history or past plastic strain history) exhibit distinct differences in mechanical behaviour. These differences are most effectively observed through idealized laboratory triaxial tests. Thus, with the reconstituted UGL-2 representing the normally consolidated sample and the natural UGL-2 representing the overconsolidated sample, the triaxial test apparatus is ideal for comparing the behaviour of such materials in this dissertation.

4.2 The triaxial test theory

4.2.1 Introduction

Cylindrical specimens are commonly employed for conducting triaxial tests. On-site, a soil mass is subjected to three principal stresses, designated as σ_1, σ_2 & σ_3. However, in a conventional triaxial test, the specimen is exposed to only two principal stresses, namely σ_1 & σ_3. Stress σ_3 exerts pressure evenly in all directions across the sample, while stress difference σ_d operates along the axial direction. Thus, the externally applied stress in the axial direction is represented as (Lade, 2016).

$$\sigma_d = \sigma_1 - \sigma_3 \qquad \text{(Eq. 4.1)}$$

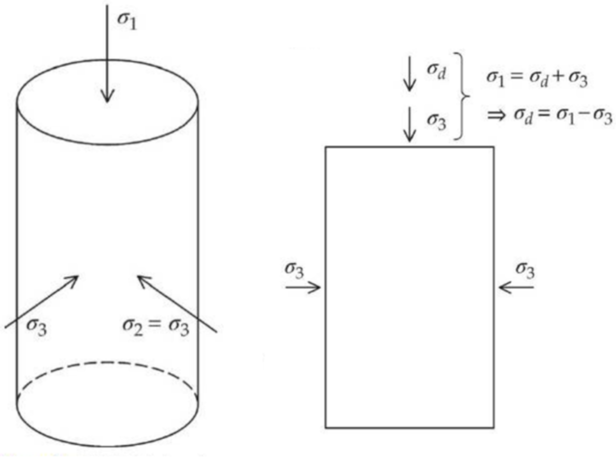

Figure 4.3 - Cylindrical specimen and stresses acting on specimen (Lade, 2016)

In the triaxial test setup, the sample is enveloped by filter paper, porous stone, and a latex membrane. This assembly is then positioned within the triaxial cell to exert cell pressure. The cell pressure applies uniform pressure from all directions on the specimen, functioning as a hydrostatic confinement. Additionally, a piston is utilized to impose a vertical load on the specimen, which is known as a deviator stress. In a triaxial test, various quantities are measured, including confining pressure, deviator load, axial deformation, and pore water pressure (Lade, 2016).

4.2.2 Consolidated-undrained tests

Isotropic consolidation tests are employed for the scope of this dissertation. Initially, the cylindrical specimen undergoes consolidation, ensuring that the applied stress results in equilibrium while permitting any excess pore pressure to escape within the specimen during the process. Prior to the undrained shearing phase, the drainage valve is shut to prevent any water from escaping the cell during the subsequent shearing stage. This lack of drainage prohibits volume change but anticipates a shift in pore pressure. Thus, the second phase of the consolidated undrained test is distinguished by (Lade, 2016):

$$\Delta V = 0$$

$$\Delta u \neq 0$$

In relation to the effective stress principle $\sigma' = \sigma - u$, the effective stresses vary from the total stresses in consolidated undrained test. Change in pore pressure is directly related to the soil's change in volume. This concept is shown in Figure 4.4. Therefore, variations in pore pressure are guaranteed in undrained tests. Some variables such as water content, void ratio will not change during the test, since there is no change in volume (Lade, 2016).

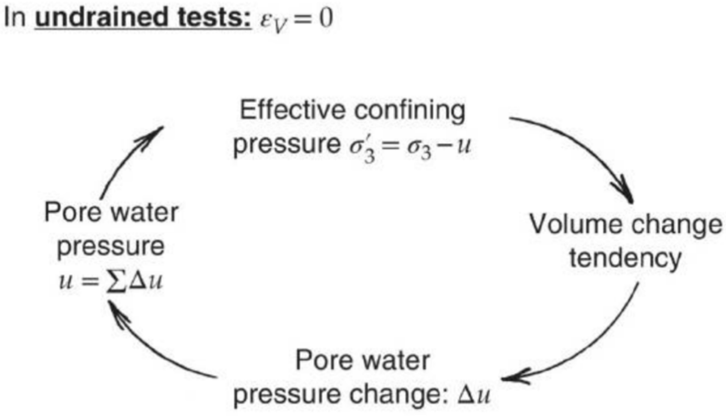

Figure 4.4 - Pore water pressure behaviour in undrained tests (Lade, 2016).

A Mohr diagram is a useful tool for deriving strength outcomes from consolidated undrained tests. Due to the emergence of pore pressure, two types of soil strength can be discerned: total strength and effective strength. Despite having the same diameter for their respective Mohr circles, these two strengths differ by the displacement Δu between them (Lade, 2016).

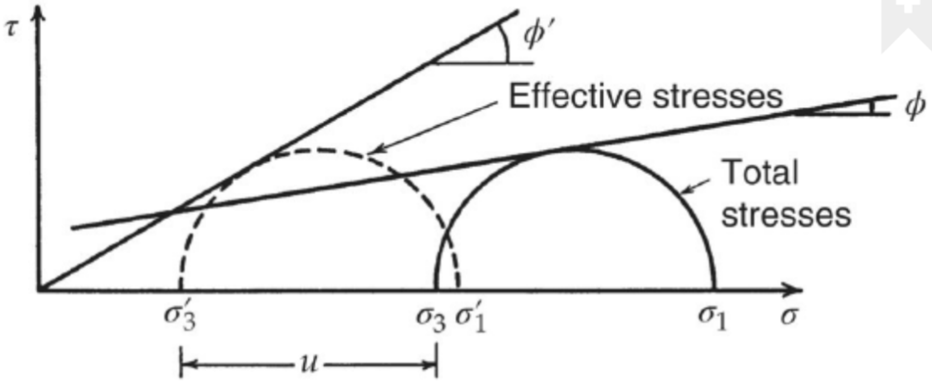

Figure 4.5 - Mohr diagram illustration with total stress and effective stress failure envelopes from CU-tests on soils (Lade, 2016)

Total and effective stress envelopes of clayey soils illustrate a strengthening trend as the confining pressure rises. In the drained state, the effective friction angle $\emptyset'$ diminishes with escalating confining pressure. Notably, the effective strength envelope in consolidated undrained tests closely mirrors that of drained tests. Consequently, the effective cohesion c' is zero for cases like remoulded and compacted soils (Lade, 2016).

The effective stress friction angle $\emptyset'$ surpasses the total stress friction angle $\emptyset$. Conversely, the total stress cohesion c might yield a higher value. It's important to note that the total stress friction angle differs from the effective stress friction angle. The effective stress friction angle $\emptyset'$ is a measure of strength acquired from the typically applied stress, whereas the total friction angle $\emptyset$ is a measure of strength derived solely from consolidation stress. In undrained tests, the friction angle is theoretically zero, as the diameters of the Mohr circles cannot change. Thus cohesion c becomes equal to the undrained strength S_u (Lade, 2016).

4.3 Triaxial tests

Triaxial tests were performed on both natural and reconstituted specimens, with seven tests being completed in total: four on natural specimens and three on reconstituted ones. This approach allows for a comparative analysis of the behavioural differences between the two materials.

The relatively low effective stresses applied were chosen due to the triaxial load cell's threshold of 10kN. As detailed later in this dissertation, specimen labelled as N4_U_800, subjected to a confinement pressure of 800kPa, nearly reached this threshold, preventing the application of higher effective stresses. Therefore, the tests employed a range of effective stresses that were proportional to each other, creating a comparative scale. Additionally, the reconstituted specimens were subjected to the same confinement pressures as the natural specimens, enabling direct comparison since both forms of UGL-2 were sheared under identical effective stresses.

The void ratios of the natural samples are relatively uniform, whereas those of the reconstituted samples show variation. This variation means that the void ratio differs across various sections of the reconstituted sample. The natural samples exhibit smaller void ratios, which is expected because they have been significantly compressed during sedimentation. This process causes the sediment particles to be more tightly packed due to the additional pressure from overlying sediment. In contrast, the reconstituted samples experienced much less overlying stress, resulting in higher void ratios.

Specimen No.	Effective Stress, p' (kPa)	Initial Voids Ratio, e
N1_U_200	200	0.77
N2_U_400	400	0.73
N3_U_600	600	0.69
N4_U_800	800	0.72
R1_U_200	200	0.86
R2_U_400	400	1.057
R3_U_800	800	0.93

Table 4.1 – List of triaxial tests

4.4 Sourcing of Samples

4.4.1 Natural Samples

The UGL-2 specimens examined in this dissertation were obtained from a block sample extracted from a trial pit in proximity of the Mellieha Bay Hotel, adjacent to Ghadira Bay in Mellieha, Malta. The location of the site was illustrated in Figure 2.4.

Figure 4.6 precisely indicates the trial pit exact coordinates from where the UGL-2 block was retrieved. Falzon (2022) outlines, that the trial pit is situated within a car parking next to the hotel. Initially, the top layer of asphalt was removed to access the material, followed by the use of a bucket excavator for the excavation process. The employment of the bucket excavator suggests the relatively soft nature of the ground material under examination.

Figure 4.6 - Trial pit location of UGL-2 samples (35°58'36.26" N, 14°21'14.66" E) (Falzon, 2022)

Falzon (2022) provides a depiction of the trial pit measurements in Figure 4.7. The green square on the Figure 4.7 denotes the precise retrieval position of the UGL-2 sample. The block sample was retrieved from a depth of 3.4 meters from the surface and 17 meters above sea level. The UGL-2 layer in the sampling area was found to be around 7 to 7.5 metres thick (Solidbase, 2023).

In order to extract the UGL-2 sample with minimal disruption, the excavation aimed to reach a predetermined level based on analyses of borehole cores conducted as part of a broader ground investigation in the region (Falzon, 2022).

Subsequently, Falzon details that narrow trenches were dug around the perimeter of the block sample using manual tools and vertical cuts surrounding the UGL-2 sample were dug. The UGL-2 sample was then split into four smaller subsamples. Each subsample was undercut, extracted, and subsequently covered in multiple layers of cling film and paraffin wax.

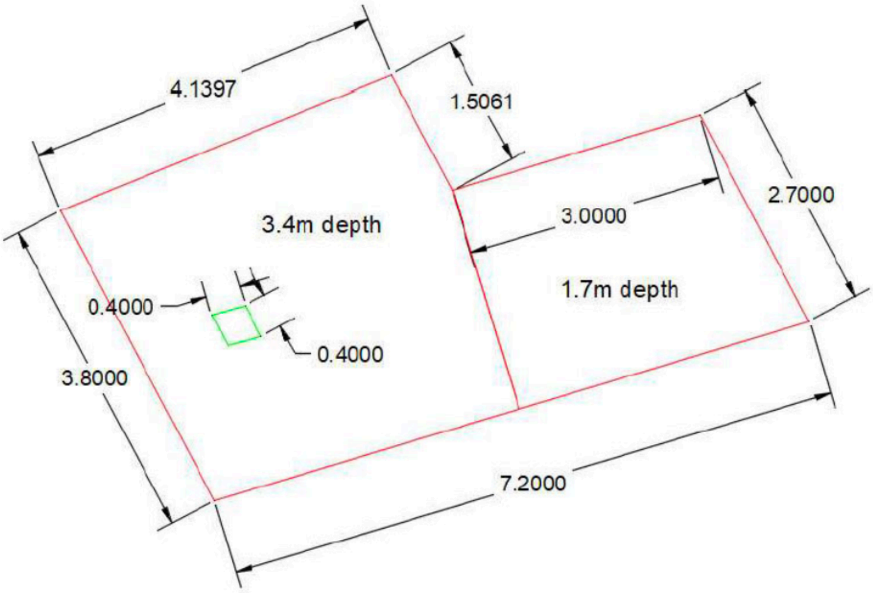

Figure 4.7 - Dimensions of trial pit (Falzon, 2022)

This pit was originally dug to extract a UGL-2 sample for research purposes (Solidbase, 2023) and (Falzon, 2022). Part of the UGL-2 sample remained unused, thus the remaining portion was partially utilized for this dissertation.

Figure 4.8 - Trial pit dug in the Upper Globigerina Limestone (Falzon, 2022)

4.4.2 Reconstituted Samples

The reconstituted UGL-2 sample was prepared as part of a dissertation by Grima (2024), which was conducted concurrently with this dissertation. The reconstituted sample was prepared using the trimmings from the natural specimens used for this dissertation. This reconstituted sample was created by breaking the natural UGL-2 into fine pieces, sieving them to a specific size (< 4mm) in a bucket, then water was added to the bucket and was desegregated in a whirlpool of water. The material was then consolidated one-dimensionally in a consolidometer and in this way the reconstituted sample was created (Grima, 2024).

Figure 4.9 shows the reconstituted UGL-2 sample created by Grima for his research. For testing purposes, this reconstituted sample was divided into four sections using a thin cross-wire, after being compressed one-dimensionally with a vertical effective stress incrementally increasing from an initial value of 5kPa and reaching a maximum stress of 334kPa (Grima, 2024). Three of these sections were allocated to this dissertation for triaxial testing, while Grima retained one section for one-dimensional consolidation analysis.

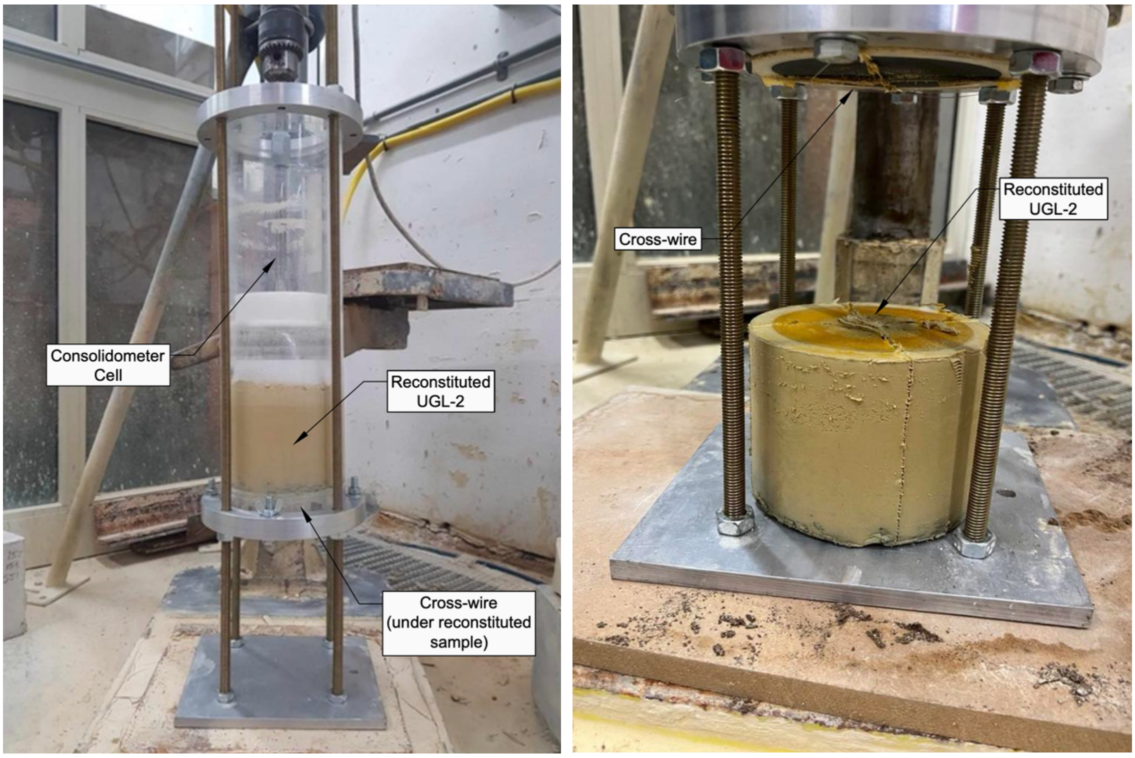

Figure 4.9 - Reconstituted UGL-2 in a consolidometer cell (left) and after divided into four pieces (right) by Grima, 2024

4.5 Upper Globigerina Limestone Specimen Preparation & Mounting for Testing

All specimens were trimmed to a diameter ratio of 2:1, at 76mm height and 38mm in diameter. The specific particle density (for UGL-2), G_s was taken as 2.63Mg/m^3 (Busuttil, 2021). The plasticity index (for UGL-2) was assumed to be 25%, categorizing it as a high plasticity clay (Falzon, 2022). The void ratio for the natural UGL-2 ranged from 0.69 to 0.77, whereas the reconstituted equivalent exhibited a range from 0.86 to 1.057.

4.5.1 Natural Upper Globigerina Limestone Specimen Preparation & Mounting for Testing

4.5.1.1 Pillar drilling

In preparing the natural UGL-2 specimen, the process initially involved using a pillar drill to extract samples from the undisturbed block sample of UGL-2. As previously mentioned, the block sample was wrapped in multiple layers of clingfilm and paraffin wax immediately after extraction by Falzon (2022). The wrapped and sealed specimen, after being stored for roughly three years in damp sawdust, was now securely affixed to the pillar drill using angle bars and G-clamps to prevent any shifting during the coring procedure. A coring tool with a diameter of 60mm was employed to extract cylindrical specimens from the block. The block remained wrapped in clingfilm and wax during the coring process, to retain moisture in the block. During the coring process the specimen was wetted with water to prevent overheating of the material due to the friction of the core with the material.

Figure 4.10 - Pillar drilling of natural Upper Globigerina Limestone

4.5.1.2 Trimming of specimen using lathe machine

Once a cylindrical core sample was extracted from the block, an engineering lathe was used to trim these core samples to the desired dimensions, in a precise manner, to produce the required triaxial test specimens.

Figure 4.11 - Lathe machine tool used to trim the natural UGL-2 sample to size

The initial step involved mounting the cylindrical core sample onto the chuck of the lathe. The end of the core sample was initially faced to achieve a smooth surface. After being faced, the sample was rotated, and the facing procedure was repeated on the other side. This ensured that the faced side of the sample would be in perfect alignment with the main longitudinal axis of the lathe, thus, permitting a precise and successful trimming procedure for specimen preparation. Following this, a cylindrical specimen was precisely trimmed to the specified size of 76mm x 38mm, using the automatic longitudinal feed of the engineering lathe. This process was executed swiftly to ensure the preservation of the specimen's water content. After the specimen was trimmed to its desired size, it was carefully wrapped with three layers of clingfilm and covered in wax to preserve its moisture content.

4.5.2 Reconstituted Upper Globigerina Limestone Specimen Preparation & Mounting for Testing

4.5.2.1 Trimming of specimen using manual soil lathe

The reconstituted material exhibited a much softer consistency compared to its natural counterpart, making use of the engineering lathe impossible in this case. Extra caution was necessary to prevent any disturbance to the material during handling. Due to the softness of the material, manual tools such as a manual-revolving soil lathe and a cross-wire were used to trim the specimen to the required size.

Initially, the reconstituted sample was approximately trimmed to the desired size using a cross-wire positioned beneath the consolidometer's base, immediately on extraction from the consolidometer itself (Grima, 2024).

Subsequently, a mould measuring 38mm by 76mm was positioned atop the specimen and pressed into it, thereby cutting the specimen to the desired dimensions using the mould. Finally, a cylinder was utilized to gently push the specimen out of the mould, ensuring a smooth removal process.

However, this procedure proved unsuitable upon post-test assessment. During compression within the sampler, the material automatically consolidated, possibly following a normal compression line during sampler insertion and then a swelling line upon release from the sampler, thus becoming slightly overconsolidated. This method was applied only to sample R1_U_200. This result was found to be undesirable because the goal was for the reconstituted sample to remain normally consolidated. Therefore, a different approach was taken for the other specimens, where they were trimmed to size (76mm x 38mm) using only a thin cross-wire mounted on a hacksaw, omitting the use of the mould sampler. This method ensured the specimens were prepared as normally consolidated.

Figure 4.12 - Manual soil lathe

4.5.3 Calculating water content

Trimmings from both types of specimens, produced during preparation were collected and weighed in their wet state. These trimmings were then dried in an oven at 105°C for 24 hours. After drying, their dry weight was measured. This allowed for the calculation of the mass of solids and the mass of water, assuming all the water had evaporated. This process enabled the determination of the water content at the initial state.

4.5.4 Mounting of natural and reconstituted specimen

Before commencing the testing process, careful handling of the sample was paramount. Initially, the clingfilm and wax coatings were meticulously removed from the specimen (This step was exclusively applied to the natural specimen, as it was typically trimmed a day before testing. In contrast, the reconstituted specimen was trimmed just before the start of the test, thus not requiring clingfilm). Subsequently, the specimen was weighed on a balance for measurement. Meanwhile, the triaxial apparatus underwent cleaning and de-aeration, as detailed further in this dissertation, while Whatman 42 circular filter paper discs of 38mm in diameter and two porous stones were also de-aired.

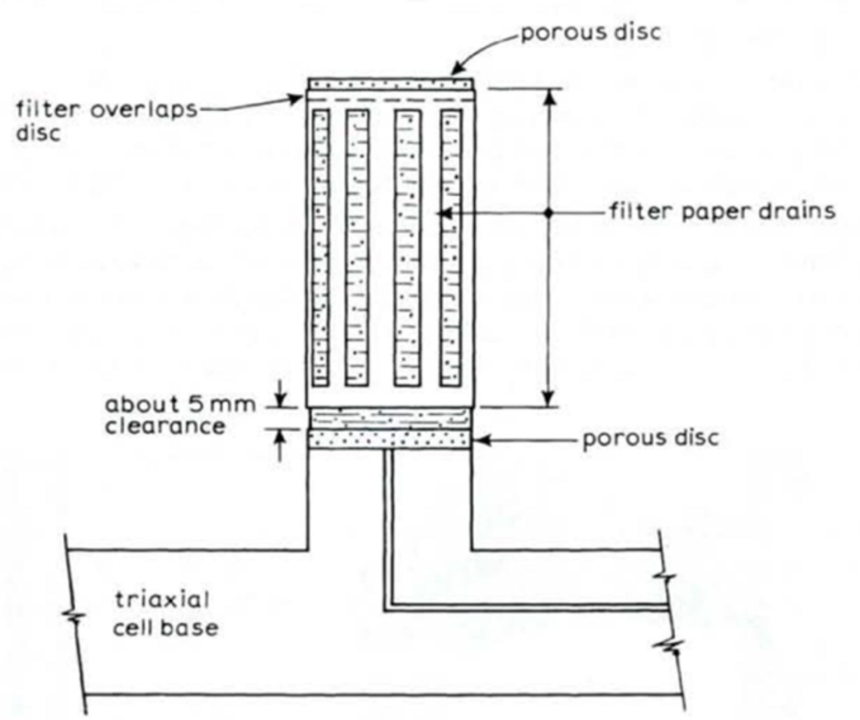

Figure 4.13 - Vertical drains on specimen avoiding overlap of lower porous disc (Head, 1998)

Figure 4.14 – UGL-2 specimen mounted on triaxial cell before set-up (left) and after set-up (right)

Upon successful completion of this step, the de-aired porous stone was delicately positioned on the base pedestal, followed by placing a circular de-aired filter paper (of the same diameter as the specimen) on top of the porous stone. The specimen was then gently placed on this setup. An additional disc filter paper disc was added on top of the specimen, followed by an additional porous stone. The scope of these filter paper discs was to prevent the porous stone from becoming clogged with soil particles during test, thus compromising drainage.

A de-aired filter paper lantern-type drain was wrapped around the natural specimen (however not in the case of the reconstituted specimen), primarily to accelerate the saturation and consolidation of the specimen given perceived the low permeability of the specimen. Also, a clearance of around 5mm was left between the bottom face of the specimen and the lower side of the lantern-type to avoid short-circuiting of the water during the saturation and the consolidation stages. Then the top cap was carefully positioned on the mounted specimen. Subsequently, a 3mm thick latex membrane was wrapped around the specimen with the assistance of a membrane stretcher. The membrane was tightened using a series of O-rings placed in an orderly manner. This process is necessary to isolate the specimen from the pressurised water in the cell creating the confining pressure. Upon successful completion of these steps, the cell was lowered and tightened, ensuring the piston and loadcell were perfectly aligned with the top cap. This setup is illustrated in Figure 4.13 and Figure 4.14

4.6 De-airing of triaxial system

Bleeding the lines is essential in triaxial systems with pore pressure measurement systems to ensure no air is trapped. The removal of air is essential because air is compressible. If air remains present, the pressure applied will cause the air to compress, hence the principle of effective stress within a saturated medium cannot work and the test readings are invalid or become very difficult to interpret.

Figure 4.15 - Bishop pump

A vacuum pump was utilized to de-air water in a tank situated above the triaxial system. Once de-aired for several minutes, this body of water was used to establish a water pressure in the lines, thereby facilitating the removal of all trapped air bubbles through bleeding. A Bishop pump, connected to volume gauges and pressure sensors, was used to pump this de-aired water from the tank into the drainage lines. This bleeding procedure was carried out before each test commenced, making sure that each part of the system was free of entrapped air.

4.7 Test Stage procedures and the corresponding analysis of data

Upon completion of the de-airing process and specimen preparation and mounting, the triaxial testing could commence. This test is divided into 3 phases: saturation, isotropic consolidation, and undrained shear. Some analyses are included in this section to complement the procedures mentioned.

The subsequent sub-sections include essential values for analysing, plotting, and interpreting the data. The values mentioned were programmed into a spreadsheet in order to obtain the necessary results efficiently.

The analysis began with the initial conditions of the specimens, which were: the cross-sectional area (A_0), the initial volume (V_0), the initial density (ρ), the initial moisture content (w_0), the bulk density (ρ_D), the void ratio (e_0), and the initial degree of saturation (S_0). After saturation stage, the actual change in the specimen's volume (m_s) was calculated by measuring the total volume of water that entered the specimen. Upon consolidation phase: the volumetric strain (ε_{cv}), length of specimen after consolidation (L_c), area of specimen after consolidation (A_c) and volume of specimen after consolidation (V_c) were determined.

Next, the consolidation characteristics of the specimens were determined by: the coefficient of consolidation (c_{vi}), the coefficient of volume compressibility (m_{vi}), and the coefficient of permeability (k).

Finally, after the undrained shear stage: the axial strain of the specimen $(\varepsilon\%)$, the calculated deviator stresses $(\sigma_1 - \sigma_3)_m$, and the corrected deviator stresses $(\sigma_1 - \sigma_3)$ were determined. Next: the minor effective principal stresses (σ_3'), the major effective principal stresses (σ_1'), stress ratio $({}^{\sigma_1'}\!/_{\sigma_3'})$, deviator stress (q) and mean effective stress (p').

All these parameters were necessary to obtain the results.

4.7.1 Initial Conditions

Table 4.2 presents the initial conditions of all the specimens. These values are crucial as they provide an overview of the starting points for each test, offering insight into the baseline conditions from which the experiments began.

Specimen No.	**A_0 (mm^2)**	**V_0 (mm^3)**	**ρ (Mg/m^3)**	**w_0 (%)**	**ρ_D (Mg/m^3)**	**e_0 (Ratio)**	**S_0 (%)**
N1_U_200	1,122.21	85.96	1.74	15.73	1.51	0.74	55.56
N2_U_400	1,137.70	86.44	1.77	16.15	1.52	0.73	58.29
N3_U_600	1,116.28	84.50	1.80	15.94	1.56	0.69	60.87
N4_U_800	1,156.91	87.74	1.80	17.54	1.53	0.72	64.35
R1_U_200	1,134.11	86.19	1.92	35.75	1.41	0.86	109.01
R2_U_400	1,122.21	85.29	1.75	37.04	1.28	1.06	92.09
R3_U_800	1,134.11	86.19	1.86	36.69	1.36	0.93	103.74

Table 4.2 - Initial conditions of specimens

4.7.2 Saturation

Saturation is achieved when the pore pressure reaches a sufficient level to enable dissolution of all entrapped air into the liquid phase. The confining pressure was elevated to generate a slight positive effective stress within the specimen. Both the cell pressure and back pressure were continuously and simultaneously raised, keeping a constant difference between them until the specimen was deemed fully saturated. Full saturation is essential because the pressure in trapped pore air is different from that in pore water, which can lead to inaccuracies in test results (Head, 1998).

The most common method in practice involves incrementally applying a back pressure to the pore fluid, alternating with increments of confining pressure. The back pressure was kept slightly lower than the cell pressure, typically by about 5 kPa, to ensure that the effective stress remained positive. The coefficient B value was checked each time the confining pressure was increased.

The saturation stage proved to be the lengthiest phase among all the triaxial stages. For the natural UGL-2 specimens, multiple saturation stages were necessary, typically around 3 or 4, each involving incremental increases in cell pressure and back pressure. In contrast, the reconstituted samples had a high initial saturation ratio. As a result, the specimens required only 1-2 days of saturation, with just one saturation stage needed, to achieve a B-value of 0.95 or higher.

These incremental increases were essential to ensure complete saturation of the specimen. As pressure increased, more water permeated the specimen's skeleton, expediting the achievement of full saturation. By applying higher cell pressure and back pressure with each increment, any remaining air bubbles within the specimen were eliminated and replaced by water. Once the B-test reached a value of 95% or higher, indicating full saturation, the saturation process was considered complete, and subsequent stages could proceed.

4.7.3 B – Test

Accurate pore water pressure measurement is crucial in undrained triaxial tests. To ensure this, the pore-pressure coefficient B, as introduced by Skempton (1954), is measured at the outset of testing to assess water pressure gauge sensitivity and specimen saturation conditions. The pore-pressure coefficient B is defined as the ratio of the change in pore water pressure to the change in cell pressure applied to the specimen in undrained triaxial tests (Head, 1998).

Specimen No.	Final B-Value
N1_U_200	98%
N2_U_400	96%
N3_U_600	97%
N4_U_800	95%
R1_U_200	99%
R2_U_400	96%
R3_U_800	95%

Table 4.3 - Final B-Value of specimen

For a fully saturated specimen, the theoretical B-value is 1.0, following the effective stress equation. Head (1998) indicates that achieving a B-value of 0.95 or higher ensures reasonably acceptable undrained test results.

The B-test was conducted at regular intervals during the saturation stage, by employing a cell pressure increase of 50kPa, while back pressure remaining constant. During this step, a change in pore pressure of the specimen could be observed. Once the B-test yielded a value ranging between 95% to 100%, indicating full saturation of the specimen, it was deemed suitable to proceed to the next stage, namely the isotropic consolidation stage.

4.7.4 Isotropic Consolidation

During isotropic consolidation, the specimen undergoes isotropic conditions where it is subjected to equal increments of stress in all directions ($\sigma_1 = \sigma_2 = \sigma_3$). This allows the specimen to consolidate both laterally and vertically, making it a three-dimensional process. Isotropic consolidation is achieved by maintaining a high difference in cell pressure and back pressure, both of which are held constant until excess pore pressures have dissipated, indicating consolidation process complete (Head, 1998).

Isotropic consolidation differs from one-dimensional consolidation. In one-dimensional consolidation, the material experiences stress from a single direction, specifically vertical compression.

Cell pressures were increased to exceed the back pressure by a desired effective stress, causing pore pressures to rise until reaching a steady state. Subsequent to this, the drainage valve is opened, and water starts to be expelled from the specimen and the volume of the drained water is measured (Head, 1998). The applied effective stresses are documented in Table 4.4. This process helps determine the specimen's field conditions within the triaxial test setup (Lade, 2016).

Mohammed (2015) defines “Consolidation as the process by which soils decrease in volume”. Consolidation is the process through which a saturated soil dissipates excess pore water, without replacement by either water or air. This results in a reduction in volume, achieved through the expulsion of water under static loads. Essentially, consolidation occurs when a load is applied to a soil, causing soil particles to compact, and resulting in a reduction in the soil's overall bulk volume.

In coarse-grained soils such as sand and gravel, pore water can be rapidly expelled because it can easily flow within the larger spaces between particles. However, in fine-grained soils such as silty or clayey soils, the consolidation process takes longer (Mohammed, 2015).

Specimen No.	**Cell Pressure (kPa)**	**Back Pressure (kPa)**	**Effective stress, p'**	**Drainage conditions**	**Time to 100% consolidation(mins)**	**Void ratio, e prior to shear**
N1_U_200	650	450	200	One end & Radial Boundary	306.25	0.78
N2_U_400	700	300	400	One end & Radial Boundary	60.06	0.75
N3_U_600	895	295	600	One end & Radial Boundary	88.36	0.76
N4_U_800	1145	345	800	One end & Radial Boundary	81.00	0.74
R1_U_200	265	65	200	One end	1075.84	0.89
R2_U_400	468	68	400	One end	888.04	0.83
R3_U_800	900	100	800	One end	985.96	0.77

Table 4.4 - Consolidation results

The consolidation process for the natural UGL-2 specimens was completed in less than one day. However, this process was accelerated by the shorter drainage path length resulting from the use of radial filter paper wrapped around the natural specimens, rendering determination of the consolidation parameters unreliable, as the exact drainage path length is non-uniform along the specimen, and hence cannot be accurately determined. In contrast, the consolidation of the reconstituted UGL-2 specimens took approximately two days to reach 95% consolidation, which is an overall amount considered to be acceptable (Head, 1998), given that the consolidation process is asymptotic to time and hence of infinite duration (Terzaghi, 1948).

Consolidation characteristics such as coefficient of consolidation, coefficient of volume compressibility and coefficient of permeability were obtained during the consolidation stage. These characteristics play a crucial role in classifying soil properties and behavior. In the testing of the natural specimen (not in the case of the reconstituted ones), side drains were employed to accelerate saturation and consolidation processes.

4.7.4.1 Coefficient of consolidation (C_v)

The coefficient of consolidation pertains to consolidation under isotropic conditions. The coefficient of consolidation is a fundamental factor in the study of saturated fine-grained soils and is particularly important for analyzing settlement in clay layers. It plays a crucial role in estimating how soils compact over time (Mittal, 2021).

Mittal continues that clayey soils typically experience significant consolidation when subjected to sustained foundation loads. Settlement analysis is commonly performed to determine both the total settlement and the rate of settlement over time, with a significant portion of this settlement attributed to the consolidation of underlying soil layers.

Various methods are available to determine the coefficient of consolidation. Taylor and Casagrande proposed graphical methods for C_v determination, which are commonly employed. These methods rely on the characteristic properties of the theoretical consolidation curve (Mittal, 2021).

Based on the coefficient of consolidation results of Table 4.5, it can be concluded that the rate of consolidation for the natural specimen is very low to low, as illustrated in Figure 4.16, hence justifying the use of the radial filter paper. Additionally, the reconstituted specimen exhibited a medium rate of consolidation.

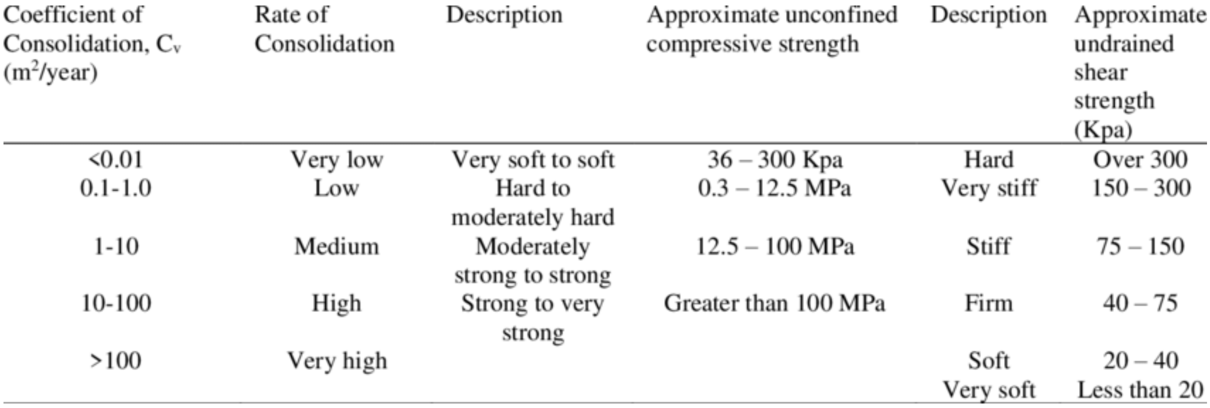

Coefficient of Consolidation, C_v (m^2/year)	Rate of Consolidation	Description	Approximate unconfined compressive strength	Description	Approximate undrained shear strength (Kpa)
<0.01	Very low	Very soft to soft	36 – 300 Kpa	Hard	Over 300
0.1-1.0	Low	Hard to moderately hard	0.3 – 12.5 MPa	Very stiff	150 – 300
1-10	Medium	Moderately strong to strong	12.5 – 100 MPa	Stiff	75 – 150
10-100	High	Strong to very strong	Greater than 100 MPa	Firm	40 – 75
>100	Very high			Soft	20 – 40
				Very soft	Less than 20

Figure 4.16 - Values of the Coefficient of Consolidation and consistency of soils (Falowo & Dayo, 2020)

4.7.4.2 Coefficient of Volume Compressibility (m_v)

The coefficient of volume compressibility is a measure of how much a unit volume of soil decreases for each unit increase in effective pressure upon compression. As a result, a higher coefficient indicates a softer soil skeleton (Das & Henderson, 2016). The coefficient of volume compressibility is a valuable parameter for predicting settlement in such soils (Frazi, 2017).

From the results in Table 4.5, it is observed that the natural specimen exhibited a lower coefficient of volume compressibility. According to Das & Henderson (2016), a lower coefficient of volume compressibility indicates that the specimen is less compressible. Thus, the natural specimen exhibits a lower coefficient of volume compressibility compared to the reconstituted specimen. Consequently, this indicates that the natural specimens are less prone to compression in contrast to their reconstituted counterparts. Thus, it can be inferred that the reconstituted specimen demonstrates greater compressibility than the natural specimen. This is expected as the natural specimen is bonded, while the reconstituted is not.

4.7.4.3 Coefficient of permeability (k)

The coefficient of permeability is fundamental in determining the flow characteristics. Generally, coarse-grained soils exhibit higher permeability compared to fine-grained soils. Hence, the coefficient of permeability quantifies the ease with which water can flow through the specimen (Das & Henderson, 2016).

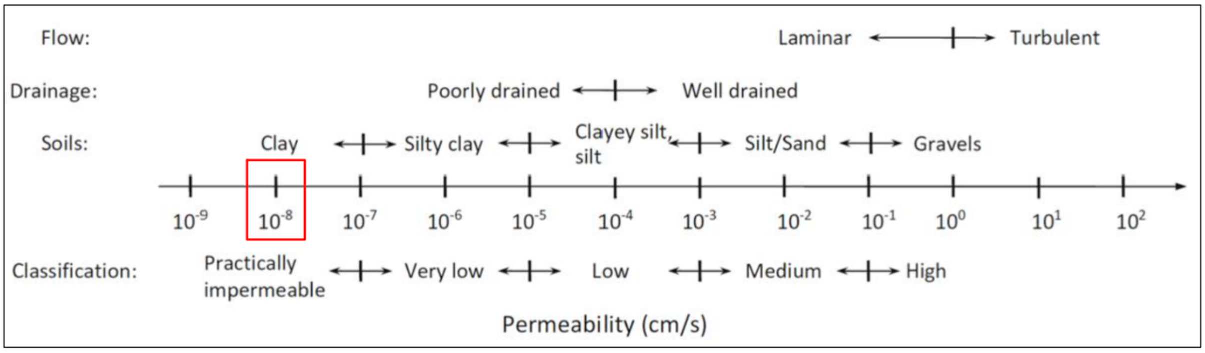

Figure 4.17 - Typical values of permeability (Das & Henderson, 2016)

Figure 4.17 exhibits values of the coefficient of permeability for a range of soils. The values resulted from the natural specimen were omitted. Head (1998) explains that the use of side drains short-circuits the process, and thus, the values obtained are not reliable. However, since no side drains were implemented for the reconstituted samples, a comprehensive analysis can be conducted. It can be inferred that the reconstituted samples lie within the 'practically impermeable' range of this assessment as indicated by the red rectangle in Figure 4.17, suggesting a high level of impermeability for these specimens.

Specimen No.	Applied Effective Stress, p' (kPa)	Coefficient of Consolidation, C_v (m^2/yr)	Coefficient of Volume Compressibility, m_v (m^2/MN)	Coefficient of Permeability, k (cm/s)
N1_U_200	200	0.095	0.11	-
N2_U_400	400	0.49	0.07	-
N3_U_600	600	0.32	0.08	-
N4_U_800	800	0.37	0.05	-
R1_U_200	200	2.13	0.30	2.00×10^{-8}
R2_U_400	400	2.49	0.25	1.93×10^{-8}
R3_U_800	800	2.19	0.20	1.33×10^{-8}

Table 4.5 - Consolidation properties

4.7.5 Undrained Shear

After completing the saturation and isotropic consolidation stages, the next step is the undrained shearing stage. In this stage, the specimen is sheared at a constant rate of axial deformation while maintaining constant cell confining pressure. Since it is an undrained test, no change in the volume of water is allowed.

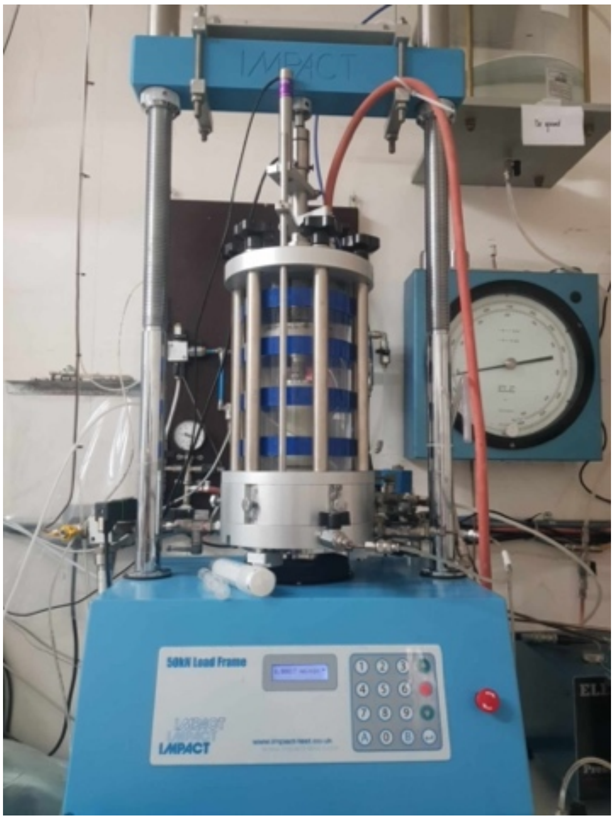

Figure 4.18 - Triaxial apparatus during shearing stage

During this undrained test, the shearing stresses and pore water pressure increases. An increase in shear stress is a result of axial load applied by the ram, as the cell is pushed upwards bodily against it by the loading frame in which the cell is located. The load cell thus, measures the force created on the specimen, located between the ram (at its top) and the pedestal/base of the cell (at its bottom). It is essential for compression by the triaxial apparatus to be very slow, allowing pore pressures to equalize throughout the specimen before failure is reached (Head, 1998).

The analysis of data for the undrained shear is detailed in the Results chapter, as the undrained shear was the primary objective of this dissertation.

4.8 Dismantling of specimen

Initially, the undrained shear strength test was concluded by decreasing the cell pressure to 0kPa, releasing the applied deviator stress, followed by closing the valves for both pressures. Subsequently, the water creating the confining pressure was drained from the cell through the triaxial's drainage pipe until the triaxial cell was fully dewatered. Once drained, the cell walls and top cap were raised to expose the sheared specimen. At this point the specimen is still mounted on the base pedestal. Then a series of photographs were taken to document the failure mode of the specimen. Next, the specimen was meticulously disassembled from the pedestal, starting with the removal of the O-rings, membrane, filter paper, and finally, the porous stones. Additional photographs were captured from four different angles after this disassembly process. After disassembly, the specimen was weighed in its wet state using a balance. It was then placed in an oven for a minimum of 24 hours to obtain its dry weight. By comparing the wet weight with the dry weight, the final water content of the specimen could be calculated.

4.9 Test Corrections

Several corrections were applied to obtain the corrected deviator stress, which include the initial moisture content, system compliance, area corrections, membrane corrections and side drain corrections.

4.9.1 Initial water Content

The final water content measured after the sheared specimen was left to dry in the oven for at least 24 hours was more reliable than the water content measured from offcuts. Mifsud (2019) explains that this phenomenon may occur because the fabric and texture of the offcuts taken from the sample can differ from the actual sample as a result of uneven texture.

Furthermore, it was noticed that the water content decreased when the sample was exposed to air. Therefore, during the preparation of the materials, particularly the natural sample that required trimming on a lathe, water content evaporated from the specimen. This evaporation could explain why the moisture content of the sheared specimen and that of the trimmings did not match exactly. Consequently, the initial water content was adjusted to align with the final water content.

4.9.2 System Compliance

During axial compression of the specimen at shearing stage, a load cell was used to measure the applied load, while a LVDT measured the axial displacement of the material. However, due to the nature of the triaxial testing environment, this sensor measured the deformation of all components within the triaxial apparatus, not just the specimen. These additional deformations, known as system compliance, included the deformation of the filter paper, porous stones, base pedestal and other components (Head, 1998). The gradients of the compliance curves measured by Mifsud (2019) for the same triaxial equipment used for this dissertation were utilized in this dissertation, because the setup and apparatus was identical to that used in Mifsud's research. These gradients were used to calculate the compliances for the specific confining and deviator pressures that were used in this research. Careful corrections were necessary to account for these deformations.

4.9.3 Area Corrections

Upon reaching their peak deviator stress, all the natural specimens displayed an inclined shear plane and continued deforming along this plane. This variability in deformation modes leads to differing degrees of changes in the cross-sectional area of the sample, consequently impacting stress calculations. Hence, adjustments for the corrected area assumed for the required calculations were made during the shearing stage (La Rochelle, Leroueil, Trak, Blais-Leroux, & Tavenas, 1988). The area correction was applied once the maximum peak was reached, where the shear plane had formed, splitting the specimen into two parts. At this stage, the two parts began to move and deform relative to each other and thus, area correction is required.

4.9.4 Membrane Corrections

Membrane restraint demanded careful attention, particularly in the case of the reconstituted specimen. The latex membranes separating the specimen from the water in the cell, creating the confining pressure, creates an additional restraint for the specimen, especially during slip failure, and in the case of soft specimens like the reconstituted ones, this restraint can be significant and hence it can adversely impact the results of the tests, thus, underscoring the critical importance of correction. The membrane corrections were quantified and applied as per recommendations by Head (1998) and measured by Mifsud (2019), because the same batch of latex membranes of 0.3mm thickness were used.

4.9.5 Side Drain Corrections

Side drains were employed for the natural specimen, necessitating their inclusion in the corrections. However, the reconstituted specimen did not require side drain correction, thus, deemed negligible. The correction was applied only to the natural UGL-2. For specimens failing by slip failure, which is typical of natural specimens, Head (1998) suggests using simplified drain correction curves as shown Figure 4.19.

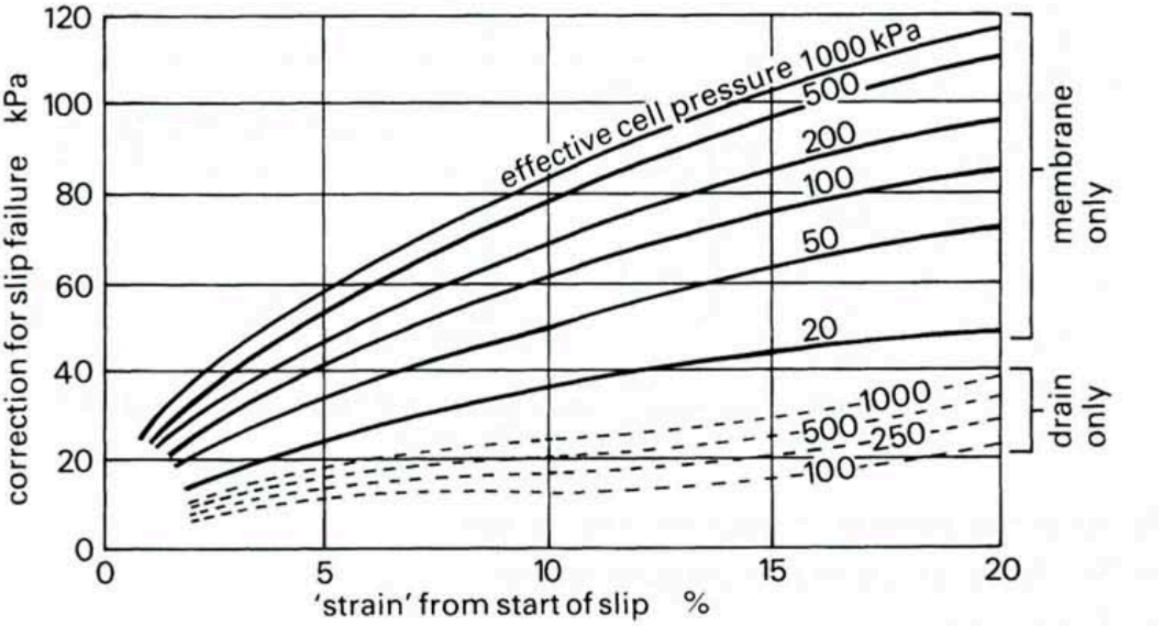

Figure 4.19 – Membrane and side drain correction curves (Head, 1998)

5. Results

This chapter will discuss and interpret the undrained shear characteristics observed from the triaxial tests performed after the specimens underwent saturation and isotropic consolidation. It will compare the mechanical behaviour exhibited by both the natural and reconstituted forms of UGL-2. Each form of the sample is consolidated under different confinement pressures, with the same pressures applied to both forms of UGL-2 for comparative analysis. This comparison is the primary focus of this research.

The chapter will begin by exhibiting the consolidation curves obtained from the isotropic consolidation stage and then move on to examining the engineering behaviour of three reconstituted samples, serving as a benchmark analysis. Then the engineering behaviour of the natural samples will be analysed. Finally, the chapter will conclude by analysing the undrained shear modulus of both forms of UGL-2. This analysis will employ various parameters essential for understanding the mechanical behaviour of these materials.

It is important to note that the three reconstituted specimens tested represent the destructured form of the Upper Globigerina Limestone, while the four natural samples represent its structured form. The following section will describe the mechanical behaviour observed in these specimens during typical isotropic compression triaxial tests conducted under undrained conditions.

5.1 Isotropic Consolidation

Prior to undrained shear testing, all specimens underwent isotropic consolidation to eliminate any excess pore pressure. This process involved expelling water from the specimens, resulting in each specimen reaching a particular void ratio. The void ratio values after isotropic consolidation and before shear (which are identical) are provided in Table 5.1.

Specimen No.	**Cell Pressure (kPa)**	**Back Pressure (kPa)**	**Effective stress, p'**	**Void ratio, e prior to shear**
N1_U_200	650	450	200	0.78
N2_U_400	700	300	400	0.75
N3_U_600	895	295	600	0.76
N4_U_800	1145	345	800	0.74
R1_U_200	265	65	200	0.89
R2_U_400	468	68	400	0.83
R3_U_800	900	100	800	0.77

Table 5.1 - Void ratio of all specimens prior to shear

Figure 5.1 and Figure 5.2 presents graphs depicting the volume change of the specimens plotted against the square root of time and logarithmic time respectively, illustrating the consolidation curves for each specimen. These curves closely align with the consolidation curves predicted by Terzaghi's theory for most soils.

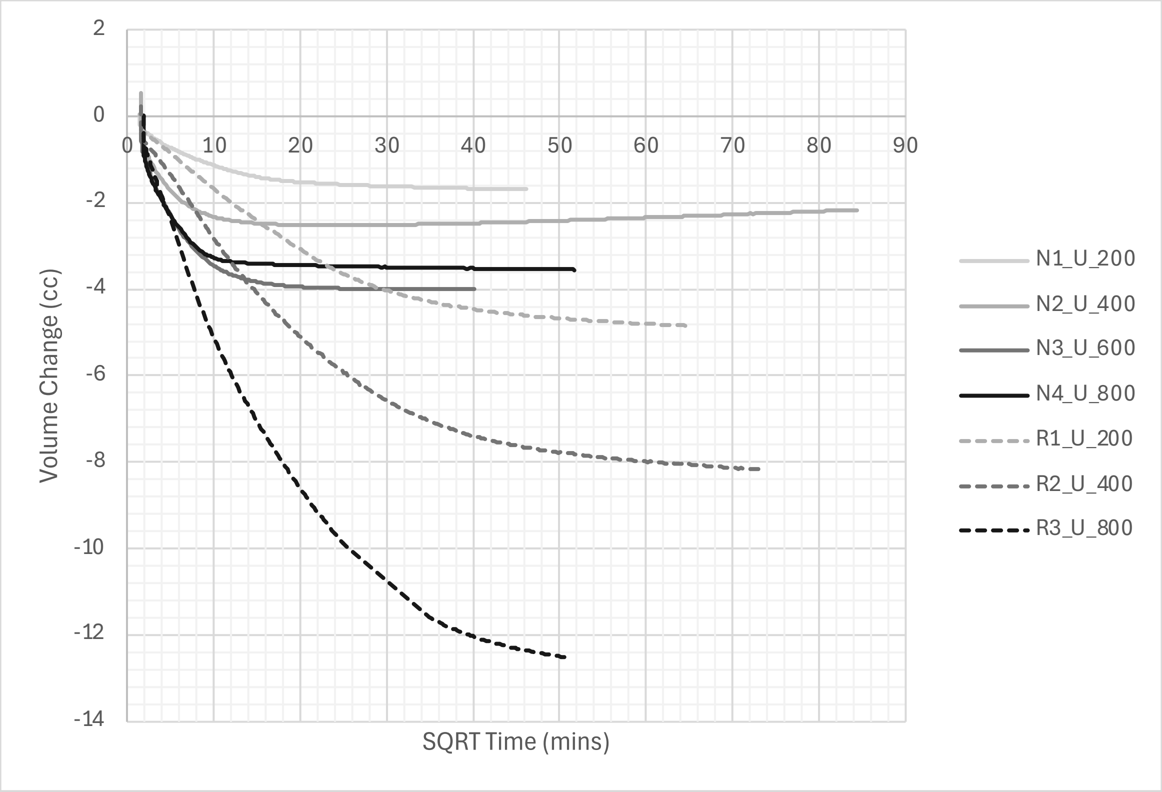

Figure 5.1 - Isotropic consolidation curves in Volume Change (cc) vs Square Root Time (mins) Graph for all specimens

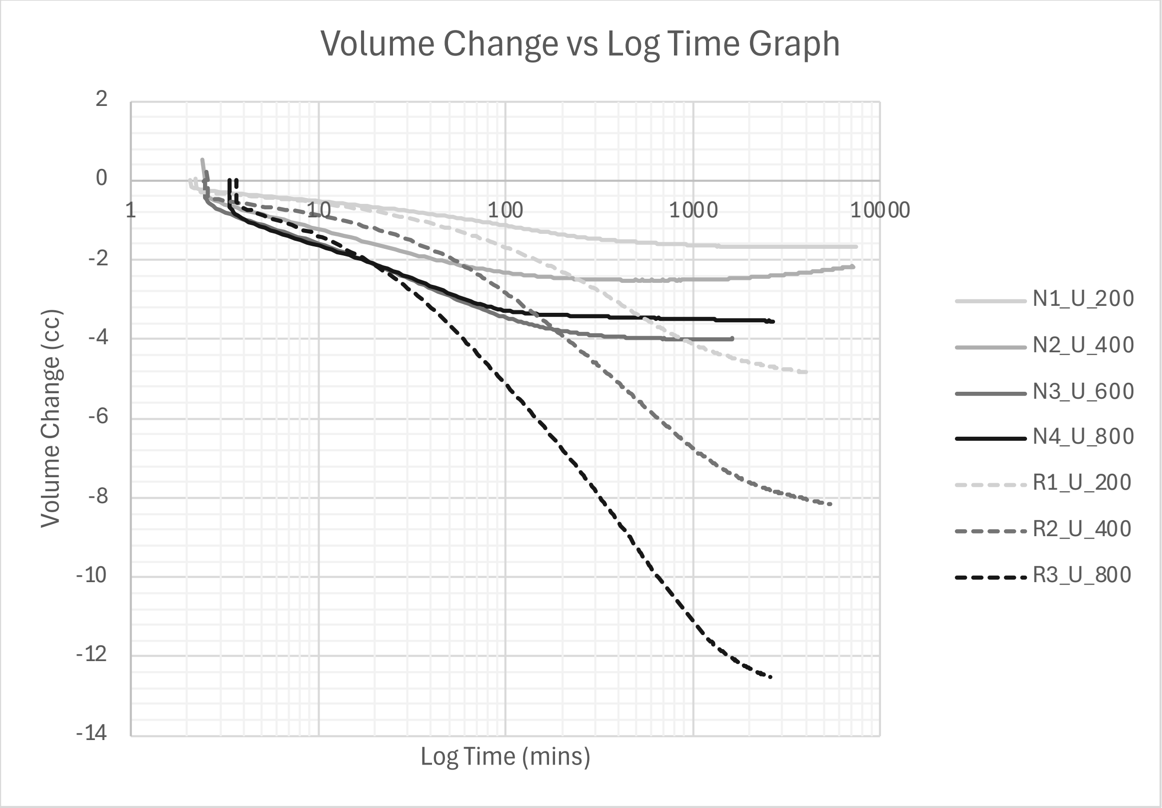

Figure 5.2 – Isotropic consolidation curves in Volume Change (cc) vs Logarithmic Time (mins) Graph for all specimens

The isotropic consolidation curves were analysed using Taylor's root time method on the volume change readings to determine the time to 90% consolidation. This analysis established the minimum shear speed rate required for the boundary conditions of the tests. The shear speeds are illustrated in Table 5.2.

After undergoing isotropic consolidation, the endpoints of all the specimens can be plotted on a Void Ratio vs Mean Effective Stress ($e\ vs\ p'$) space. When plotting the endpoints of the three reconstituted specimens (which were isotropically consolidated to different mean effective stresses as indicated in Table 5.1) these endpoints lie at different locations on a ($e\ vs\ p'$) space, as shown in Figure 5.3. All reconstituted specimen endpoints are observed to lie on an imaginary smooth curve (this curve is shown in Figure 5.3). This behaviour is congruent with that seen in Figure 3.6 by Atkinson and Bransby (1978). When the same endpoints are plotted on a ($e\ vs \ln p'$) graph in Figure 5.4, the three endpoints lie on an 'imaginary' straight line, which is also congruent with findings by Atkinson and Bransby (1978). This curve or line is known as the Isotropic Compression Line. It can be argued that at these points, the material has been erased from all its past memory as the response is controlled by its mean effective stress, and it is suggested by Leroueil & Vaughan (1990) that such states are structureless. Thus, such a curve is labelled as an Intrinsic Compression Curve (INCL). Burland (1990) emphasizes that different saturated ground materials possess unique Intrinsic Compression Curves. These isotropic consolidation endpoints, which lie on the mentioned Intrinsic Compression Line, are the starting points of the undrained shearing stage.

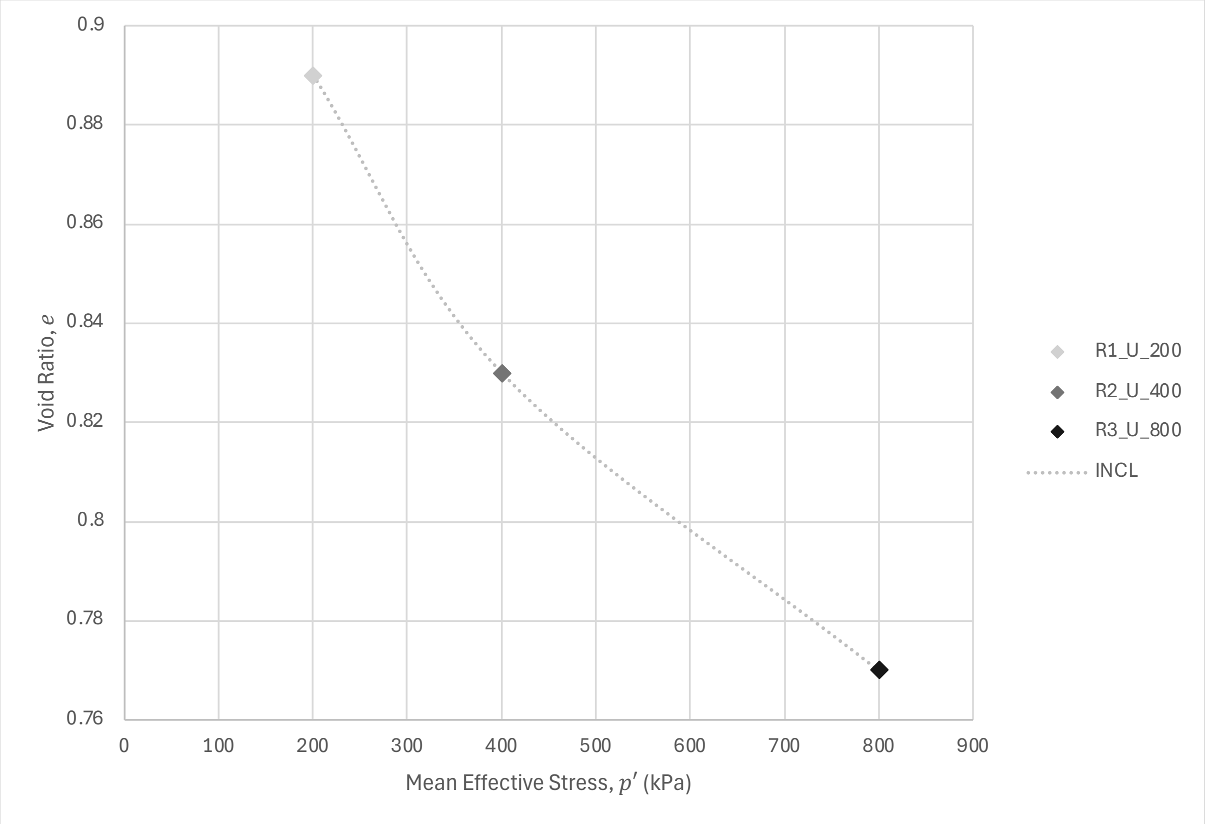

Figure 5.3 – Endpoints of all three reconstituted specimens after undergoing isotropic consolidation at different p' values in Void Ratio (e) vs Mean Effective Stress (p') Space

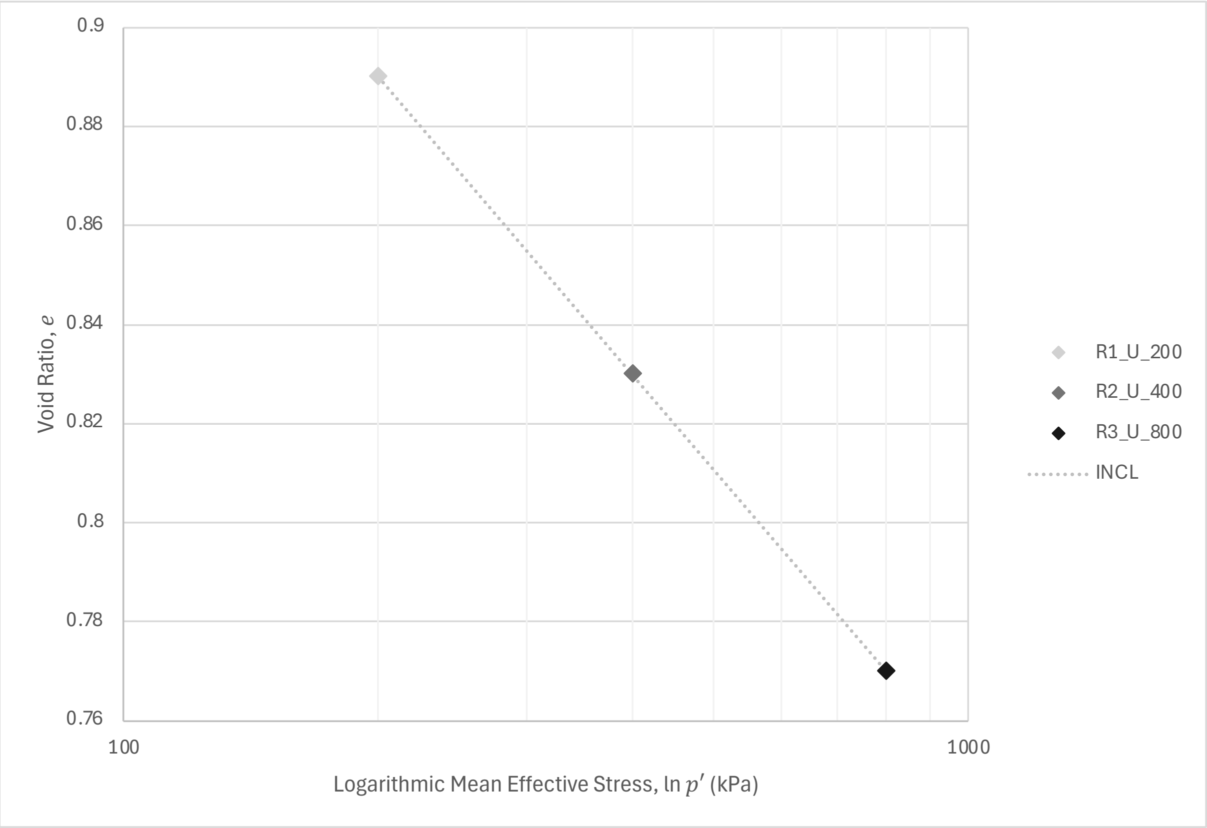

Figure 5.4 - Endpoints of all three reconstituted specimens after undergoing isotropic consolidation at different p' values in Void Ratio (e) vs Logarithmic Mean Effective Stress (ln p') Space

Using (Eq. 3.4), the Intrinsic Compression Line (INCL) derived from the reconstituted UGL-2 specimens is:

$$e = -0.0002 \ln p' + 0.93 \qquad \text{(Eq. 5.1)}$$

Where the gradient (λ) of the INCL is -0.0002 and the y-intercept is +0.93.

5.2 Undrained Shear

All tests conducted on the specimens involved monotonic shear at a constant cell pressure and constant strain rate. Furthermore, the final values attained from the isotropic consolidation stage were utilized to compute the maximum shearing rate. Specimens were sheared undrained under the different calculated shear speeds as depicted in Table 5.2.

Specimen No.	Applied Effective Stress, p' (kPa)	Shear Speed (mm/min)
N1_U_200	200	0.00017
N2_U_400	400	0.0009
N3_U_600	600	0.001
N4_U_800	800	0.00067
R1_U_200	200	0.001
R2_U_400	400	0.001
R3_U_800	800	0.001

Table 5.2 - Specimen shear speed

For all the reconstituted and natural graphs below, the symbols represent the following: the grey cross (x) indicates the initial yield as determined from the change in gradient of the stress-strain curve, the red circle marks the maximum deviatoric stress or the max dilation rate, the red triangle points the location of the phase transformation (a phenomenon which was observed and which will be explained later in this chapter), and the grey circle denotes the final states of the stress paths.

5.2.1 Behaviour of the reconstituted UGL specimen

This initial sub-section will present the mechanical behaviour exhibited by the three reconstituted specimens when subjected to shear. It will illustrate this behaviour through stress-strain graphs, pore pressure changes, stress paths, stress ratios, critical state line and by a description of the final deformed shape of the specimens after undergoing monotonic shear in the triaxial apparatus.

Considering the stress history of the reconstituted sample, this had only undergone loading and unloading once, while being formed in the consolidometer. Therefore, based on its stress history and the method of preparation used, the reconstituted sample is classified as normally consolidated. Its state, prior to the formation of the triaxial specimens , should lie on an intrinsic isotropic compression line.

Figure 5.5 and Figure 5.6 exhibit the response observed in the three reconstituted specimens. In the initial stage, all specimens exhibited linear behaviour, albeit with varying stiffness across the three specimens, where the specimens compressed to higher confinement pressures showed enhanced stiffness, notwithstanding specimens R2_U_400 and R3_U_800 almost exhibited identical stiffnesses. All specimens maintained linear stress-strain behaviour until the point termed as the initial yield, where the stress-strain curve no longer follows the original gradient.

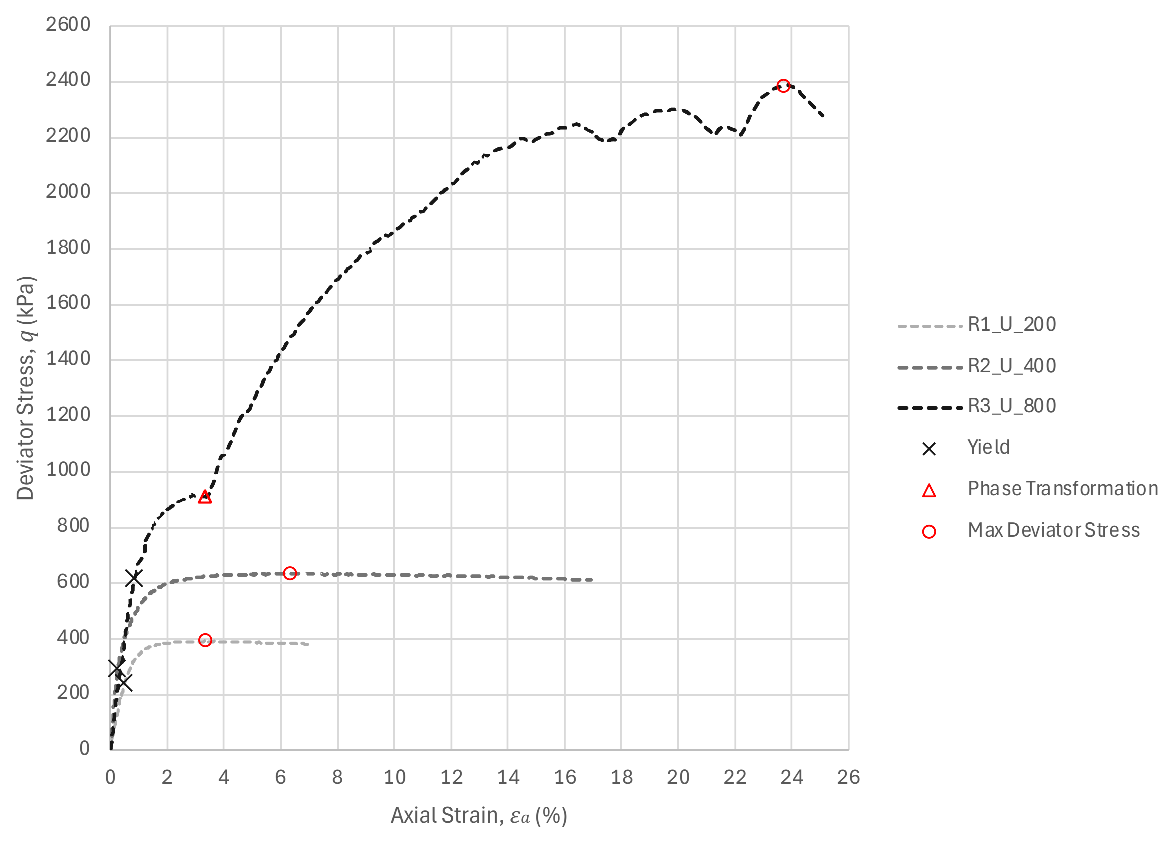

Figure 5.5 - Deviator Stress (q) vs Axial Strain (ε_a) Graph for the reconstituted specimens

During the shearing process of the normally consolidated samples, pore pressure rises quickly in the initial stages. This indicates that the specimens would have experienced a volume decrease and eventually contracted had the test been performed drained.

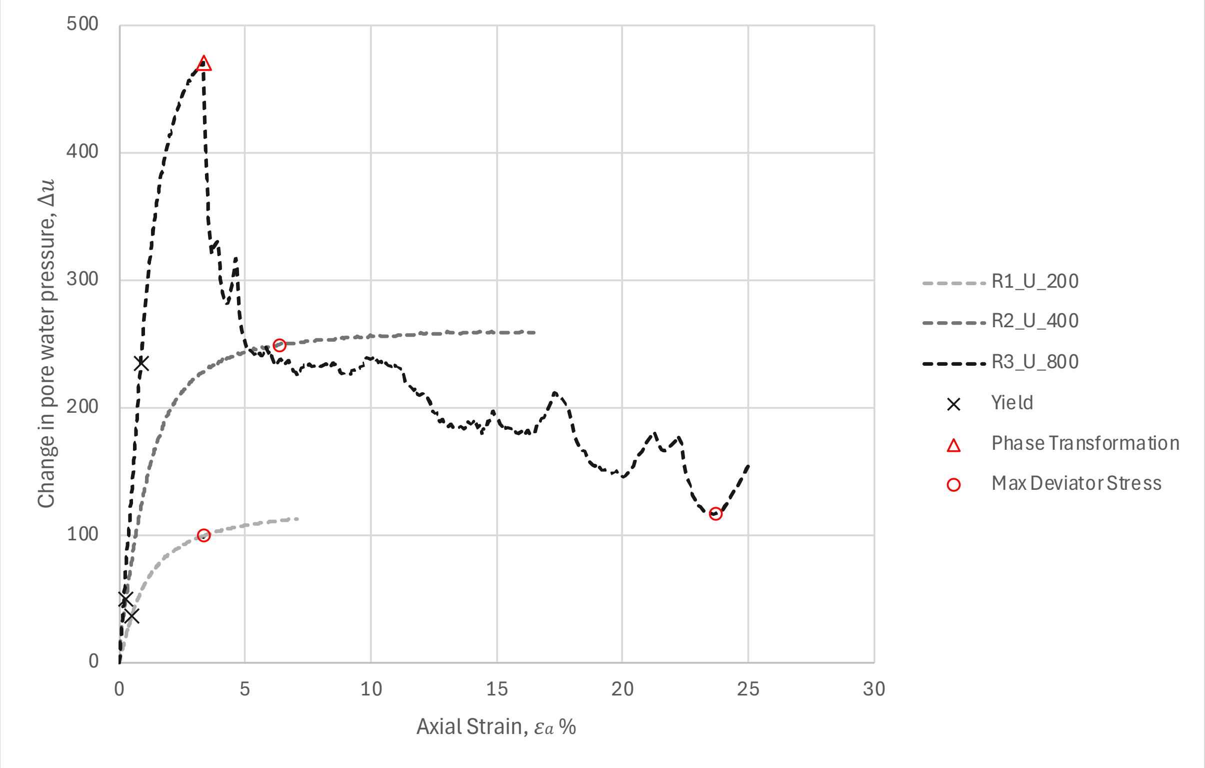

Figure 5.6 - Change in Pore Water Pressure (Δu) vs Axial Strain (ε_a) Graph for the reconstituted specimens

The deviatoric stress at initial yield is lower than the deviatoric stress at peak which indicates that after this point, both deviator stress and pore pressure continued to increase. Both deviatoric stress and pore pressure increased gradually and non-linearly after initial yield, with a decrease in stiffness indicated by the change in gradients of the curves. This happened in all reconstituted specimens, irrespective of the applied confining stress p'.

Specimens R1_U_200 and R2_U_400 reached a peak shortly after the yield point, and after this point, the specimens continued shearing at a roughly constant deviator stress. Specimen R2_U_400 was observed to reach a stage where the specimen started shearing with zero change in pore pressure and thus at constant volume. It can be hypothesized that specimen R1_U_200 would have behaved similarly to the R2_U_400 specimen had the test not been stopped prematurely.

All specimens exhibited ductile behaviour and strain hardened, albeit to different degrees. Table 5.3 illustrates the relationship experienced between the axial strain and deviator stress at initial yield and at peak deviator stress.

Notably, the greater the confinement pressure applied the greater the deviatoric stress exhibited by the specimens. Also, specimens compressed under higher confinement pressures reached an initial yield at higher deviatoric stresses. Both Figure 5.5 & Figure 5.8 supports this. Despite this variation, all specimens demonstrate similar behaviour and similar stress paths, until phase transformation occurred in specimen R3_U_800.

Specimen No.	**Axial Strain at Initial Yield**	**Deviatoric Stress at Initial Yield**	**Axial Strain at Peak**	**Deviatoric Stress at Peak**	**Yield Stress as a percentage of Peak Stress**
R1_U_200	0.50%	242.19	3.38%	391.31	62%
R2_U_400	0.25%	293.52	6.37%	634.33	46%
R3_U_800	0.85%	619.42	23.73%	2388.15	26%

Table 5.3 - Stress and Strain values at different stages of the test for the reconstituted specimens

As indicated by the stress paths in Figure 5.7, all specimens shift from right to left, suggesting they are situated on the wet side of the critical state and are attempting to reach the critical state line. The starting point of all stress paths is where the INCL intersects with them, and they end at the final state indicated by the grey circle. This behaviour indicates that the samples are either normally consolidated or lightly overconsolidated. The stress paths are all horizontal in a ($e\ vs \ln p'$) space, which is attributed to the fact that the specimens are being sheared under undrained conditions, where no volume change is possible.

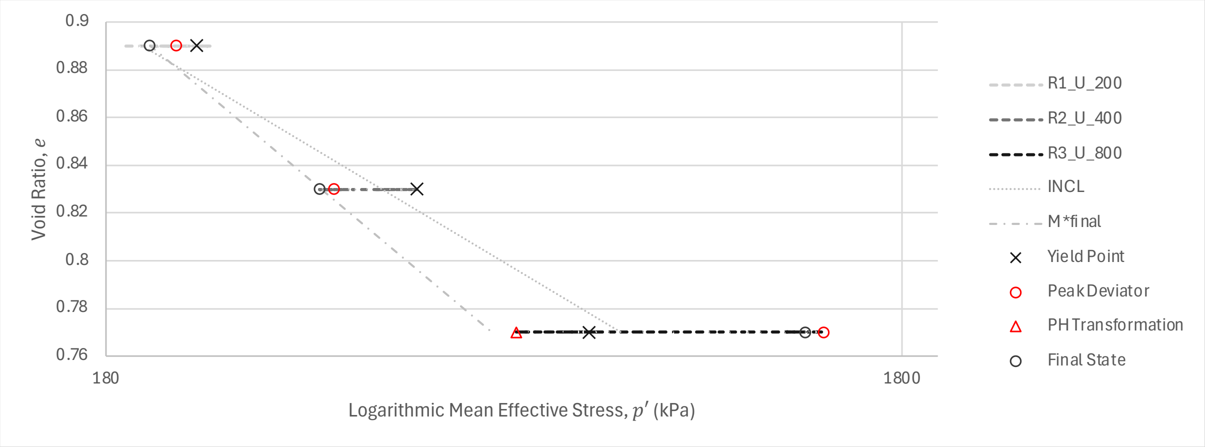

Figure 5.7 - Void Ratio (e) vs Logarithmic Mean Effective Stress (p') Space for the reconstituted specimens

From Figure 5.7, a critical state line (denoted as M^{*}_{final}) could be derived from the final states of specimens R1_U_200 and R2_U_400 (which will be explained in further detail later in this chapter), as shown below:

$$e = -0.00034\, lnp' + 0.91 \qquad \text{(Eq. 5.2)}$$

All specimens initially ascend almost vertically before veering left as exhibited in Figure 5.8. All specimens seem to reach the same imaginary boundary termed the Roscoe-Rendulic surface, which they then travel onto. While travelling on this boundary, specimen R3_U_800, behaves strangely from the rest were the p' stopped decreasing and started increasing, changing stress paths to the right. This kind of behaviour (first shift in stress path) is known as phase transformation and is a common feature in fine sands and silts (Lade & Ibsen, 1997).

After reaching the maximum deviatoric stress, specimens R1_U_200 and R2_U_400 maintained a nearly constant stress ratio. In contrast, specimen R3_U_800, after reaching its maximum deviatoric stress, showed a reversal in its stress path, with both q and p' decreasing. This decrease occurred very close to the original stress path it followed before reaching the peak, decreasing along a line with a nearly constant stress ratio.

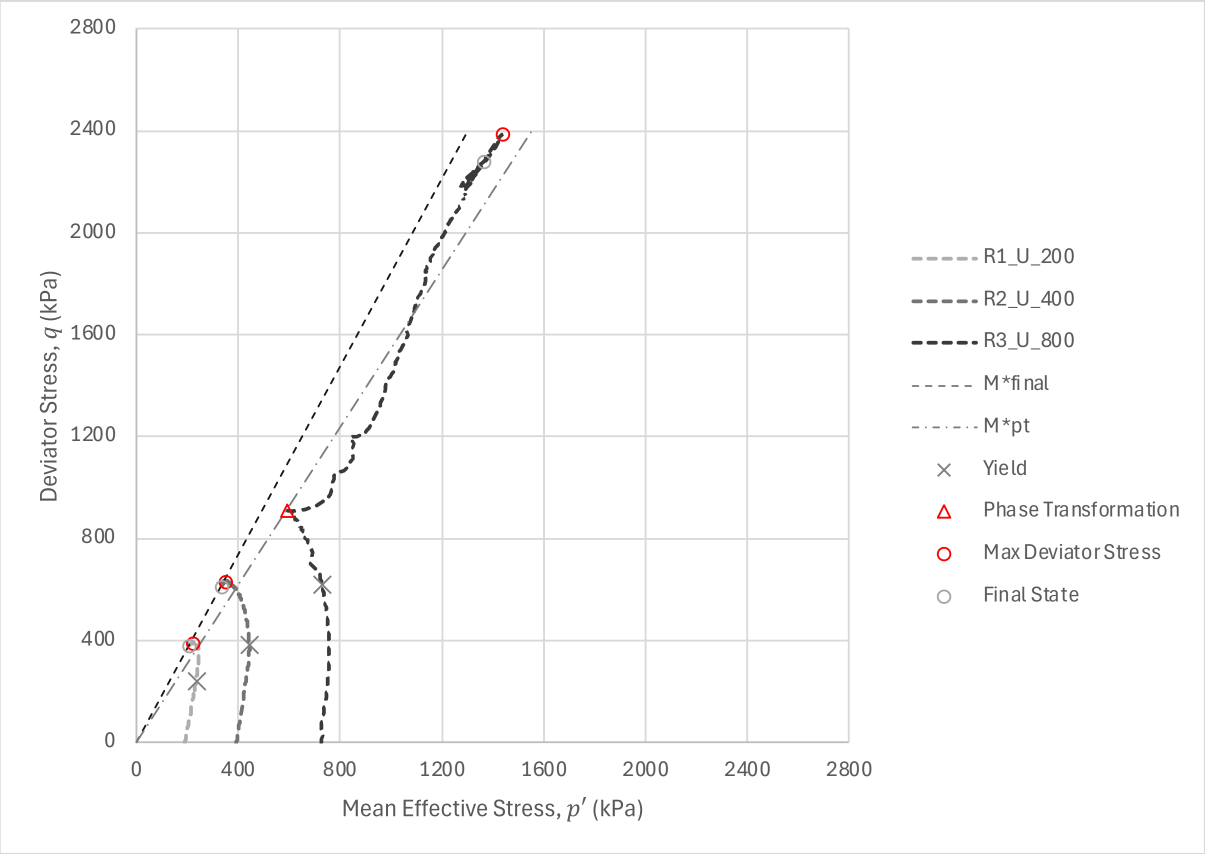

Figure 5.8 - Deviator Stress (q) vs Mean Effective Stress (p') Space for the reconstituted specimens

The shape of all the stress paths observed resemble those of normally consolidated samples shown in Figure 3.14 by Atkinson & Bransby (1978). The shape and direction of R1_U_200 and R2_U_400 stress paths indicate that positive pore water pressure is being generated and maintained, until a constant pore pressure was reached. Specimen R3_U_800 displayed the same behaviour during the initial stage before phase transformation occurred.

Specimen R3_U_800 was observed to behave similar the other specimens initially, with pore pressure increasing in the initial stages indicating contractive behaviour. Upon phase transformation, this specimen experienced a sudden drop in pore pressure, indicating a shift from contractive behaviour to dilative behaviour. This dilation contributes to increased strength, as shown by the rising deviatoric stress in Figure 5.5 after phase transformation. This specimen exhibited much higher strength compared to the other two specimens. It was the only normally consolidated specimen that experienced dilation during shear. During this dilative phase, a shear plane likely started to develop in this specimen, as observed in the Figure 5.13.

Phase transformation was observed in specimen R3_U_800, occurring after the specimen experienced barrelling due to contraction, where particles were compelled to move closer together. However, since the test is undrained, this is balanced by an increase in pore pressure.

Specimen R2_U_400 shears at constant pore pressures and a constant stress ratio in the final stages of the test. Specimen R1_U_200 seems to be reaching similar constant conditions, although this is an assumption based on observations. Such zero changes in pore pressure indicate that specimen R2_U_400 is neither contracting nor dilating at this point, suggesting that the specimen may be at the critical state. Consequently, a best fit line in Figure 5.8, denoted as M^{*}_{final}, was plotted from the origin through the final stress path states of specimen R2_U_400, which coincidentally matched the final stress path states of specimen R1_U_200, thus indicating that specimen R1_U_200 may be close to critical. Therefore, this line is proposed to represent the critical state line at the final states of the specimens.

In contrast, the final states of specimen R3_U_800 does not align with the proposed critical state line. However, at the juncture of phase transformation of this specimen, the mean stress ceases its descent and is on the verge of ascending again, while the maximum pore pressure immediately is reached surpassed beyond this point. This indicates that at this precise point, the mean stress increment change is equal to zero, signifying that the incremental volume of elastic and plastic strains would also be zero, as indicated by the peak in the change of pore pressure. Hence, the phase transformation point epitomizes a state of constant volume, albeit an exceedingly transient one.

The condition of constant volume in such materials is interpreted differently in literature. Some researchers, like Coop (1990), considered the phase transformation as an indicator of the critical state, while others, such as Razoaki (2000), used the final stress ratio to define the critical state. Therefore, the final state of specimen R2_U_400 or the phase transformation of specimen R3_U_800 could both represent the critical state.

Initially, all specimens exhibit a gradual increase in stress ratio. Specimen R2_U_400 eventually reaches a nearly constant stress ratio, converging towards a horizontal line at a stress ratio value of 1.84. If specimen R1_U_200 had not been stopped prematurely, it would probably have converged somewhere close to this horizontal line. This stress ratio at 1.84 corresponds to the gradient of the critical state line labelled as M^{*}_{final} in Figure 5.8. Similarly, specimen R3_U_800 also reaches a roughly constant stress ratio, although it converges below this line. However, this stress ratio is not considered reliable as it was reached after the specimen developed a shear plane. At the phase transformation of specimen R3_U_800, another horizontal line was drawn to represent the gradient of the critical state line in Figure 5.8, denoted as M^{*}_{pt}.

Both behaviours suggest that the specimens may be reaching critical state. By plugging this value in Equation (Eq. 3.9) by Wood (1990), the angle of shearing resistance of the specimen, denoted as $\emptyset_{cv}$, can be determined which is shown in Table 5.4.

Reconstituted UGL	**Gradient, M**	**Angle of Shearing Resistance, $\emptyset_{cv}$**
At Final State (M^{*}_{final})	1.84	44.76°
At Phase Transformation (M^{*}_{pt})	1.54	37.78°

Table 5.4 - Obtained angle of resistance

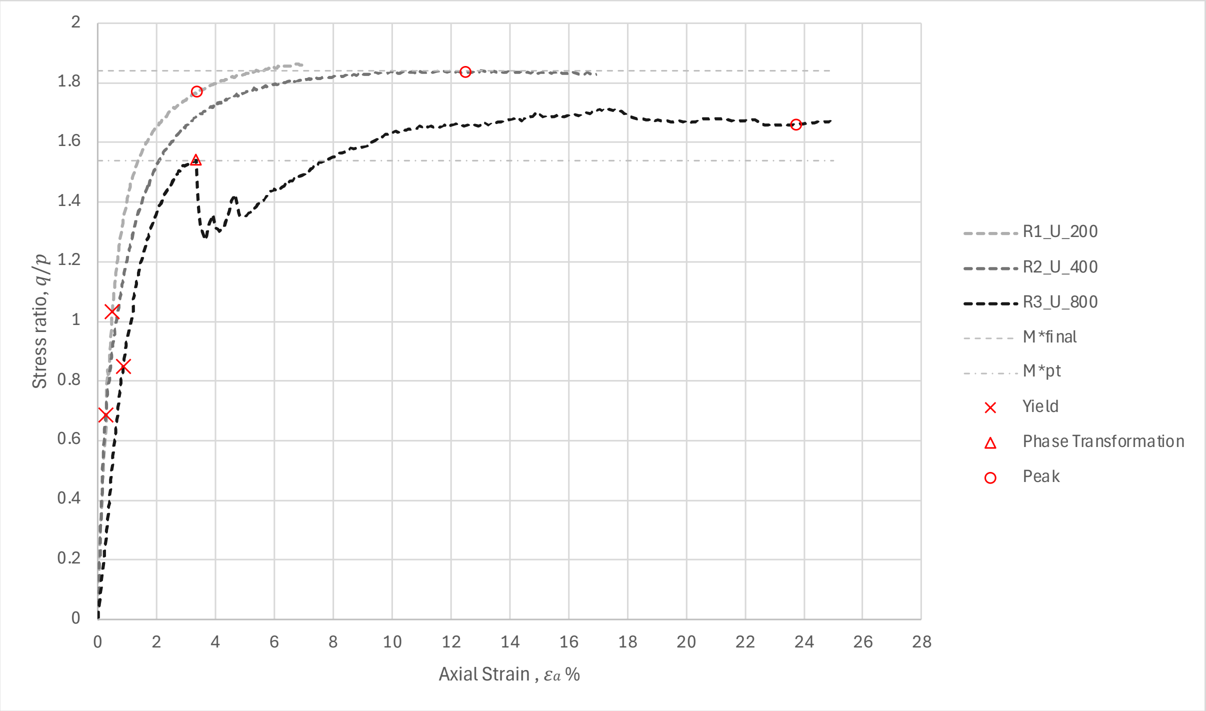

Figure 5.9 - Stress ratio (q/p') vs Axial Strain for (ε_a) Graph for the reconstituted specimens

Figure 5.7 and Figure 5.8 clearly illustrate the critical state at the final state. However, the critical state at the phase transformation is only depicted in Figure 5.8 due to a lack of data to determine the precise gradient of the CSL at phase transformation in a void ratio vs mean effective stress space.

All specimens experienced barrelling behaviour during shear, although to varying extents, as seen in Figure 5.10. Specimen R1_U_200 shows this deformation to a very low degree, the reason being that the test was stopped too prematurely. Specimen R2_U_400 showed this behaviour clearly. Specimen R3_U_800 also showed this behaviour, however, this particular specimen stopped contracting at a certain axial strain, thus stopped barrelling and started experiencing dilative behaviour, which is probably why a shear plane began to form within this specimen. It can be argued that this change in behaviour is a result of phase transformation. Moreover, the upper face of specimen R3_U_800 did not remain horizontal but became slightly inclined during compression.

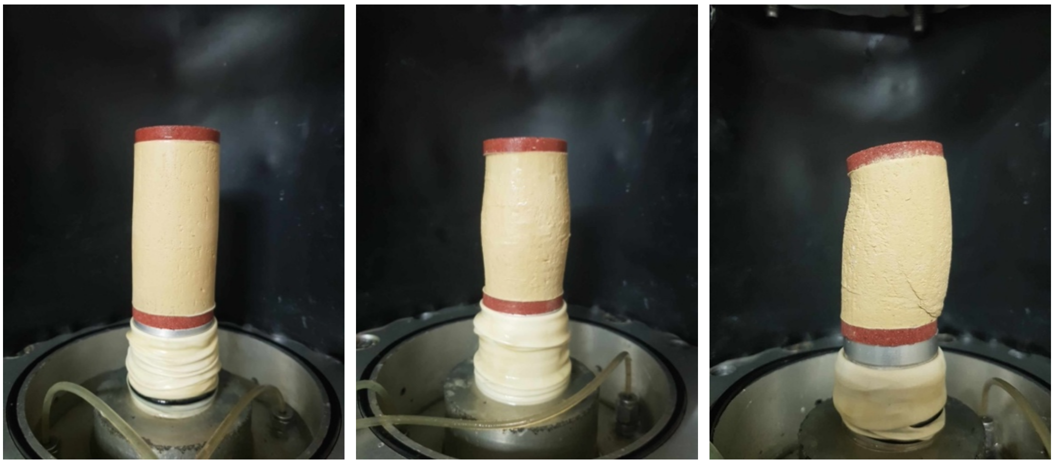

Figure 5.10 – Failure mode of the Reconstituted R1_U_200 (Left), R2_U_400 (Middle) & R3_U_800 (Right)

The contractive response of the reconstituted specimen caused an internal flow that led to a symmetrically bulging shape, hence resulting in barrel-shaped specimens. Figure 5.11 to Figure 5.13 illustrate the deformed state of all reconstituted specimens following isotropic compression. Each specimen is depicted from four different angles.

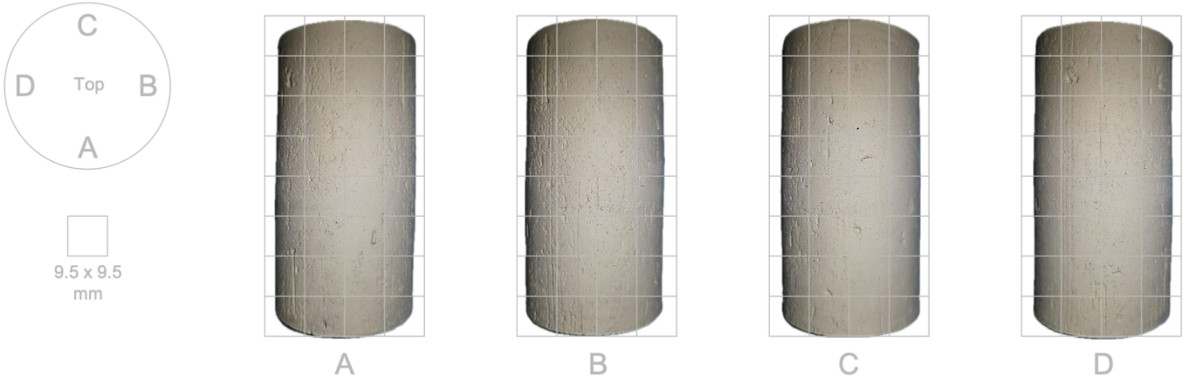

Figure 5.11 - Photos representing the failure mode of specimen R1_U_200 from four different angles

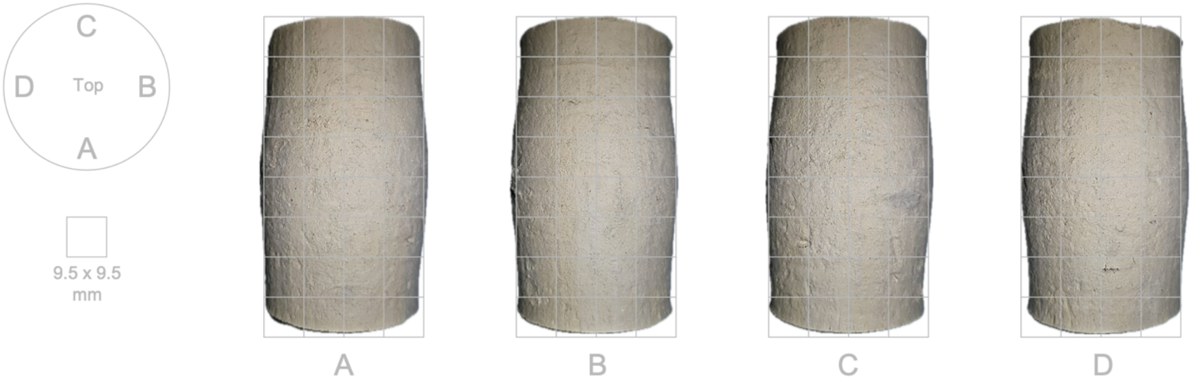

Figure 5.12 - Photos representing the failure mode of specimen R2_U_400 from four different angles

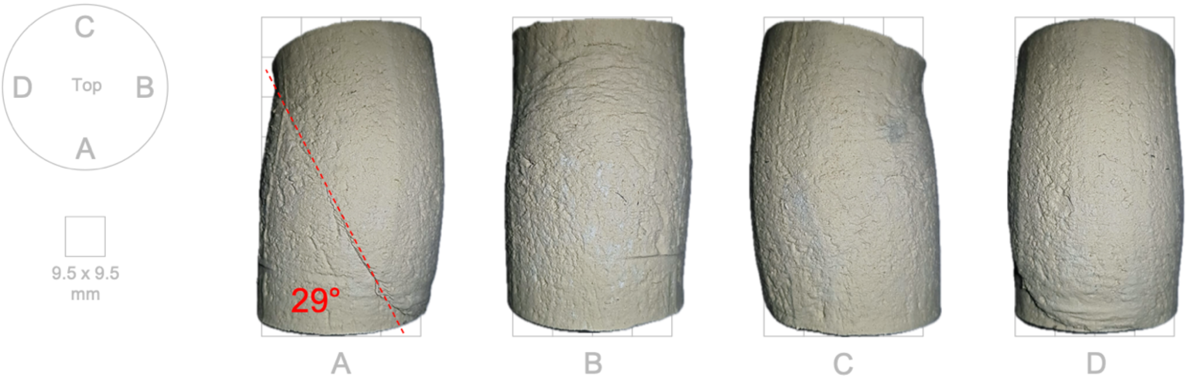

Figure 5.13 - Photos representing the failure mode of specimen R3_U_800 from four different angles

5.2.2 Behaviour of the natural UGL specimens

This sub-section presents the mechanical behaviour exhibited by the four natural specimens when subjected to shear. It illustrates this in a similar manner to that adopted for describing shear of the reconstituted specimens, thus allowing comparisons to be made.

The natural UGL-2, being a component of the geological strata in Mellieha, experienced loading due to sedimentary deposits accumulating on top of it (Scerri, 2019) over an extended period. Subsequently, as the upper strata eroded away, the UGL-2 experienced unloading. Therefore, since the UGL-2 experienced different degrees of overburden stress which invariably exceed those of the present-day stresses, the material must exist somewhere along a swelling line (as further evidenced in Figure 5.15) and thus, can be regarded as an overconsolidated material.

Similar to the reconstituted, the endpoints of the natural specimens can be plotted on a Void Ratio vs Mean Effective Stress space ($e\ vs\ p'$). When plotting the isotropic consolidation endpoints of all four specimens (which were isotropically consolidated to different mean effective stresses as indicated in Table 5.1) these endpoints also lie at different locations on a ($e\ vs\ p'$), as shown in Figure 5.14. It is observed that the endpoints of the natural specimens lie within a thin band, similar to how the reconstituted lie on the isotropic compression line. This thin band is also congruent with that seen in Figure 3.6 by Atkinson and Bransby (1978), where the isotropic consolidation endpoints of the natural specimens fall on another 'imaginary' smooth curve. When the same endpoints are plotted on a Void Ratio vs Logarithmic Mean Effective Stress ($e\ vs \ln p'$) graph in Figure 5.15, the four endpoints lie on a best fit straight line, which intersects the INCL, which is also congruent with the findings by Atkinson and Bransby (1978). This imaginary curve or line is known as a Swelling Line. These isotropic consolidation endpoints, which lie on the mentioned Swelling Line, are the starting points of the undrained shearing stage for the natural specimens.

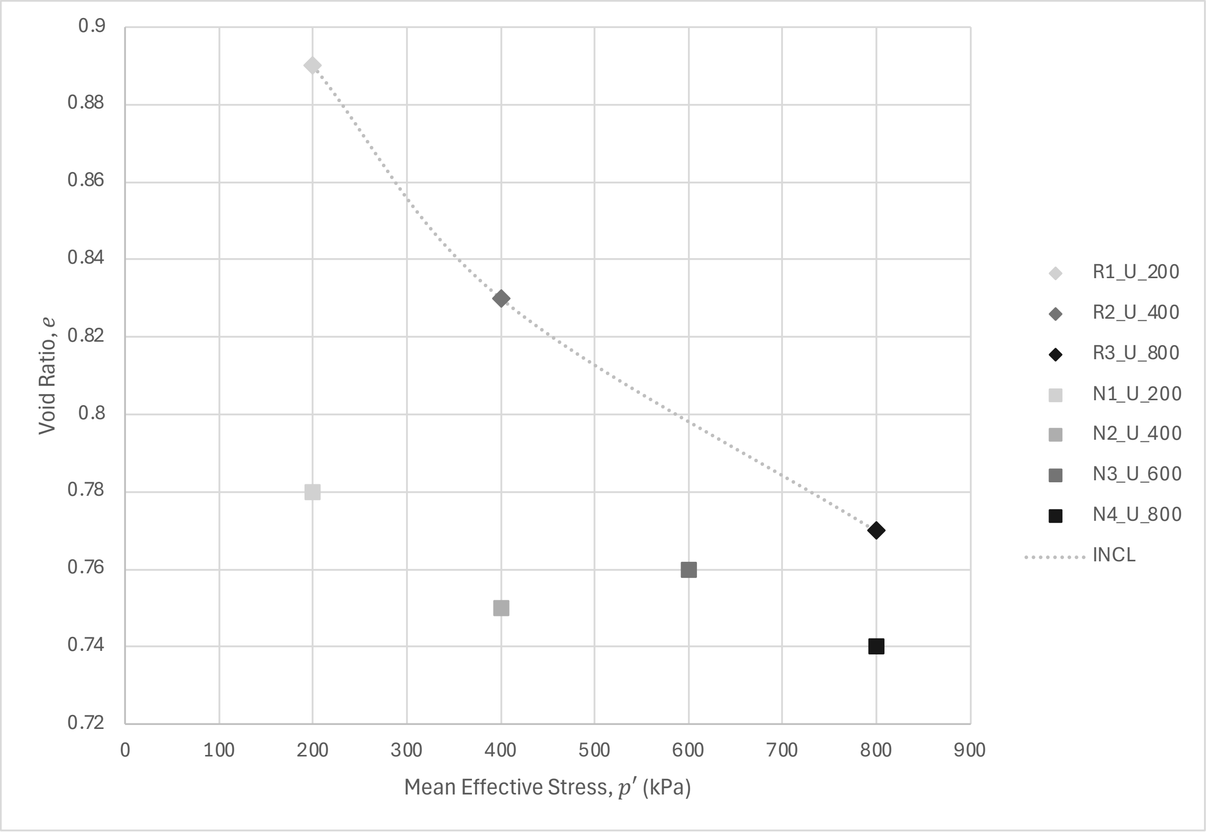

Figure 5.14 - Endpoints of all four natural specimens after undergoing isotropic consolidation at different p' values in Void Ratio (e) vs Mean Effective Stress (p') Space

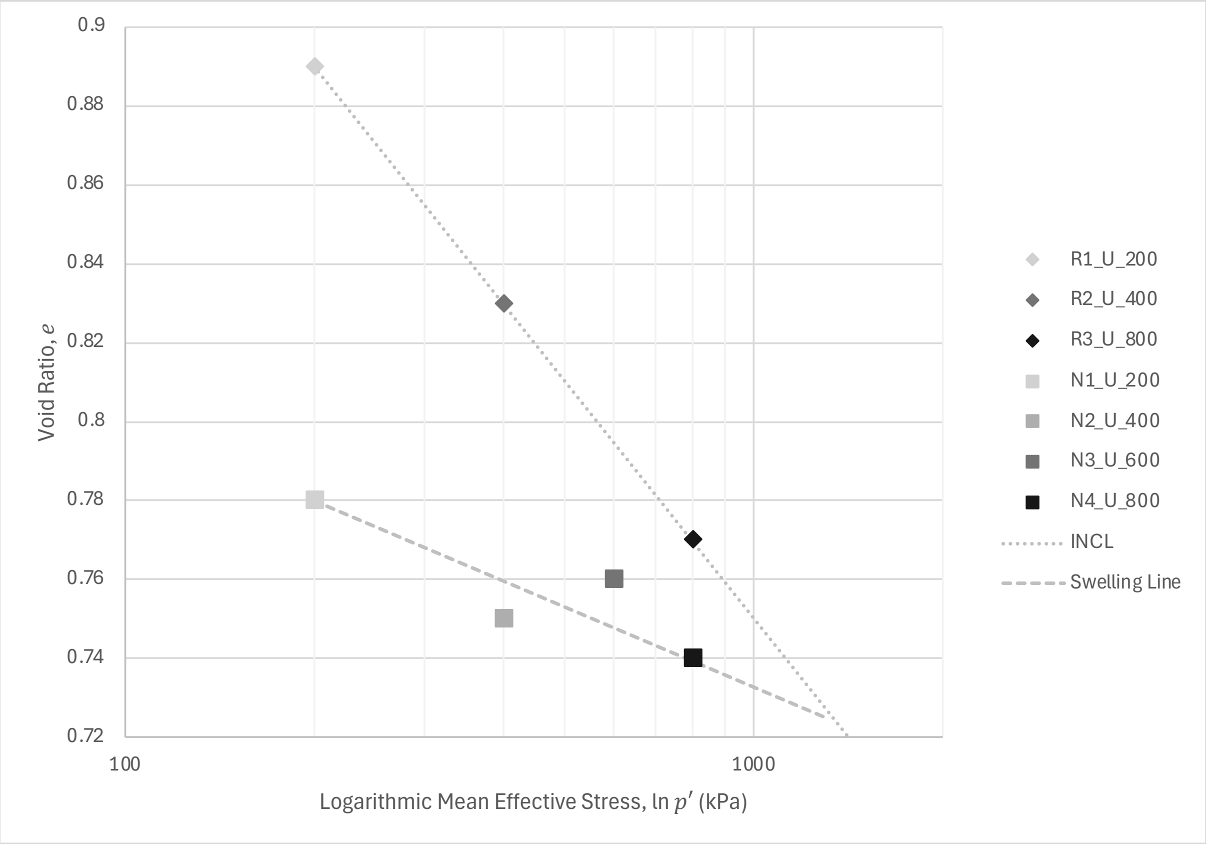

Figure 5.15 - Endpoints of all four natural specimens after undergoing isotropic consolidation at different p' values in Void Ratio (e) vs Logarithmic Mean Effective Stress (ln p') Space

Figure 5.16 and Figure 5.17 provide crucial insights into the mechanical behaviour of the specimens under study.

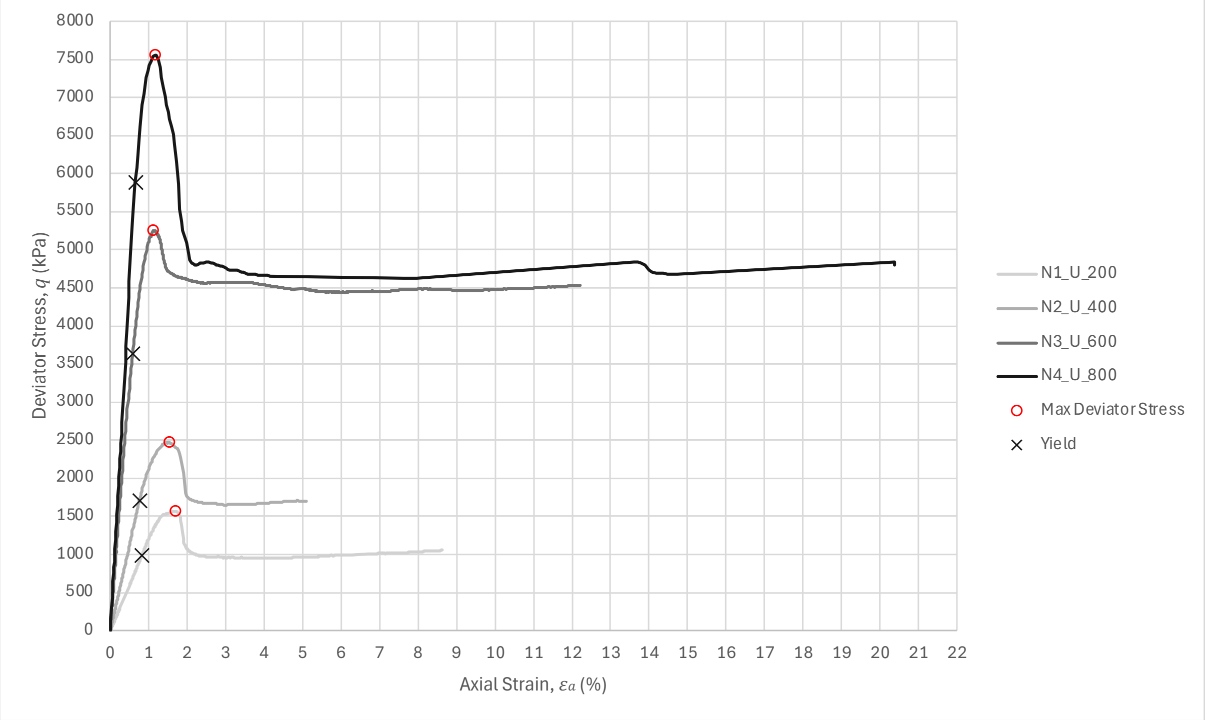

Figure 5.16 - Deviator Stress (q) vs Axial Strain (ε_a) Graph for the natural specimens

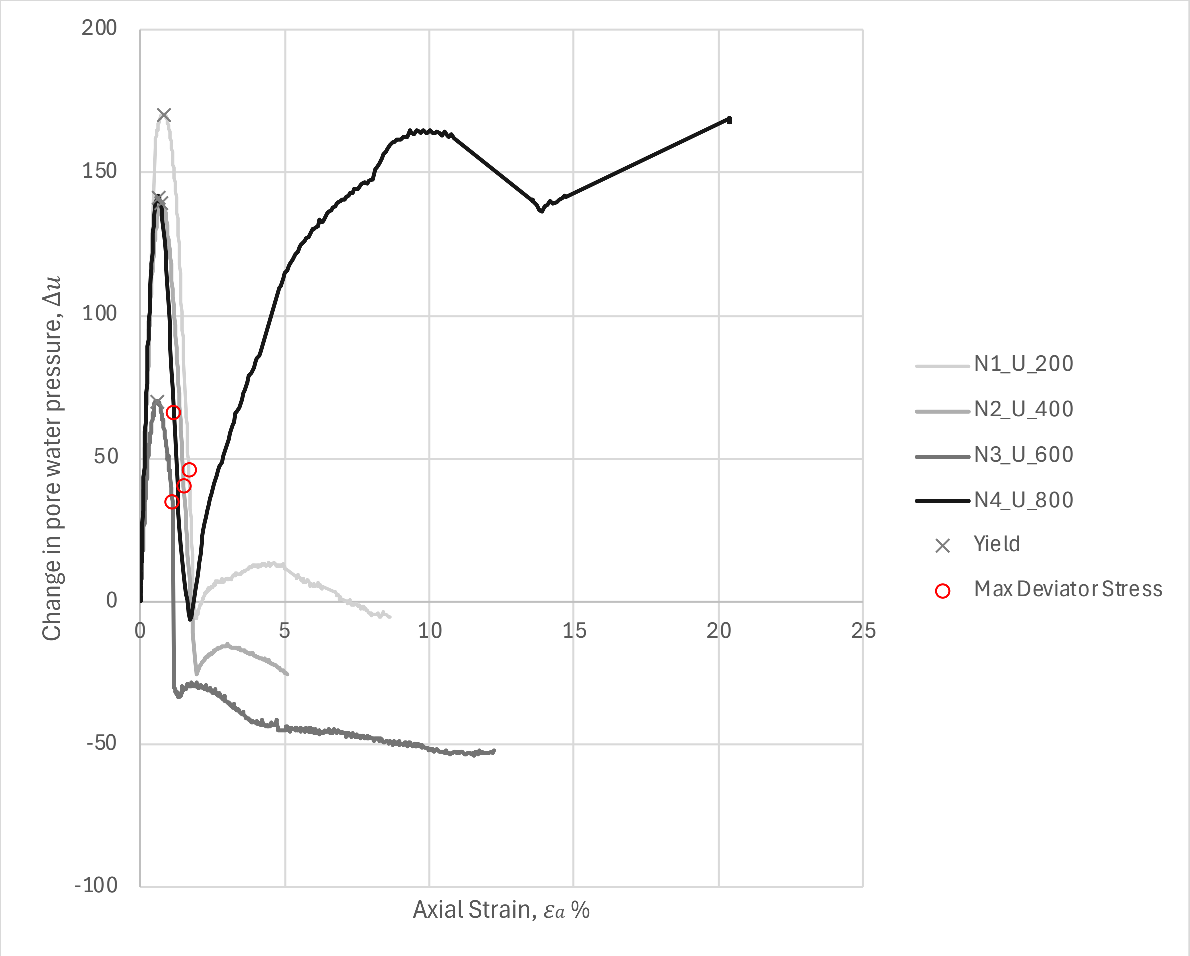

Figure 5.17 - Change in Pore Water Pressure (Δu) vs Axial Strain (ε_a) Graph for the natural specimens

Initially, all natural specimens exhibit rapid contraction behaviour, marked by a buildup in pore water pressure. During this contractive phase, all specimens display initial stiffness and linear behaviour until reaching the initial yield point, which coincides exactly with the initial peak in pore water pressure. After reaching this peak in pore pressure, all specimens show a sudden drop in pore pressure indicating dilative behaviour. During this dilative behaviour the specimens continued to show an increase in deviatoric stress, albeit with a decrease in stiffness, until a peak deviatoric stress was reached. This increase in deviatoric stress is contributed to the dilative behaviour of the specimens. The point of maximum deviator stress coincides during the maximum rate of dilation in Figure 5.17. The maximum rate of dilation, and thus the peak, represents the highest energy the sample can exhibit. This peak energy results from the combined effects of the frictional interactions between particles and the rate of dilation, leading to the formation of the major slip plane, observed in all specimens in Figure 5.21. When these two factors reach their maximum, the peak occurs. The peak deviator stress, and consequently the formation of the major shear plane in all specimens, occurs during this dilation phase. After peak, all specimens exhibited a post-rupture strength, due to strain localization which varied in proportion to the applied confining pressure. All specimens exhibit a rapid decrease in shear stress (due to strain localisation), which then stabilizes and maintains a nearly constant value with further displacement. Softening behaviour is evident in the graph, where the yield stress curve shows a decreasing trend, and a well-defined plateau is formed. The remaining strength in the post-rupture state is due to the normal stress acting on the failure surfaces, which is a result of the cell confining pressure. After the peak is reached, local axial strains decrease as a result of the unloading process. The post-rupture deformation region consists of near-rigid body sliding along the shear plane (Burland, 1990).

The higher confinement pressures resulted in higher and sharper peaks, indicating greater strength and stiffness in these specimens. Conversely, specimens subjected to lower confinement pressures exhibited lower and more gradual peaks. Interestingly, the specimens confined to the lowest pressures showed peaks at higher axial strains compared to those at higher confinement pressures. Furthermore, as the confinement pressure on the specimens increased, the specimens exhibited more brittle behaviour. This mechanical behaviour is summarized in Table 5.5.

Table 5.5 also exhibits that the higher the confinement pressure applied to the specimen, the smaller the percentage difference between the deviatoric stress at initial yield and the deviatoric stress at peak. This suggests that with higher confinement pressures, the specimen exhibits brittle behaviour for a relatively higher stress.

Specimen No.	Axial Strain at Initial Yield	Deviatoric Stress at Initial Yield	Axial Strain at Peak	Deviatoric Stress at Peak	Yield Stress as a percentage of Peak Stress
N1_U_200	0.82%	983.04 kPa	1.68%	1565.45 kPa	63%
N2_U_400	0.76%	1709.65 kPa	1.52%	2472.39 kPa	69%
N3_U_600	0.58%	3629.34 kPa	1.11%	5252.18 kPa	69%
N4_U_800	0.65%	5882.79 kPa	1.16%	7556.65 kPa	79%

Table 5.5 - Stress and Strain values at different stages of the test for the natural specimens

As reported by Henkel (1956), in overconsolidated natural clays, pore pressure initially increases as the sample is strained. This is followed by a characteristic drop in pore pressure with strain and becomes negative. Moreover, in heavily overconsolidated Cam-Clay model tests by Asaoka, Nakano and Noda (1997) it was noticed that the pore pressure initially rose until the initial yield was reached, after which the pore water pressure then dropped due to the tendency for dilation until the material approaches the CSL. This behaviour is consistent with that exhibited by all the natural UGL-2 samples in this study.

Ladd and Foott (1974) noted that overconsolidated natural clays in general tend to show strain softening when undergoing shear. This phenomenon is also similarly observed in the natural UGL-2 as the samples reach a post-rupture state after the peak strength was reached.

Following the initial increase and decrease in pore pressure, secondary minor contraction and dilative behaviours were observed in samples N1_U_200, N2_U_400, and N3_U_600. These additional behaviours likely caused the minor fractures seen in these samples. Specimen N4_U_800 exhibited the same pattern, however, the second increase in pore pressure (contraction) was significantly greater than in the other samples. This pronounced contraction was likely contributing to the formation of another major slip plane throughout the specimen that was still yet to happen.

Figure 5.18 exhibits the INCL (the starting points of the stress paths of the reconstituted), the swelling line (the starting point of the natural), the undrained stress paths of the natural specimens and the critical state reached by the reconstituted specimens is also included as a reference. The grey/black square indicates the starting point of the stress path of the natural specimens, and the grey circle indicates the final state of the stress paths. As indicated in Figure 5.18 all stress paths of the natural specimens are traveling from left to right, a path typically followed by overconsolidated samples. All stress paths are perfectly horizontal. This occurs because the specimens are being isotropically compressed under undrained conditions, where no volume change is allowed.

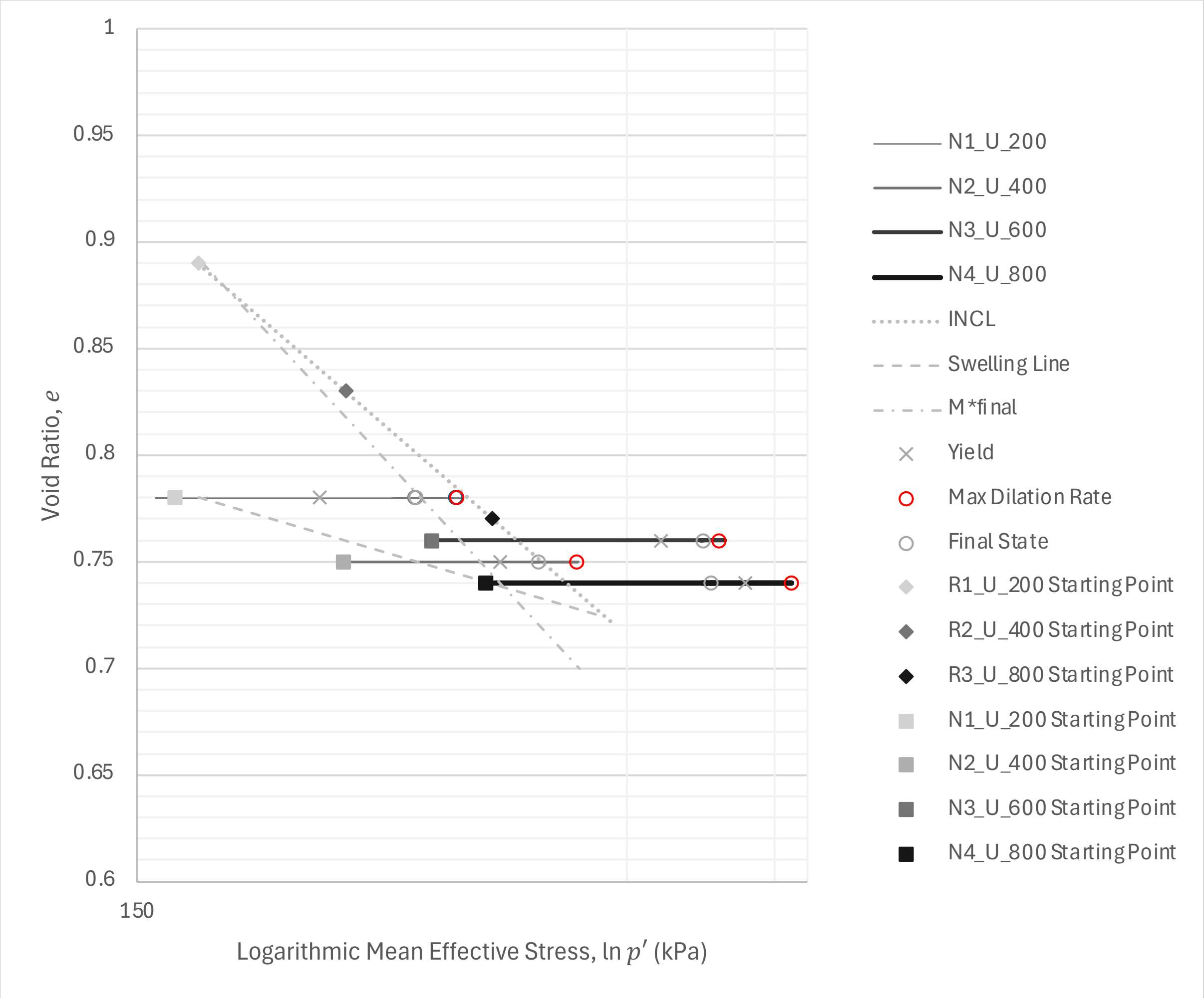

Figure 5.18 - Void Ratio (e) vs Logarithmic Mean Effective Stress (p') Space for the natural specimens

Figure 5.19 displays all stress paths reached a specific peak in deviatoric stress, which then decreased due to the formation of a major shear plane. Burland (1990) supports this statement, noting that the point of maximum dilation indicates the creation of a major slip plane throughout the specimen. As the specimens neared this peak stress, a dramatic drop in pore water pressure was observed. All specimens seem to have reached critical state however strain localization prohibits the reliability of such measurement. This is evidenced by the fact that neither specimen sheared at a constant pore pressure (or volume change). The proposed critical state lines for the final stage (M^*_{final}) and at phase transformation (M^*_{pt}) of the reconstituted specimens is provided as a reference in Figure 5.19, showing that the final states of the natural specimens did not coincide with neither critical state line although the final states and stress ratio of specimens N1_U_200 and N2_U_400 are very close to this critical state line at final state (M^*_{final}).

Clear observations in Figure 5.16 and Figure 5.19 show that specimens compressed at a higher mean effective stress demonstrated greater maximum deviatoric stresses, while specimens compressed at a lower mean effective stress experienced lower deviatoric stresses.

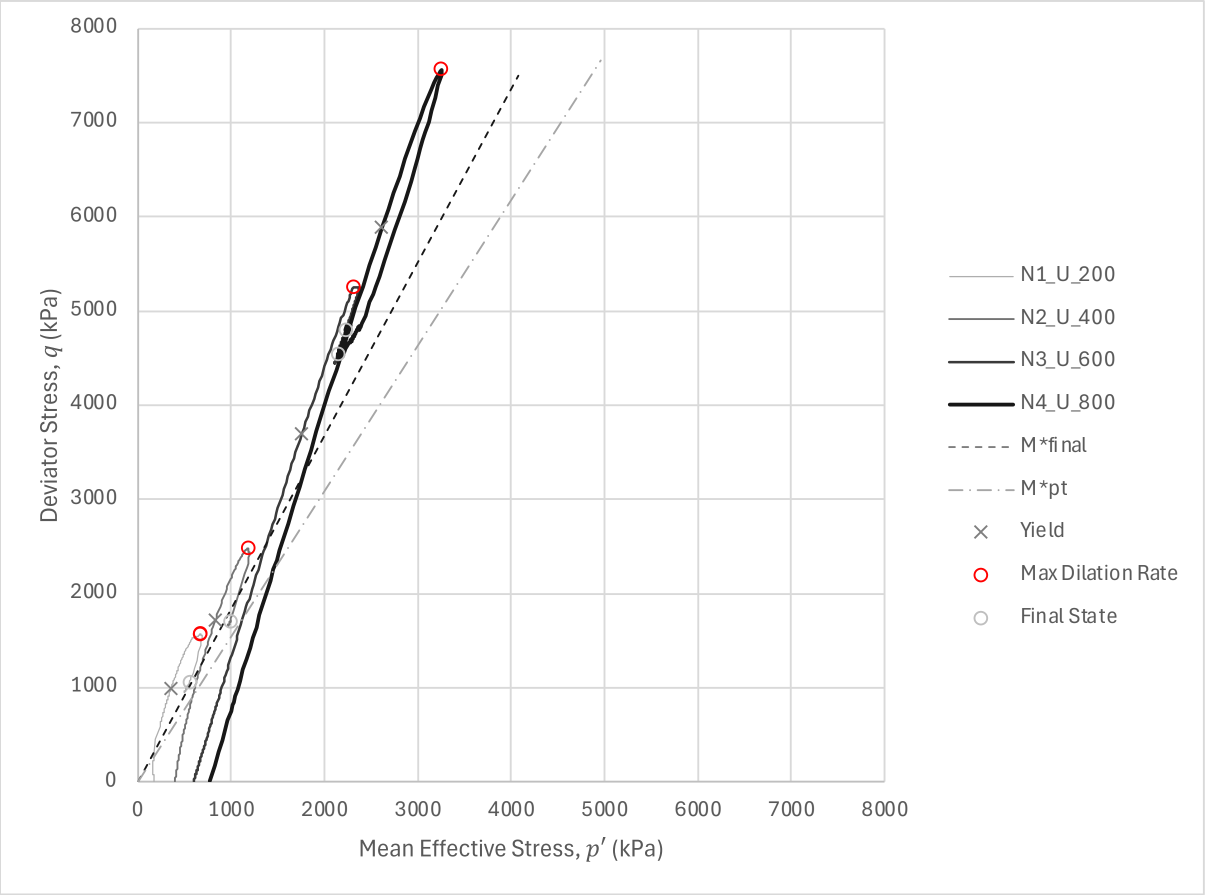

Figure 5.19 - Deviator Stress (q) vs Mean Effective Stress (p') Space for the natural specimens

The stress path of the N1_U_200 sample initially rises almost vertically before heading to the right, while the stress paths of the other samples immediately directed towards the right. It is evident that all these stress paths climb up to reach a boundary surface resembling that of the Hvorslev surface in Figure 3.12 and then travel down again. Atkinson and Bransby (1978) anticipated this type of behaviour in overconsolidated materials.

All stress paths generated a build-up of pore water pressure, similar to findings by Atkinson and Bransby (1978) in Figure 3.14. Initially, the specimens generated a positive pore pressure, which later turned negative, a typical behaviour for overconsolidated specimens under undrained conditions. This pattern was particularly evident in specimen N1_U_200, where the stress path initially moved left before shifting right. Although all specimens experienced a rise in pore water pressure, specimens N2_U_400, N3_U_600, and N4_U_800 did not exhibit a significant pore pressure build-up and resembled drained stress paths to a certain degree. This phenomenon occurred due to a lack of pore pressure build-up during the shearing process in the latter specimens.

All specimens exhibit a sharp increase in stress ratio until a peak was reached and dropped again which all later converged towards a different horizontal stress ratio. The stress ratio peak, however, does not coincide with the peak deviatoric stress. All specimens reach a near-constant stress ratio at the final stages of the test apart from sample N4_U_800 which exhibit a slowly increasing stress ratio.

The critical state line cannot be derived from the final data points of these tests because strain localization provides unreliable measurements. This is further evidenced from the stress ratios which show that all specimen lied above or below the critical state line reached by the reconstituted samples. Additionally, the stress ratios did not converge at large strains and did not settle at a unique stress ratio.

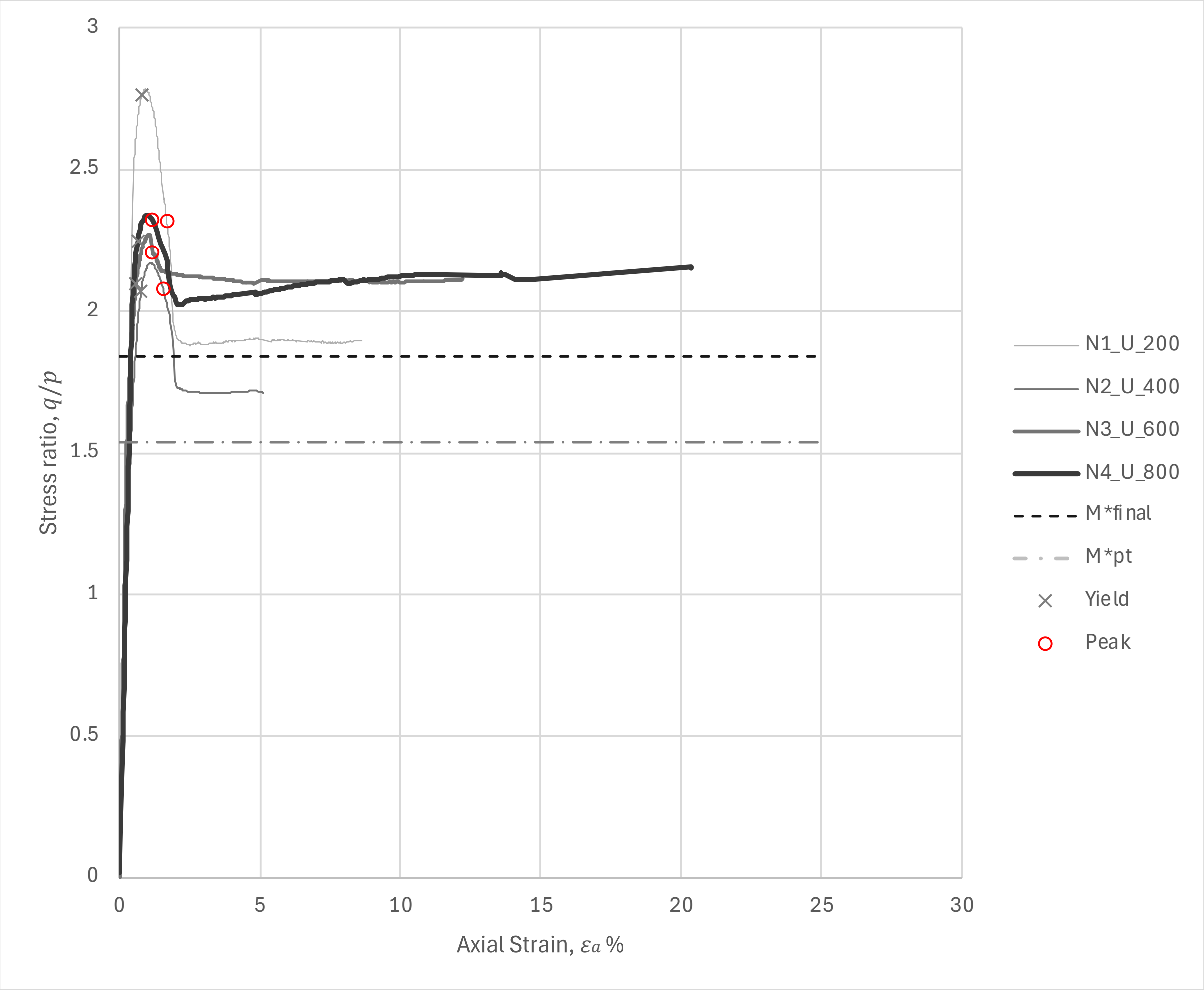

Figure 5.20 - Stress ratio (q/p) vs Axial Strain (ε_a) Graph for the natural specimens

Figure 5.22 to Figure 5.25 illustrate the deformed state of the natural specimens following isotropic compression. Each specimen is depicted from four different angles. All natural specimens failed in the same manner, developing a well-defined inclined shear plane throughout the specimen. No barrelling was observed in either specimen. The major shear plane observed in each specimen is most likely caused by strain localization. In this process, shear that was originally uniformly distributed, converges to the weaker plane within the specimen, resulting in the specimen splitting into two parts. This convergence results in the shear plane visible in all the specimens.

All specimens developed additional minor cracks, with the severity of these cracks increasing as the confinement pressure rose. Specimens N1_U_200 and N2_U_400 sustained only a few hairline cracks, whereas specimens N3_U_600 and N4_U_800 exhibited a relatively higher degree of cracking throughout.

All specimens developed a well-defined shear plane extending from the head to the mid-height, except for specimen N3_U_600, which developed a shear plane from the mid-height to its toe.

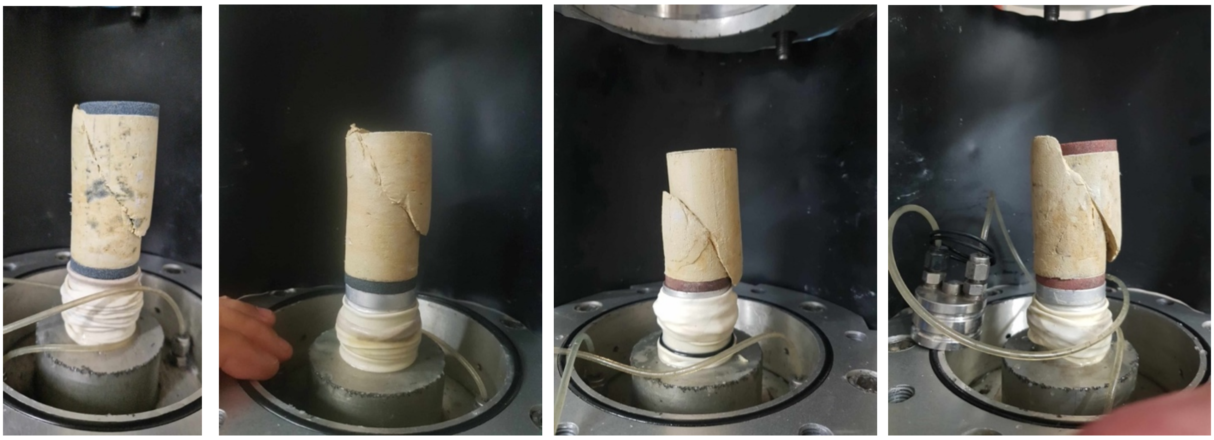

Figure 5.21 – Failure mode of the Natural UGL 1 _ 200kPa (Left), Natural UGL 2 _ 400kPa (Middle-Left), Natural UGL 3 _ 600kPa (Middle-Right) & Natural UGL 4 _ 800kPa (Right)

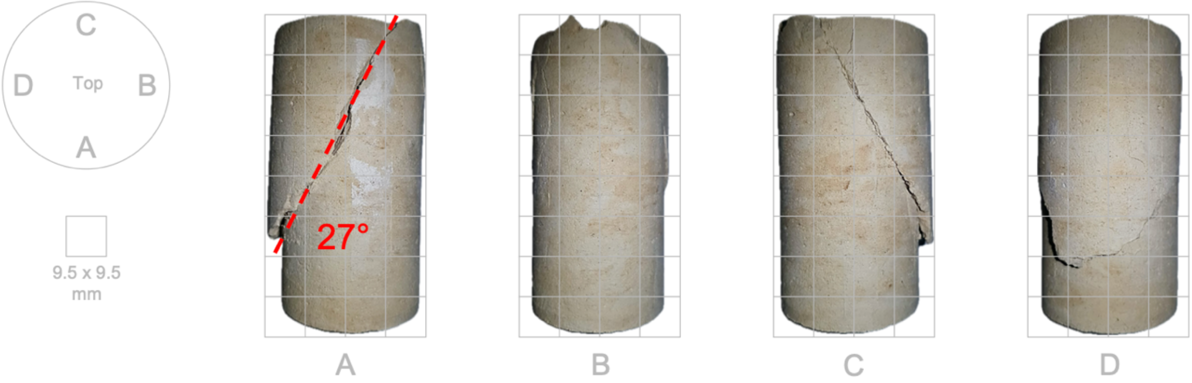

Figure 5.22 - Photos representing the failure mode of specimen N1_U_200 from four different angles

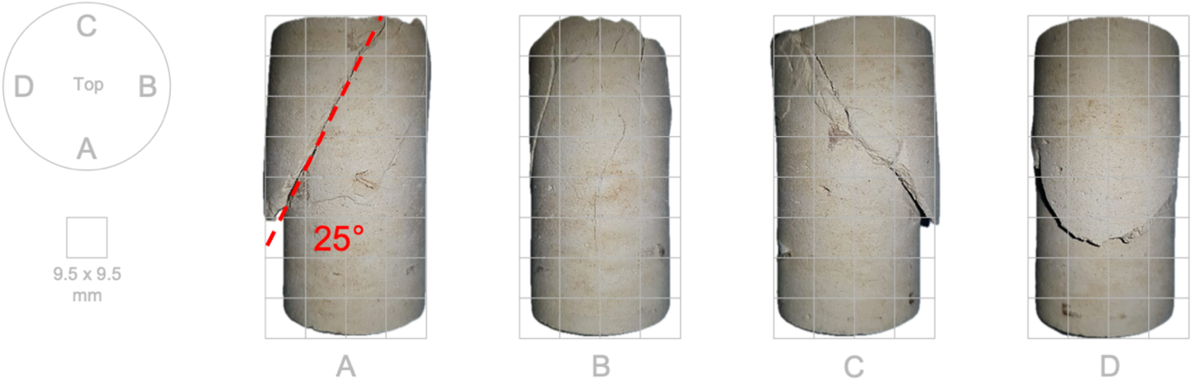

Figure 5.23 - Photos representing the failure mode of specimen N2_U_400 from four different angles

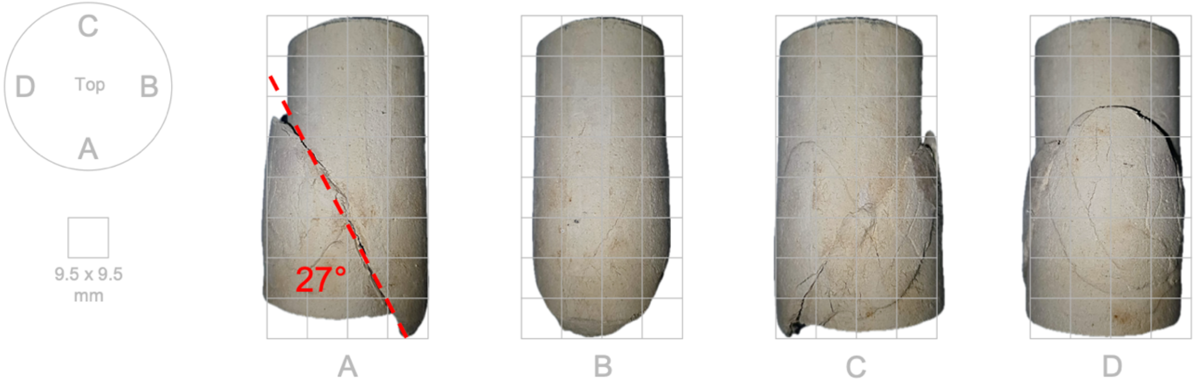

Figure 5.24 - Photos representing the failure mode of specimen N3_U_600 from four different angles

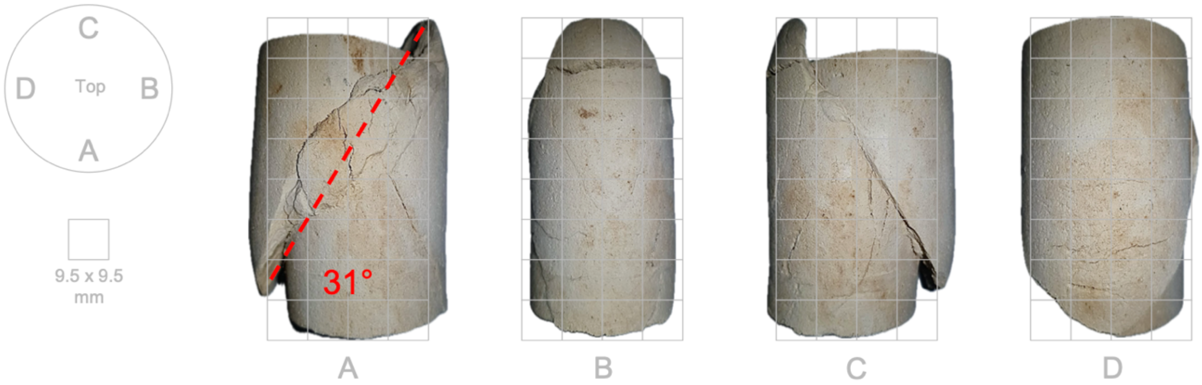

Figure 5.25 - Photos representing the failure mode of specimen N4_U_800 from four different angles

5.2.3 Normalization of plots

To compare all the natural and the reconstituted tests, normalization is necessary. The two forms of UGL-2 were normalized separately to obtain a better view of the results. This process helps in assessing the stress path shapes of all specimens. Normalization was achieved by dividing the deviatoric stresses and the mean effective stresses by the equivalent pressure at the same void ratio. According to Lade (2016), this normalization assists in identifying potential errors that may have occurred during the test. Figure 5.26 and Figure 5.27 display the normalized stress paths for both forms of UGL-2.

The stress paths of the reconstituted specimens are converging toward the same boundary, forming a narrow band that resembles the Roscoe-Rendulic surface, typical of normally consolidated materials. However, there is a discrepancy in the stress path of sample R1_U_200, which may be due to the incorrect preparation process, as previously mentioned. Specimen R3_U_800 follows this narrow band in the initial stage, which then changes direction as a result of phase transformation.

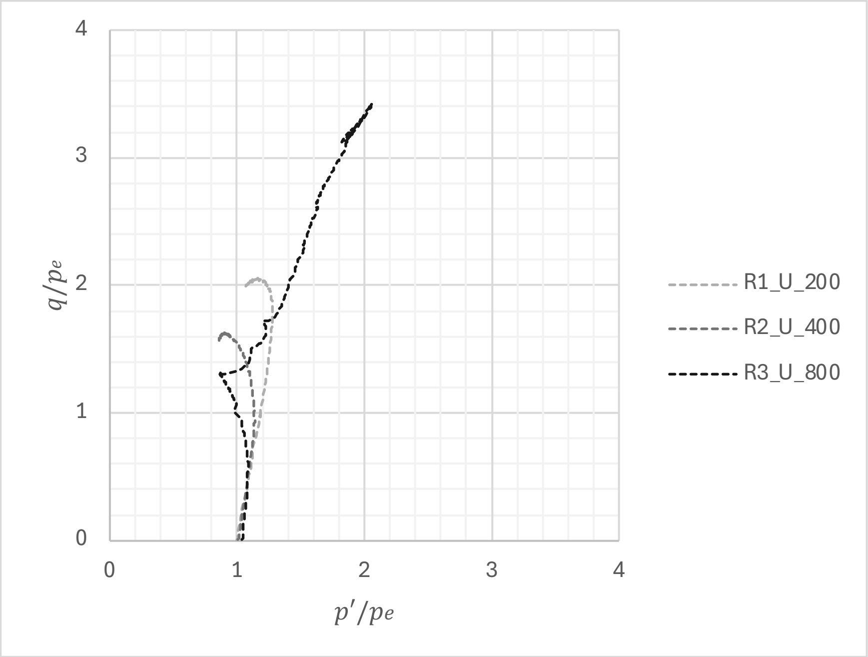

Figure 5.26 - Normalization of Stress Paths Graph for the reconstituted specimens

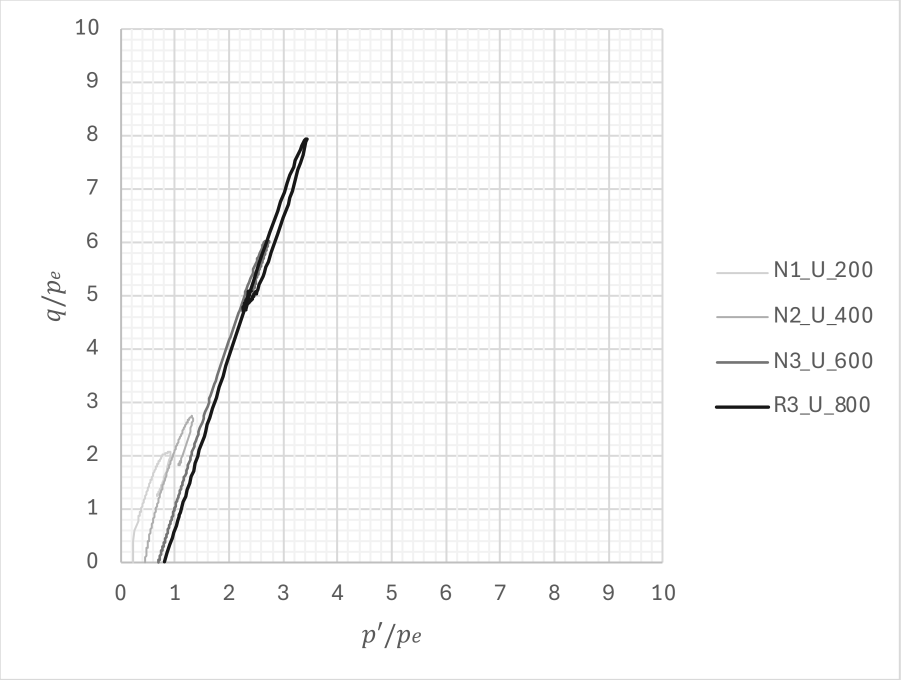

Figure 5.27 - Normalization of Stress Paths Graph for the natural specimens

The natural specimens also head towards and converge into a narrow band, resembling that of the Hvorslev surface, as expected for overconsolidated materials.

It is evident from Figure 5.28 that the state boundary surface achieved by the natural specimens is significantly larger than that of the reconstituted specimens, indicating that the natural specimens have greater strength and stiffness compared to their reconstituted counterparts. This strength results from the inherent structure of the natural UGL-2, which the reconstituted UGL-2 lacks. Therefore, it is clear that structure significantly influences the mechanical behaviour of soils, as highlighted by Leroueil and Vaughan (1990) and Burland (1990).

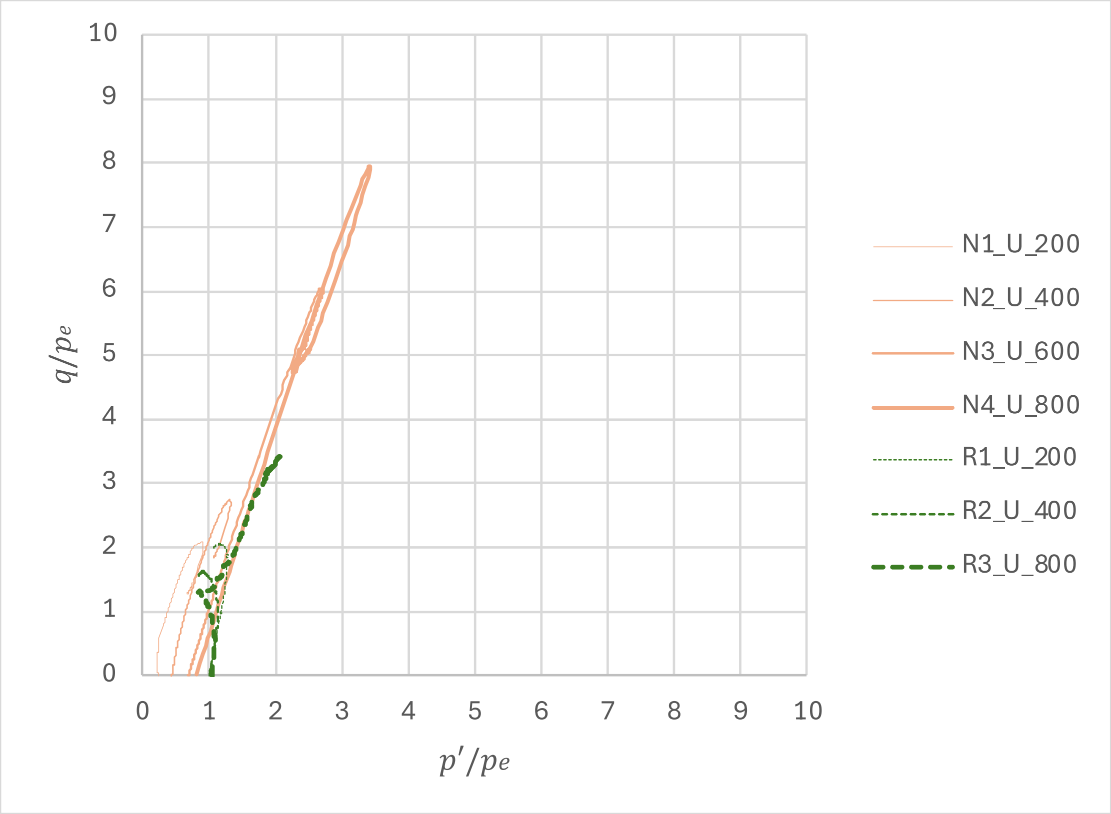

Figure 5.28 - Normalization of Stress Paths Graph for both reconstituted and natural specimens

5.2.4 Undrained Young's Modulus

The undrained Young's Modulus, E_i, for both forms of UGL-2 was determined by calculating the gradient of the initial linear region of the deviator stress versus axial strain graph. Lade (2016) notes that there exists no unique value for the undrained Young's Modulus, as it varies with different confinement pressures, which can be confirmed by the table below. The initial yield point, marked with a cross (x) for both forms of UGL-2, occurs at very low strains, especially in the reconstituted specimens. Table 5.6 presents the undrained Young's Modulus values for both the natural and reconstituted specimens at various confinement pressures.

Specimen No.	**Deviator Stress, q (kPa)**	**Axial Strain (%)**	**Young's Modulus, E_i (MPa)**
N1_U_200	983.04	0.82	120
N2_U_400	1709.65	0.76	225
N3_U_600	3629.34	0.58	626
N4_U_800	5882.79	0.65	905
R1_U_200	242.19	0.50	48
R2_U_400	293.52	0.25	117
R3_U_800	619.42	0.85	73

Table 5.6 - Obtained Values of the Undrained Young's Modulus

6. Recapitulation and Conclusion

This dissertation aimed to explore the mechanical behaviour of the Upper Globigerina Limestone, both in its natural and reconstituted states, extracted from Mellieha, Malta, to comprehend the impact of structure on the UGL-2's strength and stiffness. This analysis was conducted by subjecting the limestone to undrained shear under isotropic conditions using a triaxial apparatus.

This final chapter begins with a summary of the various mechanical behaviours observed in both the natural and reconstituted samples when subjected to shear. Finally, it will conclude by highlighting the main finding of this dissertation.

6.1 Mechanical behaviour comparison of both forms of UGL-2

As observed in Figure 6.1 the greater the confinement pressure applied, the higher the deviator stress at both the initial yield and the peak for both forms of UGL-2. The reconstituted specimens exhibited ductile behaviour and strain hardening as deviator stress kept roughly constant in specimens R1_U_200 and R2_U_400 and increased in specimens R3_U_800 after reaching peak in stress-strain graphs. On the other hand, the natural specimens displayed brittle behaviour and strain softening as indicated by the decrease in deviatoric stress after reaching peak. Higher confinement pressures increased brittleness behaviour in the natural samples indicated by the sharp peaks observed in the stress-strain graphs. The natural specimens experienced much greater peak deviatoric stress compared to the reconstituted at the same confining pressure.

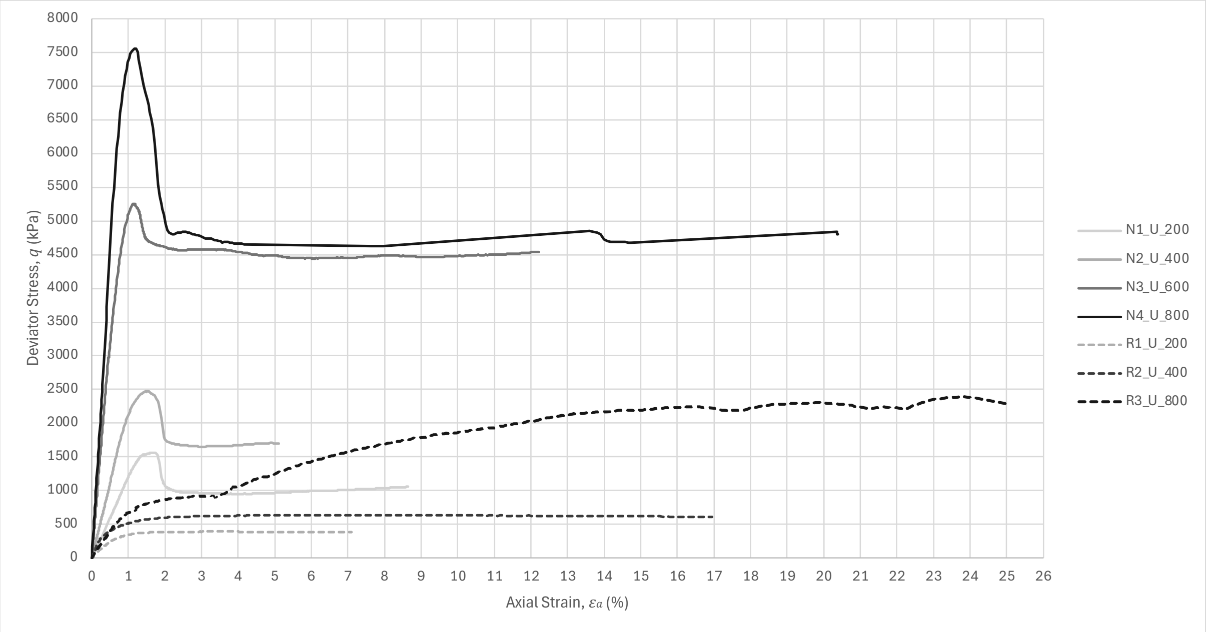

Figure 6.1 - Deviator Stress (q) vs Axial Strain (ε_a) Graph for both reconstituted and natural specimens

Figure 6.2 shows that the reconstituted specimens initially exhibited contractive behaviour, resulting in barrel-shaped specimens. After exhibiting contraction behaviour, specimen R2_U_400 reached an axial strain where it began shearing at a constant volume, and specimen R1_U_200 likely would have done the same if the test had not been stopped prematurely.

Specimen R3_U_800 also experienced contraction until phase transformation occurred, changing its behaviour to dilative, with a slip plane beginning to form at this point. The natural samples initially exhibited an abrupt contraction behaviour until reaching a peak, after which they underwent a sharp drop in pore pressure, signifying expansion behaviour. This dilation contributed to increased strength in the natural sample, and as it dilated, shear planes emerged due to strain localisation. There were no observations of barrelling deformation in these samples.

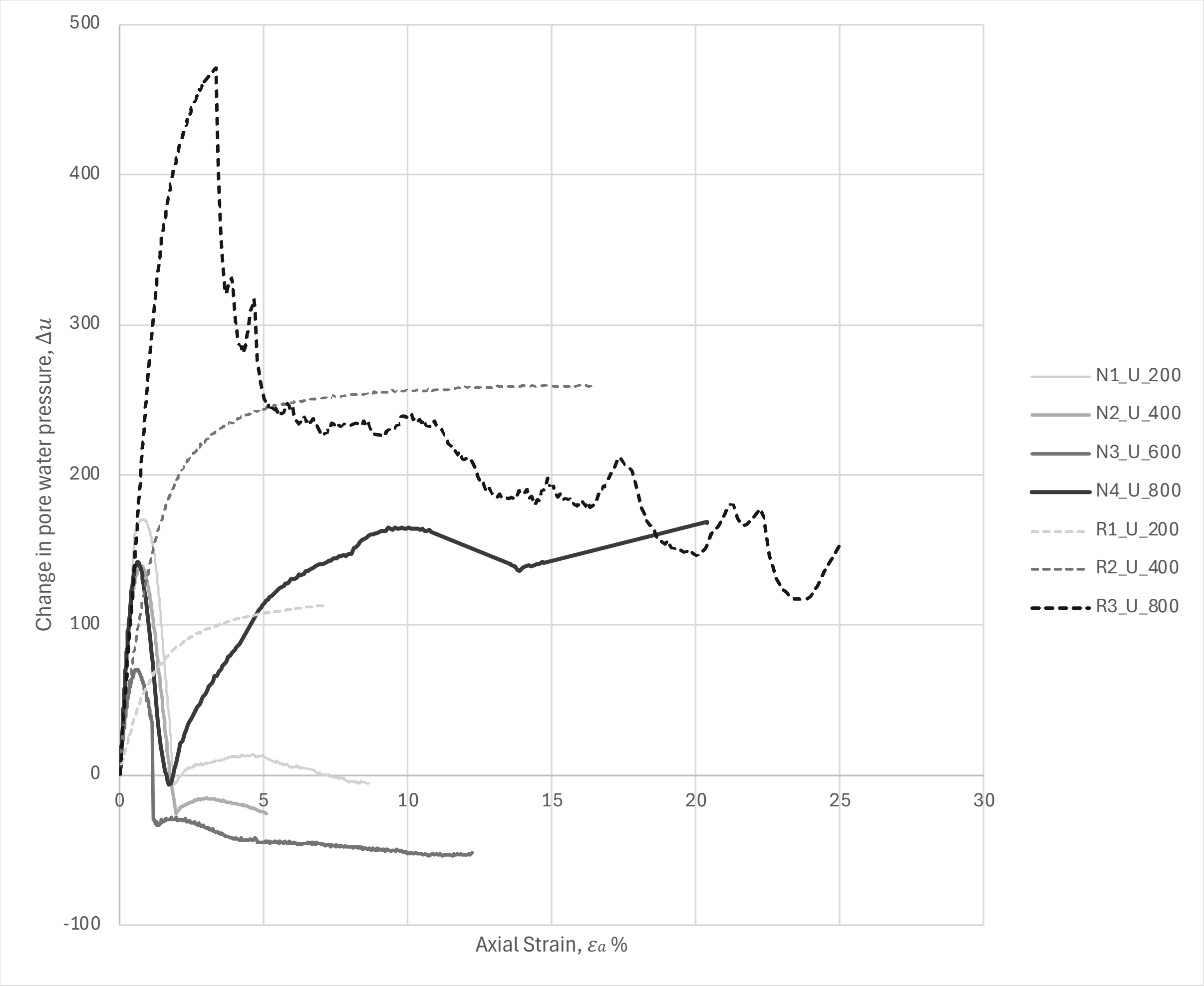

Figure 6.2 – Change in pore water pressure (Δu) vs Axial Strain (ε_a) Graph for both reconstituted and natural specimens

Figure 6.3 illustrates that all reconstituted specimens were initially located on the wet side of critical and moved to the left to reach the critical state, which is typical for normally and lightly overconsolidated specimens. In contrast, all natural specimens were initially on the dry side of critical and moved to right in an effort to reach the critical state, a common feature for overconsolidated specimens.

Critical state was reached only by specimen R2_U_400 and nearly reached by R1_U_200 in the final stages, while specimen R3_U_800 attained this state during phase transformation. All natural specimens reached the critical state as well at the post-rupture surface; however, it could not be reliably measured at this stage.

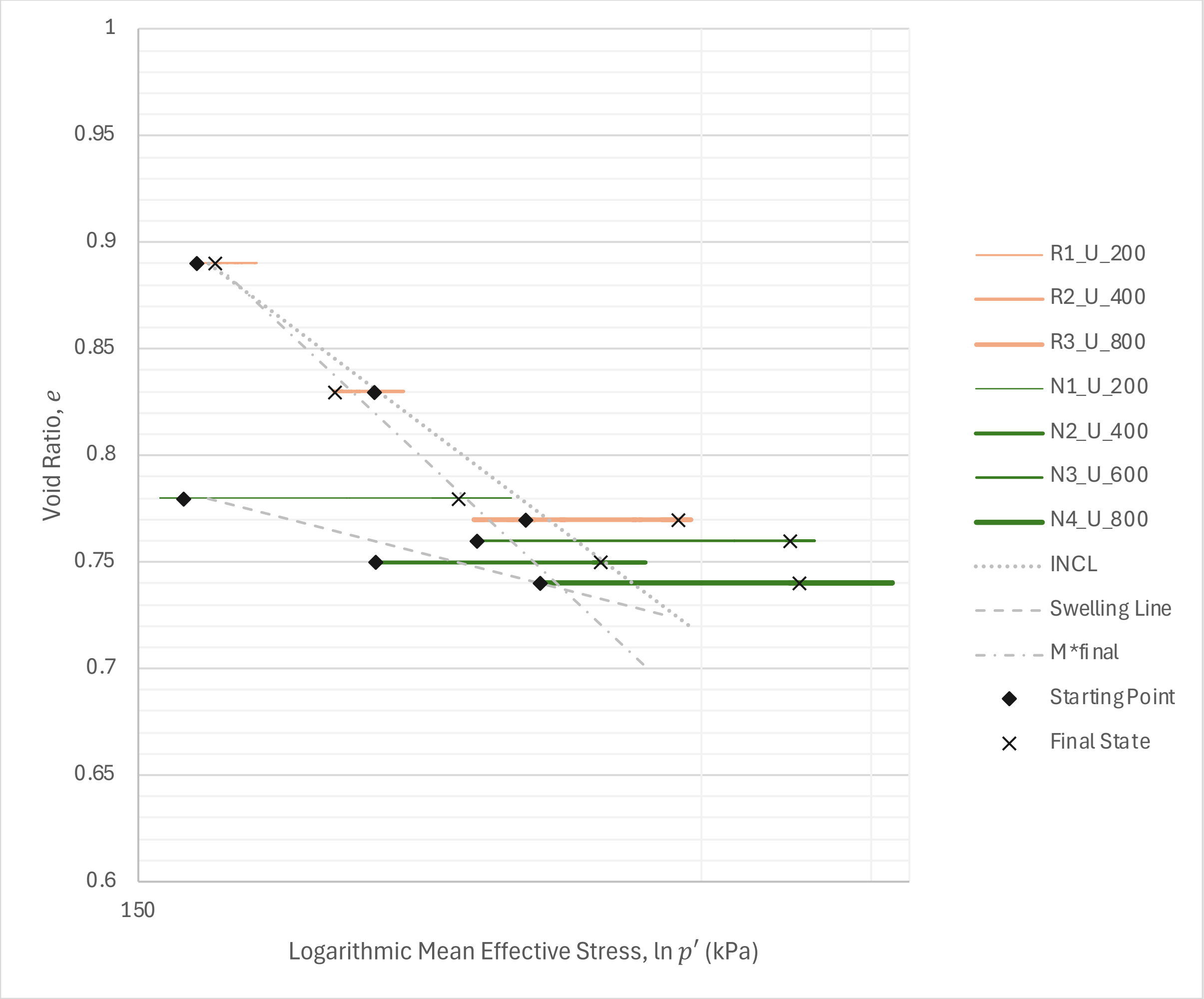

Figure 6.3 - Void Ratio (e) vs Logarithmic Mean Effective Stress (p') Space for all specimens

Figure 6.4 displays that all reconstituted stress paths follow a Roscoe-Rendulic boundary which is a common feature for normally consolidates specimens, whereas all natural stress paths follow a Hvorslev surface, which is a common feature for overconsolidated specimens.

Both Figure 6.1 & Figure 6.4 show that the strength and stiffness of the natural specimens surpasses that of the reconstituted specimens. This is demonstrated by the significantly higher deviatoric stress achieved by the natural specimens.

All specimens converged and reached a nearly consistent stress ratio as shown in Figure 6.5. Both reconstituted specimens R1_U_200 and R2_U_400 converged to an approximately equal stress ratio which indicate the critical state at the final state of both specimens. Reconstituted specimen R3_U_800 did not converge to this mentioned constant stress ratio, however another horizontal line at phase transformation could be drawn which may indicate critical state as well. However, the natural specimens did not align with a specific, unique stress ratio; instead, they displayed scattered ratios. Additionally, they did not match with any of the stress ratios seen in the reconstituted specimens (which indicate critical state). This indicates that the critical state observed in the natural specimens is unreliable and this unreliability is due to strain localization.

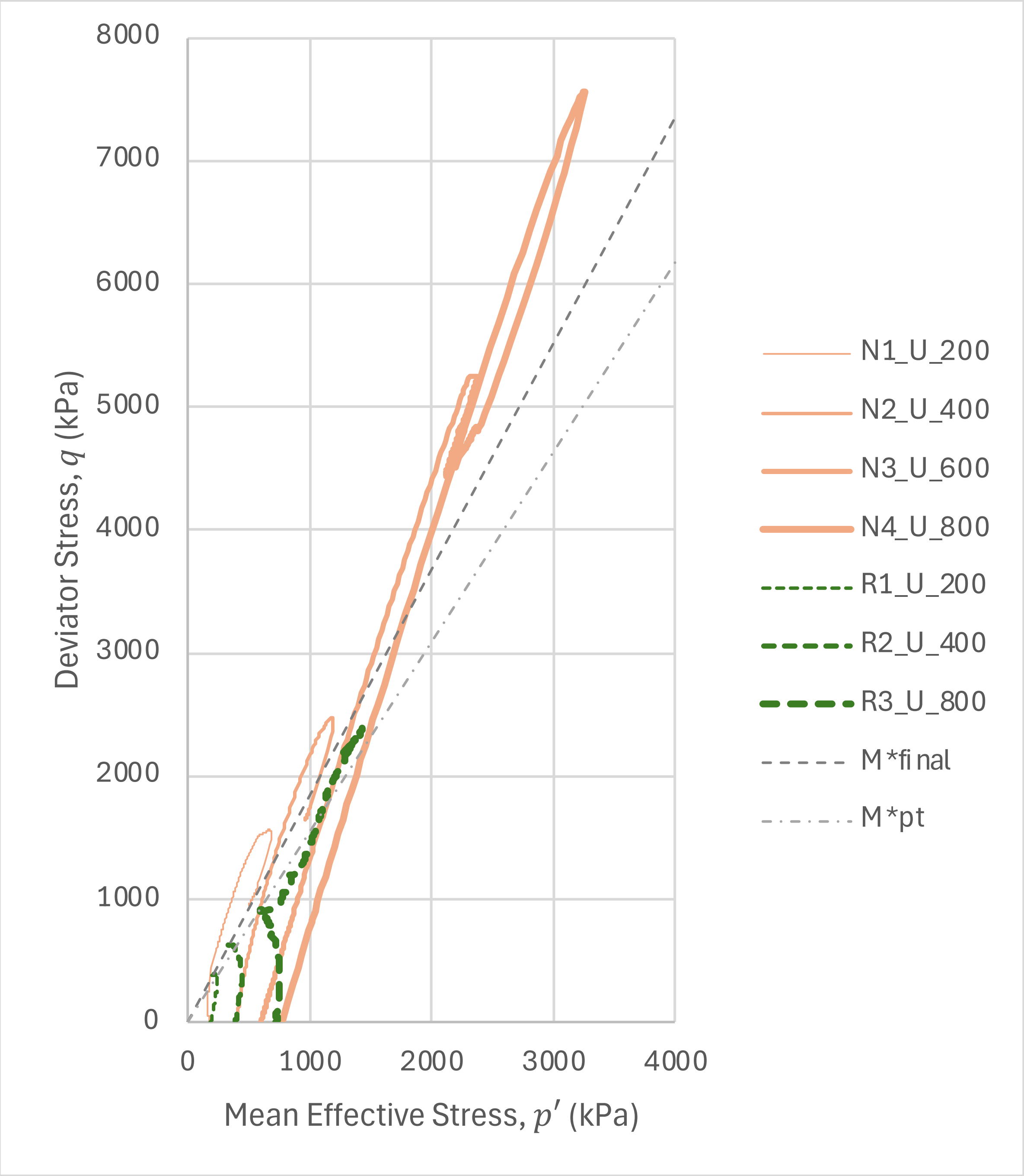

Figure 6.4 - Deviator Stress (q) vs Mean Effective Stress (p′) Space for both reconstituted and natural specimens

Figure 6.6 exhibits the normalization of graphs which shows the extended state boundary surface (red dashed SBS) of the natural specimens as compared to the state boundary surface (blue dashed SBS) of the reconstituted specimen. The SBS for the natural specimen cannot be drawn completely as more testes with higher confinement pressures are required to construct the full boundary surface. A rough and unscaled version (on the right of Figure 6.6) of the predicted complete SBS is provided to serve as reference to the SBS drawn for both forms of UGL-2 material. This extended SBS by the natural (structured) UGL-2 shows the superior strength and larger strength sensitivity (which is definitely greater than 4) of the natural UGL-2 as compared to that of the reconstituted UGL-2.

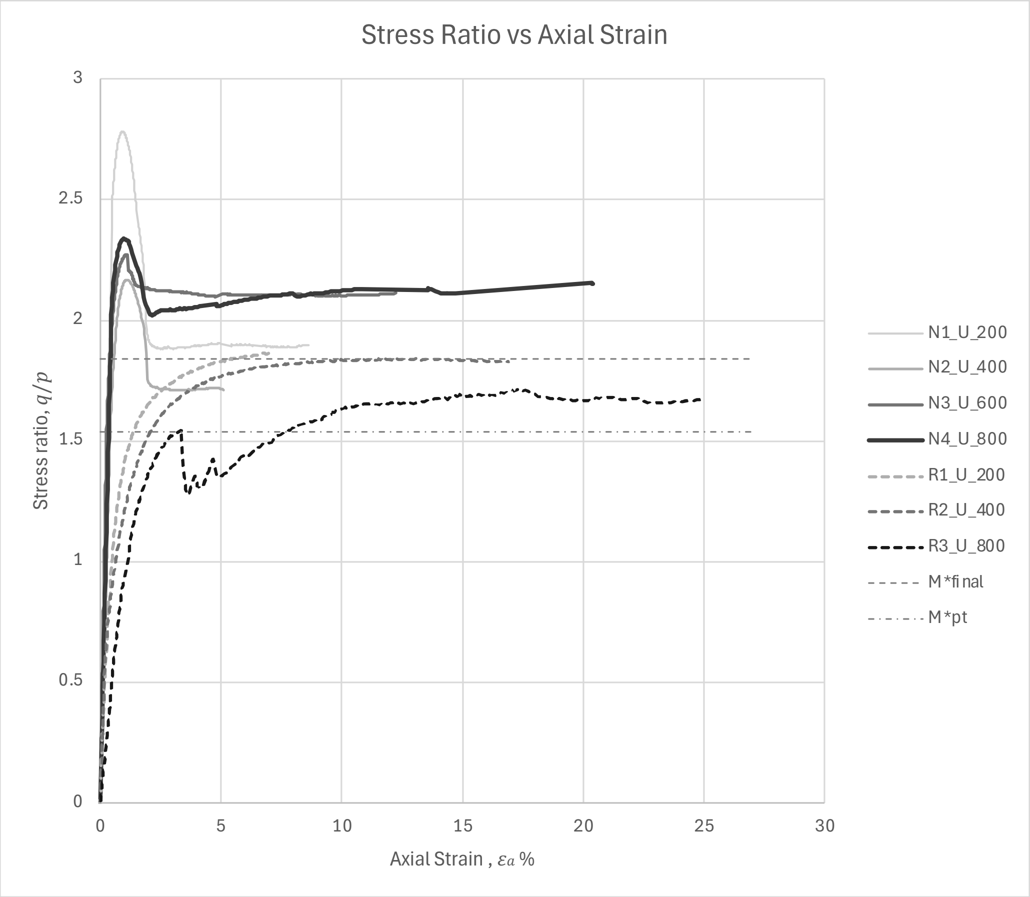

Figure 6.5 - Stress ratio (q/p) vs Axial Strain (ε_a) Graph for both reconstituted and natural specimens

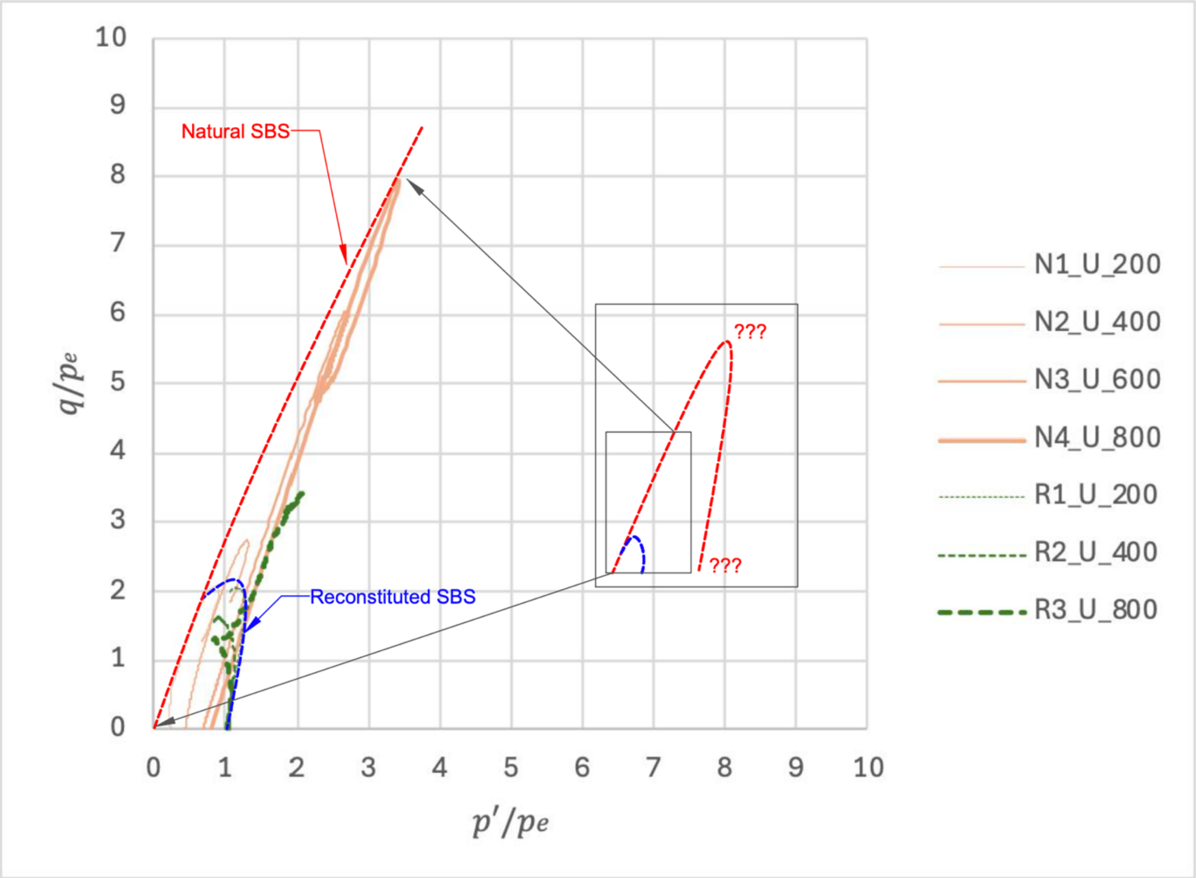

Figure 6.6 - Normalization of Stress Paths with predicted (approximated) State Boundary Surface for both natural and reconstituted specimens

6.2 Conclusion

This dissertation set out to investigate the applicability of the theory articulated by Leroueil and Vaughan (1990) and Burland (1990) to the Maltese Upper Globigerina Limestone. This theory suggests that natural soils tend to possess greater strength and stiffness compared to their reconstituted counterparts.

The findings unequivocally demonstrate that the natural UGL-2, characterized by its inherent structure, exhibits significantly enhanced strength and stiffness in comparison to the reconstituted UGL-2, which lacks such structure. Consequently, it can be firmly asserted that the presence of structure indeed plays a pivotal role in influencing the strength and stiffness of this sedimentary deposit. This conclusion lends substantial support to the theory proposed by Leroueil and Vaughan (1990) and Burland (1990). Furthermore, it was observed that the structured natural specimen exhibits stress sensitivity of definitely four times greater than that of the reconstituted specimen.

The tests performed are only applicable to UGL-2 but sheds important information onto bonded soils of this category.

6.3 Further recommended research

Although this dissertation has offered valuable insights into the mechanical behaviour of the UGL-2, there remains a substantial amount of research to be conducted to comprehensively understand this peculiar material.

1. Ground material is highly heterogeneous, meaning the results obtained for this UGL-2 can vary even within a few meters from the original retrieval site. This variability is especially true for UGL-2 samples taken from different locations. Therefore, the Mellieha UGL-2 tested in this dissertation could be compared to UGL-2 samples from other locations to observe differences in mechanical behaviour.
2. In this dissertation, the confinement pressures applied were relatively low. Consequently, the material can be further investigated by applying higher confinement pressures to the same UGL-2 to observe how its behaviour changes.
3. The material can also be examined through microstructural analysis using a Scanning Electron Microscope (SEM). This study is particularly intriguing because, when combined with the findings of this dissertation, it could reveal the origins of the UGL-2's structure, significantly enhancing the value of this research.

7. Bibliography

Agius, J., Miceli, M., & Spatola, D. (2023). A Geological Overview of the Maltese Archipelago with reference to the Area of Sliema. Department of Geosciences, University of Malta, Msida, Malta.

Asaoka, A., Nakano, M. & Noda, T. (1997a). Soil-Water Coupled Behaviour of Heavily Overconsolidated Clay near/at Critical State. Soils and Foundations, Vol. 37, No. 1, pp. 13-28.

Atkinson, J., & Bransby, P. (1978). The mechanics of soils – an introduction to critical state soil mechanics. Published by: McGraw-Hill Book Company (UK) Limited, Berkshire, England.

Atkinson, J. (1993). Mechanics of soils & foundations by Atkinson. McGraw-Hill Book Company (UK) Limited, Europe.

Bennett, S.M. (1979). Paleoenvironmental studies in the Maltese mid-Tertiary carbonates. Ph.D. thesis submitted at University of London.

Bishop, A.W, & Henkel, D.J. (1957). The measurement of soil properties in the triaxial tests. London: Edward Arnold Ltd.

Bishop, A.W., & Henkel, D.J. (1962). The Measurement of Soil Properties in the Triaxial Test, Edward Arnold, London, 2nd edition., p. 228.

Bjørlykke, K. (2013). Encyclopaedia of sediments and sedimentary rocks. Pg 161-168.

Brewer, R. (1964). Fabric and Mineral Analysis of Soils, John Wiley and Sons, Inc, pp. 129-158.

Burland, J.B. (1990). On the compressibility and shear strength of natural clays. Geotechnique 40(3), 329-378.

Burland, J.B., Rampello, S., Georgiannou, V.N., & Calabresi, G. (1996). A laboratory study of the strength of four stiff clays. Geotechnique 46, pp. 491-514.

Busuttil, M. (2021). Characterisation of Soil in Marsa.

Casagrande, A. (1936). The Determination of the Pre-Consolidation Load and its Practical Significance. Proc 1st Int. Conf. on Soil Mechanics and Foundations., pp. 60-64.

Chandler, R., & Apted, J. (1988). The effect of weathering on the strength of London Clay. Quarterly Journal of Engineering Geology, 21, 59-68.

CloudIsle. (2018). Extracted from: https://www.um.edu.mt/projects/cloudisle/

Clough, G.W., Sitar, N., Bachus, R.C. & Shaffi Rad, N. (1981). Cemented sands under static loading. J. Geotech. Engng Div., Am. Soc. Civ. Engrs 107, GT6, pp. 799-817.

Coop, M.R. (1990). The Mechanics of uncemented carbonate sands. Geotechnique, 40(4), 607-626

Coop, M.R. (2004). MSc course notes. Imperial College, University of London.

Continental Shelf Department. (2022). Extracted from: https://www.bgs.ac.uk/news/new-geological-map-of-malta/

Cotecchia, F. & Chandler, R.J. (1997). The influence of structure on the pre-failure behaviour of a natural clay. Geotechnique 47, pp. 523-544.

Cotecchia, F. & Chandler, R.J. (2000). A general framework for the mechanical behaviour of clays. Geotechnique 50, pp. 431-447.

Craig, R.F. (2004). Craig's Soil Mechanics (Seventh Edition ed.). London, UK: E & FN Spon Press.

Craig, R.F., & Knappett, J. (2012). Craig's soil mechanics (8th edition ed.). E & FN Spon, an imprint of Chapman & Hall.

Czerewko, M.A., & Cripps, J.C. (2006). The implications of diagenetic history and weathering on the engineering behaviour of mudrocks. No. 118. The Geological Society of London 2006.

Das, B., & Henderson. (2016). Correlations of Soil and Rock properties in geotechnical Engineering. Springer.

Elliot, G.M., & Brown, E.T. (1985). Yield of a soft high-porosity rock. Geotechnique 35, No. 4, pp. 413-423.

Falowo, O.O., & Dayo, D.S. (2020). Geoengineering Assessment of Subgrade Highway Structural Material along Ijebu Owo – Ipele Pavement Southwestern Nigeria. IARJSET, Vol 7, Issue 4.

Falzon, M. (2022). Creep behaviour of Upper Globigerina Limestone. Master's thesis submitted at University of Malta, Msida.

Felix, R. (1973). Oligo-Miocene stratigraphy of Malta and Gozo. Meded Landbouwhogesch. Wageningen 73(20):1-103.

Frazi, M. (2017). Evaluation of volume compressibility coefficient variations in cement stabilised bentonite clay using (wet & dry). Journal of Fundamental and Applied Science.

Galea, P. (2019). Central Mediterranean tectonics – a key player in the geomorphology of the Maltese Islands. In: Gauci R, Schembri JA (eds) Landscapes and Landforms of the Maltese Islands. Springer, Switzerland, pp 19-30

Gatt, M. (2006). Il-Geologija u L-Paleontologija Tal-Gzejjer Maltin – 1. Malta, Publikazzjonijiet Indipendenza.

Gauchi, R., & Inkpen, R. (2019). The physical characteristics of limestone shore platforms of the Maltese Islands and their neglected contributions to coastal land use development. In: Gauci R, Schembri JA (eds). Landscapes and Landforms of the Maltese Islands, Springer, Switzerland, pp 343-356.

Grima, S. (2024). Investigating one dimensional properties of reconstituted Upper Globigerina Limestone. Master's thesis submitted at University of Malta, Msida. Unpublished.

Head, K. (1998). Manual of Soils Laboratory Testing Volume 3. John Wiley & Sons Ltd.

Henkel, D.J. (1956). The effect of overconsolidation on the behaviour of clays during shear. *Geotechnique*, 6, 139-150.

Hoek, E. (1999). Putting numbers to geology – an engineer's viewpoint. Quarterly Journal of Engineering Geology, 32 (1999), pp. 1-19.

Holtz, R.D., & Kovacs, W.D. (1981). An Introduction to Geotechnical Engineering. New Jersey. Prentices-Hall, Inc.

House, M.R., Dunham, K.C., & Wigglesworth, D. (1960). Geology and structure of the Maltese Islands. In H. Bowden-Jones, J.C. Dewdney, & W.B. Fisher, Malta – Background for development University of Durham.

John, C.M., Mutti, M., & Adatte, T. (2003). Mixed carbonate-siliciclastic record on the North African margin (Malta) – coupling of weathering processes and mid-Miocene climate. Geological Society of America Bulletin, 115, 217-229.

Kavvadas, M. & Amorosi, A. (2000). A constitutive model for structured soils. Geotechnique 50, No. 3, pp. 263-273.

Kruse, Gerard, A.M., Dijkstra, T.A., & Schokking, F. (2007). Effects of Soil Structure on Soil Behaviour: Illustrated with loess, glacially loaded clay and simulated flaser bedding example. Engineering Geology. Vol. 91(1), pg. 34-35.

Ladd, C.C., & Foott, A.M. (1974). New Design procedure for Stability of Soft Clays. Journal of the Geotechnical Engineering Division.

Lade, P. (2016). Triaxial testing of soils. Chichester, West Sussex, England : Wiley Blackwell.

Lade, P., & Ibsen, L. (1997). A study of the phase transformation and the characteristic lines of sand behaviour. International Symposium on Deformation and Progressive Failure in Geomechanics. Nagoya, Japan.

Lambe, T., & Whitman, R. (1969). Soil Mechanics. New York: John Wiley & Sons, Inc.

La Rochelle, P., Leroueil, S., Trak, B., Blais-Leroux, L., & Tavenas, F. (1988). Observational Approach to Membrane and Area Corrections in Triaxial Tests. In R. Donaghe, R. Chaney, & M. Silver, Advanced triaxial testing of soil and rock (pp. 715-731). Baltimore: ASTM.

Leroueil, S., & Vaughan, P.R. (1990). The general and congruent effects of structure in natural soils and weak rocks. Geotechnique, 40(3), 467-488. 10.1680/geot.1990.40.3.467.

Ling, X. (2015). The Influence of Structure on the Behaviour of a Saturated Clayey Loess. Canadian Geotechnical Journal.

McConnachie, I. (1974). Fabric changes in consolidated kaolin. Geotechnique 24(2):207-22.

Middleton, G.V. (2003). Encyclopaedia of sediments and sedimentary rocks. Kluwer Academic Publishers.

Mifsud, A. (2019). The Middle Globigerina Limestone of the Maltese Islands. Msida: PH.D. thesis submitted at the University of Malta. Unpublished.

Mitchell, J.K. (1976). Fundamental of soil behaviour. New York: Wiley.

Mittal, M., Satapathy, S.C., Pal, V., Agarwal, B., Goyal, L.M., & Parwekar, P. (2021). Prediction of coefficient of consolidation in soils using machine learning techniques. Microprocessors and Microsystems. 82(103830).

Mohammed, J.A. (2015). Consolidation of Soils – Testing and Evaluation 10.13140/RG.2.2.20220.33923.

Nichols, G. (2009). Sedimentology and Stratigraphy. Second Edition. Wiley-Blackwell.

Oil Exploration Directorate, Office of Prime Minister, Malta. (1993). Geological Map of the Maltese Islands

Pedley, H.M., House, M.R., & Waugh, B. (1976). The geology of Malta and Gozo. Proceed Geol Assoc 87:325-341

Pedley, H.M. (1978). A new lithostratigraphical and paleoenvironmental interpretation for the coralline limestone formations (Miocene) of the Maltese Islands. Overseas geology and mineral resources, H.M.S.O:54

Pedely, H.M., Hughes-Clarke, M., & Galea, P. (2002). Limestone isles in a crystal sea: the geology of the Maltese Islands. Publishers Enterprises Group (PEG Ltd), San Gwann, Malta, 109p.

Pedley, H.M. (2011). The Calabrian stage, Pleistocene highstand in Malta: a new marker for unravelling the late Neogene and quaternary history of the islands. J Geol Soc London 168:913-926.

Razoaki, R.N. (2000). Effect of ageing on mechanics of chalk slurries – Ph.D. thesis. University of Portsmouth.

Scerri, S. (2019). Sedimentary evolution and resultant geological landscapes. In: Gauci R, Schembri JA (eds). Landscapes and landforms of the Maltese Islands. Springer, Switzerland, pp 31-47.

Schembri, J.A. (2003). Costal land use in the Maltese Islands: a description and appraisal. Ph.D. Thesis, University of Durham, Unpublished, 393p.

Schofield, A., & Wroth, P. (2004). Roscoe, Kenneth Harry (1914-1970), soil mechanics engineer. Oxford University Press. 10.1093/ref:odnb/35828.

Skempton, A.W. (1970). The consolidation of clays by gravitational compaction. Geol. Soc. Lond., 125, 373-412.

Soldati, M., Devoto, S., Prampolini, M., & Pasuto, A. (2019). The spectacular landslide-controlled landscape of the northwestern coast of Malta. In: Gauci, R, Schembri, J.A. (eds) Landscapes and landforms of the Maltese Islands. Springler, Switzerland, pp 167-178.

Solidbase Laboratory Ltd. (2023). Redevelopment of Mellieha Bay Hotel, Mellieha, Malta, Ground Investigation Report to EN 1997, Unpublished.

Sugiyama, Y., Kawai, K., & Iizuka, A. (2016). Effects of stress conditions on B-value measurement. Soils and Foundations, 56(5), pp. 848-860.

Tavenas, F., Leroueil, S., La Rochelle, P., & Roy, M. (1978). Creep behaviour of an undisturbed lightly overconsolidated clay. Can. Geotech. J. 15, No. 3, 402-423.

Tavenas, F., & Leroueil, S. (1980). The behaviour of embankments on clay foundations. Can. Geotech. J., Vol. 17, pp. 236-260.

Tavenas, F., & Leroueil, S. (1985). Discussion. Proc. 11th Int. Conf. Soil mech. Fdn Engng, San Francisco 5, 2693-2694.

Terzaghi, K. (1925). Erdbaumechanik auf bodenphysikalischer Grundlage. Vienna: Deoticke.

Terzaghi, K. (1941). Undisturbed clay samples and undisturbed clay. J Boston Soc Civil Eng 28:211.

Terzaghi, K., Peck, R.B., & Mesri, G. (1948). Soil Mechanics in Engineering Practice.

Totsche, K.U. (2018). Microaggregates in soils. Journal, Vol. 181 (1), p. 104-136.

Twenhofel, W.H. (1939). Principles of sedimentation. New York, London, McGraw-Hill Book Company, inc.

Vaughan, P.R. (1988). Characterising the mechanical properties of in-situ residual soils. Proc. 2nd Int. Conf. Geomechanics in Tropical Soils, Singapore 2, 469-487.

Viladesau Franquesa, E. (2004). The influence of swelling on the behaviour of London Clay.

Wen, Y., & Zhang, Y. (2022). Relation between void ratio and contact fabric of granular soils. 10.1007/s11440-022-01507-7.

Wikimedia. (2007). Extracted from: https://commons.wikimedia.org/wiki/File:Mellieha-map.svg

Wood, M. (1990). Critical State Soil Mechanics – Muir Wood. Published by the Press Syndicate of the University of Cambridge.

Zhenghong, Y., Yanyun, Z., Jiabao., Congzhi, Z., Donghao, M., Lin, C., & Taiyi, C. (2020). Importance of soil interparticle forces and organic matter for aggregate stability in a temperate soil and subtropical soil. Geoderma (Vol. 362).